Forschungszentrum Jülich
in der Helmholtz-Gemeinschaft

Institut für Kernphysik

Production of the η meson in nucleon-nucleon collisions

Vadim Baru

Jül-4004

Production of the η meson in nucleon-nucleon collisions

Vadim Baru

Berichte des Forschungszentrums Jülich ; 4004
ISSN 0944-2952
Institut für Kernphysik Jül-4004
(Diss., Moskau, Russland, ITEP, 2002)

Zu beziehen durch: Forschungszentrum Jülich GmbH · Zentralbibliothek
D-52425 Jülich · Bundesrepublik Deutschland
☎ 02461/61-5220 · Telefax: 02461/61-6103 · e-mail: zb-publikation@fz-juelich.de

Contents

Chapter 1

Introduction

The study of the production of different mesons in nucleon-nucleon and nucleon-nucleus collisions at intermediate energies is a rather active direction of modern nuclear physics. In spite of the fact that this topic has been investigated for many years it is still the subject of strong interest at present. This interest is not but least related to recent successful developments in the accelerator technology which led to a wealth of new and rather accurate experimental data on the production of π, η, η' and other mesons in nucleon-nucleon collisions in the near-threshold region. These data in combination with the theoretical analysis open the unique possibility to study the mechanism of the production of different mesons as well as to explore the features of the meson-nucleon and nucleon-nucleon interactions. Over the last years significant progress was achieved in case of pion production in the reaction $NN \to NN\pi$ [1–5]. However, our knowledge about reactions involving the production of heavier mesons (K, η, η', ω, ϕ, a_0, ...) is still rather incomplete. That is why the present work is devoted to the study of the production of two of those heavier mesons in nucleon-nucleon collisions, namely of the η and a_0 mesons. Note, that the theoretical understanding of the reaction $NN \to NN\pi$, which is the main inelastic channel of the NN-interaction, is very important for studying the production of heavier mesons – because it serves us as a guideline for developing corresponding models. The most consistent calculation of pion production in NN-collisions was performed by Hanhart et al. [4,5]. The authors of [4,5] utilized in their calculation a realistic model of the πN-interaction developed by Schütz et al. [6] and investigated the role of heavy meson exchanges (HME).

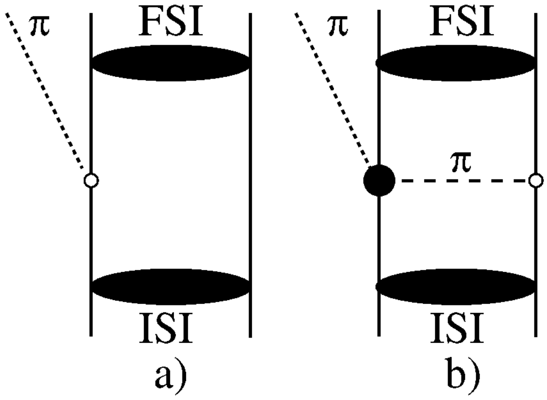

Figure 1.1: Mechanisms for the pion production in the reaction $NN \to NN\pi$.

On the basis of a good agreement with the experimental data the authors of [5] concluded that the contributions of the diagrams presented in Fig.1.1, i.e. direct production and pion re-scattering with taking into account the off-shell properties of the πN amplitude and the nucleon-nucleon interaction in the initial (ISI) and in the final (FSI) states, dominate for all channels of the reaction $NN \to NN\pi$. The only exception is the reaction $pp \to pp\pi^0$ where the contribution involving the re-scattering of heavier mesons (i.e. the so-called heavy meson exchanges) is about 40%. Thus, the results of [5] testify that effective approaches based on meson-exchange models work well, at least in the region of pion production. Therefore, a similar model approach will be utilized in the present investigation of the reaction $NN \to NN\eta$. One of the goals of the present work is a combined theoretical analysis of all channels of the reaction $NN \to NN\eta$, namely $pp \to pp\eta$, $pn \to pn\eta$ and $pn \to d\eta$, taking into account consistently NN ISI and FSI effects and utilizing a realistic model of the meson-nucleon interaction for the η-meson production process. Only such a combined analysis might allow to draw conclusions about the reliability of the approach and to determine the mechanisms of η-meson production. Another argument for the theoretical investigation of the η-meson production is the wealth of available experimental information on the different η-meson observables. Apart from recent measurements of the total cross section for the reaction $pp \to pp\eta$ [7–12], there exist also some data on the total cross sections of the reactions $pn \to pn\eta$ [13] and $pn \to d\eta$ [14, 15]. Furthermore, due to COSY and Uppsala measurements there are already new data on the differential cross sections for the η production in proton-proton collisions [12, 16, 17] and even some polarization observables in the reaction $\vec{p}p \to pp\eta$ [18].

In this work we are interested in the description of η-production in the near-threshold region, i.e for excess energies up to $Q \sim 50$ MeV. Very recent experimental data on the differential cross sections of the reaction $pp \to pp\eta$ [17] clearly indicate that in this energy region the production of the η meson still takes place primarily in S-waves. Therefore, our efforts will also be concentrated mainly on the investigation of the S-wave contributions. Another goal of our work is the investigation of NN FSI and ISI effects. The understanding of these effects is a necessary prerequisite for the analysis of production processes of different mesons (not only π and η) in NN collisions. Note, that in many papers concerned with meson production FSI effects are taken into account approximately by applying methods which are rather questionable if one wants to obtain absolute predictions for the production cross sections (see, e.g, [19–22] for the case of η-production). The situation with the ISI is even less satisfying. Indeed, its contribution is simply omitted in most papers.

Note also, that in spite of the abundance of theoretical investigations on η-meson production [19–29] the central question, namely what is the dominant mechanism for the production process, is still open. There is general consent in the literature that re-scattering processes similar to the diagram 1.1b (but with a variety of intermediate meson exchanges) will be important. However, it is not clear which one of the possible meson exchanges plays the leading role. For instance, in [21, 24, 25] it is suggested that the dominant contributions should come from the vector meson ρ, whereas in [23] that particular contribution is not even considered and in [26, 27] it is found to be of minor importance compared to other contributions. Note that the understanding of the mechanism of meson production in NN-collisions could also help to pin down the special features of baryonic resonances involved in the production process. In particular, the proximity of the $S_{11}N^*(1535)$ resonance to the ηN-threshold ($m_\eta + m_N \simeq 1486$ MeV) has an essential effect on the ηN-interaction both in the $NN \to NN\eta$ production process and in the final state.

The thesis is structured in the following way. The chapters 2 and 3 are devoted to a detailed theoretical analysis of different channels of the reaction $NN \to NN\eta$, i.e. in $pp \to pp\eta$, $pn \to pn\eta$, and $pn \to d\eta$. In the presented model calculations effects of the NN FSI and ISI are taken into account. Our model analysis suggests that the dominant role in the η-meson production process belongs to the re-scattering mechanism involving the pion exchange. The contributions of other meson exchanges have to be taken into account as well since they have an influence on the magnitude of the cross sections due to interference with the amplitude of the pion exchange. The effects of the nucleon-nucleon final state interaction in the reactions $NN \to NNM$ are studied in detail in chapter 4. It is shown that the FSI effects are indeed not universal, i.e. they do depend on the mass of the produced meson. This is in contrary to the results of Ref. [19–22] where an universal NN FSI was utilized. Furthermore, it is demonstrated that the reaction amplitude cannot be factorized into the production process and (independent) NN FSI effects if the calculation aims at predicting absolute values of the cross sections. The analysis of ISI effects performed in chapter 2 leads us to the conclusion that ISI effects are not uniform in respect to the exchanges by different mesons. It is stressed that the inclusion of the ISI has a significant impact on the absolute value of the cross sections. It leads to strong reduction of the cross sections.

Apart from the investigation of the η-meson production in NN-collisions we present also, in chapter 5, an estimation of the cross sections for $a_0(980)$ meson production in the reaction $pn \to ppa_0^-$. The goal of this calculation is to stimulate a corresponding experiment at the COSY accelerator in order to study the structure and properties of the a_0-meson, which are so far poorly known. In the present work it is proposed to study these features by measuring total and differential $(\frac{d\sigma}{dm_{\pi\eta}}, \frac{d\sigma}{dm_{K\bar{K}}})$ cross sections of the reaction $pn \to ppa_0^-$. It is worth mentioning that the spectra of the effective masses, $\frac{d\sigma}{dm_{\pi\eta}}$ and $\frac{d\sigma}{dm_{K\bar{K}}}$ respectively, are quite sensitive to the specific features of the a_0-meson (mass of the resonance, its width, ratio of branchings into the $\pi\eta$ and $K\bar{K}$ systems). That is why experimental data in combination with a theoretical analysis could allow to make a step forward in the understanding of the structure of this scalar meson.

Chapter 2

Formalism

2.1 Present theoretical status

It is quite evident, especially due to pion and photon induced processes [30, 31], that near threshold η-production is governed by the S_{11} $N^*(1535)$ resonance. This rather broad resonance (width $\Gamma \approx 150$ MeV) is located very close to the mass of the ηN-system ($m_\eta + m_N \approx 1486$ MeV) and has a large branching ratio $\sim 30-55\%$ of the decay into the ηN channel. In contrast to the πN interaction, which becomes strong only in the region of the Δ-isobar in the P_{33} partial wave, the ηN interaction is predicted to be strongly attractive already in the S wave. Due to this feature of the ηN-interaction there are even suggestions about the possibility of existence of η-nucleus bound states (see, e.g., [32, 33]). Therefore it is not surprising that the $N^*(1535)$ resonance might have a strong influence on the η production. The coupling of the η to other resonances are either forbidden by isospin arguments (like for P_{33} $\Delta(1232)$) or believed to be weak and not important near the threshold (S_{11} $N^*(1650)$, ...). In the case of near threshold η production in NN collisions the $N^*(1535)$ resonance should contribute significantly to the magnitude as well as to the energy dependence of the cross section.

The analysis of recent experimental data on the cross section of the reaction $pp \to pp\eta$ measured at the CELSIUS and COSY accelerators [9, 11] indicates that, in contrary to π-meson production, the energy dependence of the cross section for η near the threshold cannot be explained just by phase-space factors

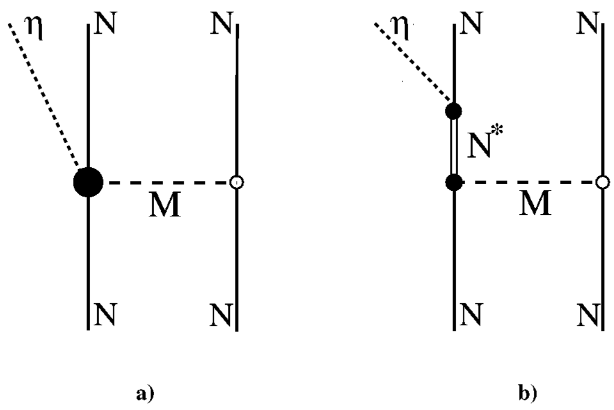

Figure 2.1: Diagrams for η production. (a) One-boson exchange contribution. The large blob • corresponds to the full $MN \to \eta N$ transition amplitude taking into account all possible intermediate processes; (b) One-boson exchange mechanism where the reaction $Mp \to \eta p$ ($M = \pi$, η, ρ, ω,...) proceeds only via the excitation of an intermediate $N^*(1535)$ resonance.

+ strong proton-proton final state interaction (FSI). A deviation from the phase-space behaviour is also seen in the reaction $pn \to d\eta$ [14]. It is commonly assumed that this discrepancy is a sign for the existence of a fairly strong $p\eta$ interaction in the final state [9, 11, 14, 34]. Another possibility is that this deviation is due to the influence of the near-by $N^*(1535)$ resonance on the primary production amplitude [23]. However, the ηN interaction in the production amplitude is averaged in the process of integration of the FSI loop. Therefore it seems to be less important for the energy dependence as compared to the FSI between the slowly moving outgoing η and the nucleons.

The reaction $NN \to NN\eta$ has been investigated theoretically in many works [19–29]. However, so far no final conclusions have been achieved — even the question what are the relevant mechanisms for the η production is not yet clarified. Though most of the model calculations assume that the production is mediated by re-scattering diagrams of the kind depicted in Fig 2.1a they differ significantly in the choice of intermediate meson exchanges. The strongest controversy in the literature concerns certainly the role of the vector mesons (ρ and ω). Since the $N^*(1535)$ is believed to play an important role the diagram of Fig. 2.1b with the intermediate ρ and ω meson exchanges might give a significant contribution. Therefore the results for the cross section depend heavily on the coupling constants $g_{\rho NN^*}$ and $g_{\omega NN^*}$, which are not directly experimentally available. The determination of these coupling constants is very model dependent. Assuming the vector-meson dominance model (VDM) hypothesis Germond and Wilkin [24] derived a rather large ρ coupling constant, $g_{\rho NN^*} = 1.66$, from the photo-production process of the η meson ($\gamma N \rightarrow N^*(1535) \rightarrow \eta N$). However, they were not able to extract the coupling constants for both vector mesons from one reaction. Therefore the contribution of the ω meson was neglected. Indeed the ρ meson plays a dominant role in their investigation. Its contribution is much larger than all other exchanges. On the other hand in the work of Vetter et al. [26] the coupling constant $g_{\rho NN^*}$ was obtained from the empirical $N^*(1535) \rightarrow \rho N$ decay width. The nominal ρN threshold is located above the mass of this resonance and hence only the tail of the ρ spectral function can contribute to this process leading a the coupling constant which is almost a factor of 3 smaller than that employed by Germon and Wilkin [24]. The coupling constant for the ω was deduced in [26] from the hypothetical relation

$$\frac{g_{NN^*\pi}}{g_{NN\pi}} = \frac{g_{NN^*\omega}}{g_{NN\omega}}. \tag{2.1}$$

Using these assumptions the authors come to the result that the contributions of ρ, ω and π mesons are basically of equal magnitude[1]. In the paper of Gedalin et al. [21] in some way a combination of the above assumptions was applied – the ρ coupling $g_{\rho NN^*}$ was deduced from VDM but $g_{\omega NN^*}$ was fixed by using the abovementioned relation (2.1) from [26]. Their conclusion is that the cross section is governed by ρ-exchange and π exchange, whereas the contribution of the ω is small. The model of Batinić et al. [23] involves only the π, η and σ-exchange contributions (i.e. no vector mesons at all are included) but is still able to describe the data for the $pp \rightarrow pp\eta$ reaction. There is also a lately published paper by M.T. Peña et al. [27] where the authors obtained the most important contributions by short-ranged mechanisms resulting from scalar meson exchange and

[1] However, it is worth mentioning that the ρNN effective Lagrangian in [26] consists of just the vector coupling part whereas the tensor part, which is the dominating piece near threshold (the ratio of tensor coupling constant to vector one is $\kappa_\rho = f_{\rho NN}/g_{\rho NN} \approx 6.1$) [35], was omitted.

from the direct η production. Finally, the very recent calculation of Nakayama et al. [29] shows that not only the ρ-exchange mechanism (with ρNN^* coupling deduced from VDM) but also re-scattering processes by pseudoscalar mesons alone, specifically by π and η, can describe the experimental data in both the pp and pn collisions. It is suggested in Ref. [29] to study spin observables to disentangle these mechanisms.

Apart from the choice of the exchanged mesons there are also essential differences in the construction of the $MN \to \eta N$ transition amplitude and in the treatment of the effects of the initial and final state interaction. Most of the models [19–21, 24, 26] are based on the calculation of tree level re-scattering diagrams and substitute instead of the full $MN \to \eta N$ T-matrix just the $N^*(1535)$ resonance, as depicted in Fig 2.1b[2]. Note, that there is no justification for these approaches but their simplicity. For instance, the experimentally measured $\pi N \to \eta N$ transition cross section contains not only the $N^*(1535)$ resonance but all other possible contributions as well (see, e.g., the realistic meson nucleon models in Refs. [6, 36, 37]). A direct consequence of this approximate approach is the fact that the relative phases between different meson exchanges are fixed by hand. This is, of course, inappropriate for obtaining quantitative predictions.

Another uncertainty is caused by the treatment of the NN FSI effects. It was shown by Watson [38] and Migdal [39] that the energy dependence of the cross section near the production threshold is predominantly determined by the interaction between the slowly moving particles in the final states. Due to a point-like region of the meson production only the scattering process in the final state should affect the energy dependence. Using these arguments, most of the authors separated the full production amplitude M into a "genuine" production part and into a piece that contains the NN FSI effects, i.e.

$$M \sim A_{prod} FSI \tag{2.2}$$

As long as one is only interested in a qualitative understanding and especially in the energy behaviour of the production cross section near threshold this simple

[2]For completeness we have to mention that some kind of background in the form of s and u-channel nucleon exchanges was taken into account in [21].

approximation is fairly reliable and therefore a good choice. However, this factorization procedure does not allow to predict the absolute magnitude of the cross section [40–43]. This peculiarity will be discussed in detail in the corresponding chapter 4. None-the-less the authors of [19–22] applied this factorization scheme in their works, whereas in [26] FSI effects were taken into account in different but also approximate manner. In Refs. [23, 27] FSI effects seem to be included consistently. This means that the full loop integration over the FSI amplitude consisting of the dynamical information about the production amplitude and the half-off-shell NN T-matrix is performed. In this case the principal value (P.V.) integral as well as 2-body unitarity cut are included.

The situation with regard to the treatment of ISI effects is even less satisfying than for the FSI. It is known for a long time that, in general, the ISI reduces the production cross section [23, 40]. On the other hand, reliable quantitative estimations for the reduction caused by the ISI, e.g. for the reaction $pp \to pp\eta$, are hard to obtain, not but least due to our poor (theoretical) knowledge of the NN interaction at those energies relevant for production of heavier mesons such as η, η' etc. In any case it is obvious that the ISI should strongly influence the absolute value of the cross section. However, in most of the model calculations this effect is simply neglected [19, 21, 22, 26] or it is taken into account in a very approximate way [24, 27, 44]. The authors of Ref. [29] utilize the approximate approach developed in [40] for the treatment of the ISI. The only more refined calculation that has been done so far is the one by Batinić et al. [23]. This work includes both FSI and ISI effects utilizing an NN model developed in [45]. However, there is a feature which looks strange in their analysis, namely the conclusion that the total distortion effect from the FSI and the ISI is not sensitive to the dynamics of the production process. We will come back to this feature in more detail in section 2.5.

Finally we would like to emphasize that many of these models yield results that are in rough agreement with the experiments for the $pp \to pp\eta$ reaction. However, most of them either do not consider other reaction channels for the η production, i.e. $pn \to pn\eta$ and $pn \to d\eta$ reactions, or are not able to describe simultaneously all experimental data. This concerns, in particular, the large cross section ratio

$\sigma_{pn\to pn\eta}/\sigma_{pp\to pp\eta}$. The appearance of new accurate experimental data for the reactions $pn \to pn\eta$ and $pn \to d\eta$ [13–15] is therefore very important because it allows to perform a combined analysis of both isospin channels for the η production and, consequently, it puts much stronger constraints on the theoretical models.

2.2 Formalism for η-production

We study η-meson production mechanism in the distorted wave Born approximation (DWBA). But let us first consider the full transition amplitude from the initial to the final state, which is given by [38, 39, 46, 47]

$$M_{2\to 3} = \left\langle \Phi_f^- \,\middle|\, A_{2\to 3} \,\middle|\, \Psi_i^+ \right\rangle = \left\langle \Psi_f^- \,\middle|\, A_{2\to 3} \,\middle|\, \Phi_i^+ \right\rangle. \tag{2.3}$$

Here $A_{2\to 3}$ is the meson production potential. Let us introduce also the full Hamiltonian H, the Hamiltonian of the NN system, H_{NN}, and the kinetic energy operator K by the relations:

$$H = K + A_{2\to 3} + V_{NN}, \quad H_{NN} = K + V_{NN} \tag{2.4}$$

They satisfy the Schrödinger equations

$$(E - H)\,|\Psi_\alpha^\pm\rangle = 0, \quad (E - H_{NN})\,|\Phi_\alpha^\pm\rangle = 0, \quad (E_\alpha - K)\,|\chi_\alpha\rangle = 0. \tag{2.5}$$

Here $|\chi_\alpha\rangle$ is the wave function of a free particle in the initial or final state ($\alpha = i, f$), $|\Phi_\alpha^\pm\rangle$ is a distorted wave function due to the NN interaction V_{NN} and $|\Psi_\alpha^\pm\rangle$ is the complete 3 particle wave function which tends asymptotically to $|\Phi_\alpha^\pm\rangle$ plus outgoing spherical waves:

$$\begin{aligned} |\Phi_\alpha^\pm\rangle &= |\chi_\alpha\rangle + (E - H_{NN} \pm i\varepsilon)^{-1} V_{NN}\,|\chi_\alpha\rangle && (2.6)\\ |\Psi_\alpha^\pm\rangle &= |\Phi_\alpha^\pm\rangle + (E - H \pm i\varepsilon)^{-1} A_{2\to 3}\,|\Phi_\alpha^\pm\rangle \\ &= |\chi_\alpha\rangle + (E - H \pm i\varepsilon)^{-1} (V_{NN} + A_{2\to 3})\,|\chi_\alpha\rangle && (2.7) \end{aligned}$$

The distorted wave Born approximation (DWBA) method consists in the replacement of the full wave function $|\Psi_\alpha^\pm\rangle$ by the distorted w.f. $|\Phi_\alpha^\pm\rangle$ in (2.3), i.e.

$$M_{2\to3} = \langle\, \Phi_f^- \mid A_{2\to3} \,|\Phi_i^+ \rangle = \tag{2.8}$$

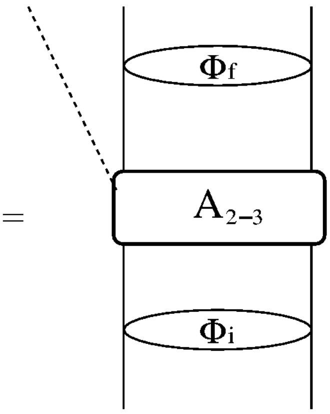

This means that the interaction $A_{2\to3}$ is assumed to be rather weak so that the first iteration of $|\Psi\rangle$ is applied. Using the relation $GV_{NN}\,|\chi\rangle = T_{NN}G_0\,|\chi\rangle$ one can express $|\Phi_\alpha^\pm\rangle$ in terms of two body NN T-matrix

$$|\Phi_\alpha^\pm\rangle = |\chi_\alpha\rangle + (E - K \pm i\varepsilon)^{-1}T_{NN}\,|\chi_\alpha\rangle = (1 + G_0T_{NN})\,|\chi_\alpha\rangle \tag{2.9}$$

Then we deduce for the reaction amplitude

$$M_{2\to3} = \langle\, \chi_f \mid (1 + T_{NN}^{FSI}G_0)A_{2\to3}(1 + G_0T_{NN}^{ISI})\,|\chi_i\rangle. \tag{2.10}$$

This expression forms the basis for our calculation. Here we have tacitly assumed that the interaction in the NN system is much stronger than the one in the ηN-system.

However, it is commonly recognized and experimentally confirmed ([9, 14, 34]) that the ηN interaction is not negligible (cf. table 2.1 to have an overview of the ηN scattering length) and presumably influences both the energy dependence and the magnitude of the cross section. Under such circumstances it would be desirable to include the ηN FSI consistently and to solve 3 body integral equation of the Faddeev type for the most difficult case when all particles are free (see c.f. [57] and references therein). However, exploring the ratios of the cross sections[3] $\sigma_{pn\to d\eta}/\sigma_{pn\to d\pi^0}$ [14, 58] and $\sigma_{pp\to pp\eta}/\sigma_{pp\to pp\pi^0}$ [9] one can conclude that the ηN interaction is important (at least for the energy dependence) only in a very narrow energy region up to 10 MeV above the η-threshold. Therefore the investigation of the η-meson production mechanism in the energy range 10 MeV $\leq Q \leq$ 50 MeV, which is the subject of our work, might be done without taking into account the

[3] For the pion production reactions the πN FSI at low energies is negligible.

Reference	Scattering length (fm)
Bennhold and Tanabe [48]	0.25+i0.16
Bhalerao and Liu [49]	0.27+i0.22
Grishina et al. [28]	$Re\, a_{\eta N} \leq 0.3$
Krehl et al. (see table 1 in Ref. [50])	0.42+i0.34
Sauermann et al. [51]	0.51+i0.21
Wilkin [52]	0.55(20)+i0.3
Abaev and Nefkens [53]	0.62+i0.3
Green and Wycech [54]	0.75+i0.27
Batinić et al. [55]	0.91(5)+i0.29(4)
Arima et al. [56]	0.98+i0.37

Table 2.1: The ηN scattering length in the literature

ηN interaction. In any case it is quite reasonable to consider the much more complicated 3-body effects only after a detailed quantitative understanding of NN ISI and FSI effects as well as of the production process has been achieved. Therefore, in this work we disregard a possible effect from the ηN FSI.

The production amplitude $A_{2\to 3}$ in our model consists of the re-scattering diagrams with π, ρ, η, σ meson exchanges and the direct η production. Diagrams calculated in our work are shown in Fig. 2.2.

One of the principal novelties of our investigation is the utilization of a realistic microscopic model in which all the elementary reaction amplitudes $MN \to \eta N$, that enter into the η production amplitude, are treated in a consistent way. Such a model has been developed recently by the Jülich group [36, 37]. It aims for describing the πN phase shifts and inelasticities from the πN threshold up to c.m. energies of about 1900 GeV, as well as of the transition cross sections for the reactions $\pi N \to \eta N$ and $\pi N \to \rho N$. This model will be discussed in detail in section 2.3. The important aspect connected with the use of this model is that the relative phases between different meson contributions are now constrained by the model.

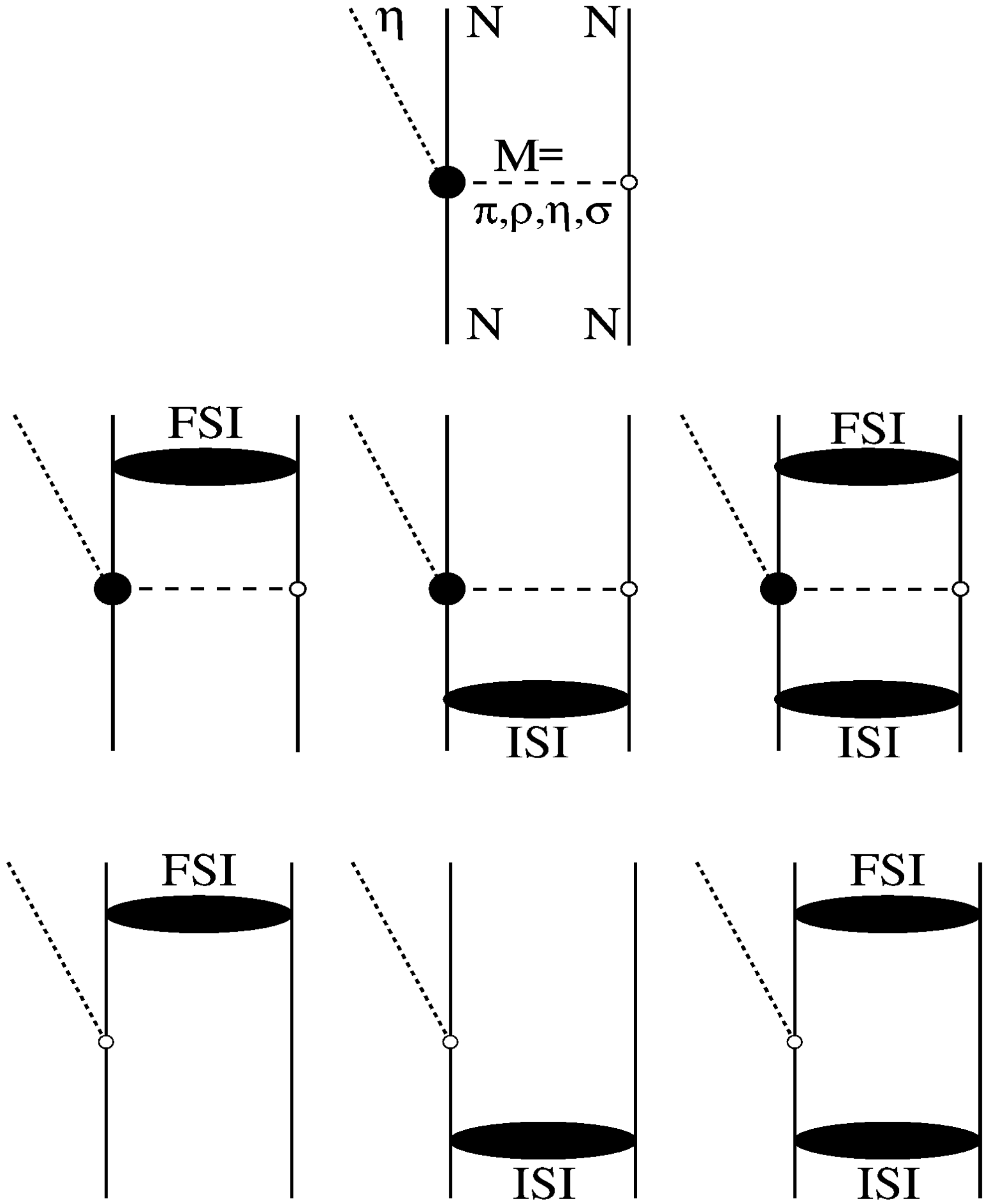

Figure 2.2: Diagrams contributing to the η production in the reaction $NN \to NN\eta$ in our model

Another merit of our model is a consistent treatment of NN FSI effects and the inclusion of ISI effects. Chapter 4 and section 2.5 will be devoted to thorough considerations of those phenomena. For the NN interaction in the final state we utilize the Bonn NN model, namely Bonn B from Ref. [59]. Uncertainties of the NN models are investigated by utilizing the CCF version of the Bonn model [60]. In the initial state the energy is so high that the standard Bonn potential is not applicable. However, the extended model CCF can be used. It contains the elastic NN potential as well as $NN \to N\Delta$ and $NN \to \Delta\Delta$ transitions which are introduced as a source of NN inelasticities (see Fig. 2.13 and 2.14).

The calculation of the MNN vertices with $M = \pi, \rho, \eta, \sigma$ has been carried out on the basis of the following effective Lagrangians:

$$\begin{aligned}
\mathcal{L}_{\pi NN} &= \frac{f_{\pi NN}}{m_\pi}\bar{\Psi}_N\gamma^5\gamma^\mu\vec{\tau}\Psi_N\partial_\mu\vec{\pi} \\
\mathcal{L}_{\eta NN} &= \frac{f_{\eta NN}}{m_\eta}\bar{\Psi}_N\gamma^5\gamma^\mu\Psi_N\partial_\mu\eta \\
\mathcal{L}_{\rho NN} &= g_{\rho NN}\bar{\Psi}_N(\gamma^\mu - \frac{\kappa_\rho}{2m_N}\sigma^{\mu\nu}\partial_\nu)\vec{\tau}\vec{\rho}_\mu\Psi_N \\
\mathcal{L}_{\sigma NN} &= g_{\sigma NN}\bar{\Psi}_N\Psi_N\sigma
\end{aligned} \tag{2.11}$$

where $\Psi_N, \vec{\pi}, \vec{\rho}, \eta$ and σ represent the nucleon and mesons fields respectively. The definition of these field operators are given in Appendix 7.2. Note, that the same Lagrangians have been utilized for the construction of the MN model.

The MNN vertex functions include also form factors which parameterize the extended character of the interactions. We utilize form factors of the monopole type, i.e.

$$F(\vec{q}_M) = \frac{\Lambda^2_{MNN} - m^2_M}{\Lambda^2_{MNN} + \vec{q}^{\,2}_M}. \tag{2.12}$$

Here Λ_{MNN} is the cut off parameter and $\vec{q}_M$ and m_M are the 3-momentum and mass of the exchanged meson, respectively.

Most of the coupling constants and cut off parameters are taken from the full Bonn model. The only exception is the ηNN parameters because the ηNN vertex is simply not present in the full version of the Bonn potential. The value of the ηNN coupling constant varies in the literature over a rather wide range, namely from $g^2_{\eta NN}/4\pi = 0.3 \simeq 0.4$ – from theoretical fits to the η photoproduction on the nucleon [61] and from the calculation of the $a_0\pi N$ triangle diagram [62] – up to $g^2_{\eta NN}/4\pi = 3 \simeq 7$ in different one-boson-exchange (OBE) versions of the Bonn NN model. A value of about 1.8 follows from SU(6) (flavour $\otimes$ spin) symmetry. For consistency reasons in our calculation we utilize $g^2_{\eta NN}/4\pi \approx 1.8$ which is the value adopted in the model [36, 37] from which the $MN \to \eta N$ amplitudes are taken. A discussion on the influence of this coupling constant on the results and a list of all parameters used in the calculation can be found in chapter 3.

Finally we would like to mention that, except for some objective ambiguities related with the phenomenological nature of the form factors and uncertainties of the ηNN coupling constant, the calculation performed in this work does not contain any free parameters.

In this investigation we are interested in the η production in NN collisions not far from threshold, in particular, for excess energies

$$Q = \sqrt{s} - 2m_N - m_\eta \leq 50MeV \tag{2.13}$$

	$pp \to pp\eta$	$pn \to pn\eta$	$pn \to d\eta$
T=1	$^3P_0 \to {}^1S_0 s$	$^3P_0 \to {}^1S_0 s$	—
T=0	—	$^1P_1 \to {}^3S_1 s$	$^1P_1 \to {}^3S_1 s$

Table 2.2: Partial waves amplitudes contributing in the near threshold region

It will be assumed that in this energy regime the relevant angular momentum L_{NN} of the final NN pair as well as the momentum l_η of the produced η are zero. The list of near threshold partial waves allowed by the Pauli principle and by parity conservation is given in table 2.2 for the different isospin channels of the reaction $NN \to NN\eta$. It is worth noting that the configuration with $L_{NN} = 0$ and $l_\eta = 1$ is forbidden for isotriplet channel, whereas states with $L_{NN} = 1$ are expected to be much less important than the extremely strong S wave NN interaction. This is actually the case for the pion production in NN collisions [63].

2.3 Model of meson-nucleon (MN) interaction.

In this section we describe the structure and results of the MN-model – which is one of most important ingredients of our calculation. This model was developed in Jülich by C.Schütz [6] and then extended by O.Krehl [36,37]. The main goal of the model is a simultaneous description of the πN phase shifts and inelasticities as well as transition cross sections for the reactions $\pi N \to \eta N$ and $\pi N \to \rho N$. The reaction amplitudes are obtained from solving the coupled-channel relativistic scattering equation of Lippman-Schwinger type

$$T_{\mu\nu}(\vec{k}, \lambda_1, \lambda_2; \vec{k}', \lambda_3, \lambda_4) = V_{\mu\nu}(\vec{k}, \lambda_1, \lambda_2; \vec{k}', \lambda_3, \lambda_4)$$
$$+ \sum_{\gamma} \sum_{\lambda_1' \lambda_2'} \int d\vec{q} V_{\mu\gamma}(\vec{k}, \lambda_1, \lambda_2; \vec{q}, \lambda_1', \lambda_2') \frac{1}{Z - W_\gamma(q) + i0} T_{\gamma\nu}(\vec{q}, \lambda_1', \lambda_2'; \vec{k}', \lambda_3, \lambda_4) \quad (2.14)$$

where $\lambda_i, \lambda_{i+2}, \lambda_i'$ are the helicities of the baryon and meson in the initial, final and intermediate states, $k(k')$ are the center of mass (cm) momenta of the initial and final baryons and μ, ν, γ are indices that label different reaction channels. The energy of the intermediate state $W_\gamma(q)$ is $W_\gamma(q) = \sqrt{q^2 + M_\gamma^2} + \sqrt{q^2 + m_\gamma^2}$ where m_γ and M_γ are the meson and baryons masses, respectively, in the channel γ.

This model contains 6 channels namely $\pi N, \eta N, \rho N, \sigma N, \pi\Delta$ and $\pi N^*(1520)$. All the MN interactions and transition potentials $V_{\mu\nu}$ are constructed in time-ordered perturbation theory (TOPT) on the basis of effective Lagrangians. Most of the coupling constants at the meson-baryon-baryon and meson-meson-meson vertices are taken from other sources. The cutoff masses at the vertex form factors are the only free parameters which were determined by a fit to the πN partial-wave amplitudes. The potentials consist of t-channel meson exchanges, s-channel resonance graphs and u-channel baryon exchanges as shown in Fig. 2.3.

The three body $\pi\pi N$ system which is an important decay channel for some resonances (e.g., $S_{11}(1535), S_{11}(1650), D_{13}(1520)$) is not present in the model explicitly. The inclusion of such three body channels is indeed a very difficult numerical problem. However, this $\pi\pi N$ channel is effectively parameterized in the model by two body channels, specifically by $\pi\Delta, \rho N, \sigma N$ which have large branching ratios into $\pi\pi N$. In order to include the width of intermediate particles like ρ, σ, Δ... the effective propagator of the meson-baryon is modified by including corresponding self energy terms Σ

$$\frac{1}{Z - W(q)} \to \frac{1}{Z - \tilde{W}(q) - \Sigma(Z)}. \tag{2.15}$$

Here $\tilde{W}(q) = \sqrt{q^2 + M_N^2} + \sqrt{q^2 + m_0^2}$ (e.g., for the ρN or σN channels) and m_0 is the bare mass of the intermediate meson, treated as a free parameter. The amplitude corresponding to the series of diagram

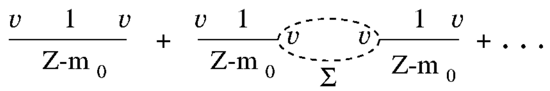

is equal to

$$T = \frac{|v|^2}{Z - m_0 - \Sigma(Z)}; \quad \Sigma = \int d\vec{q} \frac{|v(q)|^2}{Z_{sub} - 2\epsilon_i}, \tag{2.16}$$

where ϵ_i is the energy of the intermediate particles in their cm system and Z_{sub} is the energy of the decaying particle in the same system.

The value of the bare mass m_0 as well as parameters of the vertex function v for σ and ρ mesons are determined by fitting to the $\pi\pi$ phase shifts in the corresponding I=0, J=0 and I=1, J=1 partial waves. A similar procedure has been used to include the self energy term of the $\Delta \to \pi N \to \Delta$ process. These self energy contributions are very important for the correct description of the πN experimental data. The results of this model for the πN phase shifts and inelasticities are presented in the Fig. 2.4 by the solid lines. Evidently, except for the S_{31} and D_{33} partial waves where corresponding resonances $S_{31}\Delta(1620)$ and $D_{33}\Delta(1700)$ are not included in the model[4], the model provides a satisfactory description of all πN partial amplitudes with $J \leq 3/2$. Therefore it is an excellent starting point for our calculation.

[4]In the up-to-date version of this model performed recently by Gasparyan [64] these partial waves are also described quite well.

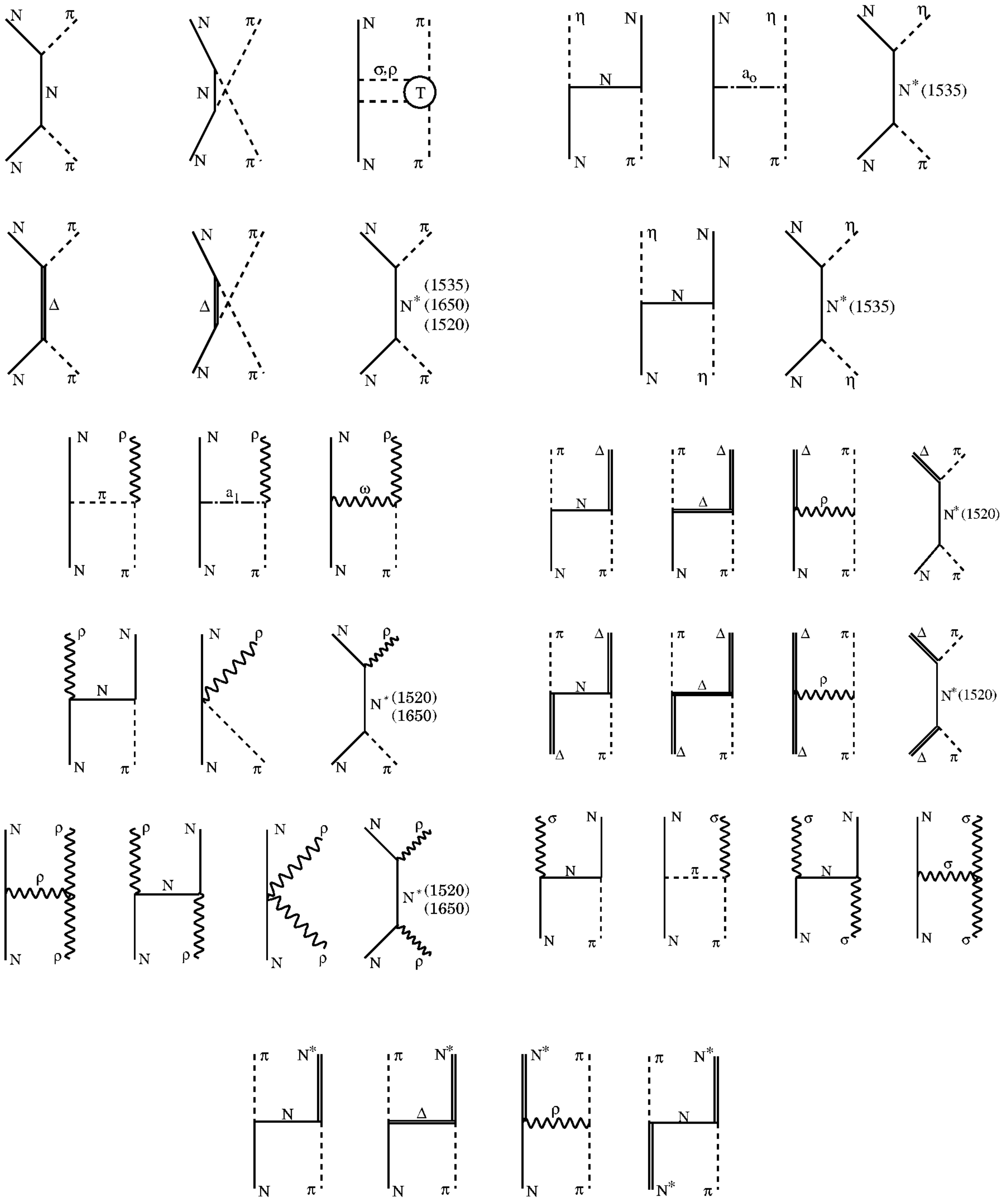

Figure 2.3: Diagrams included in the model

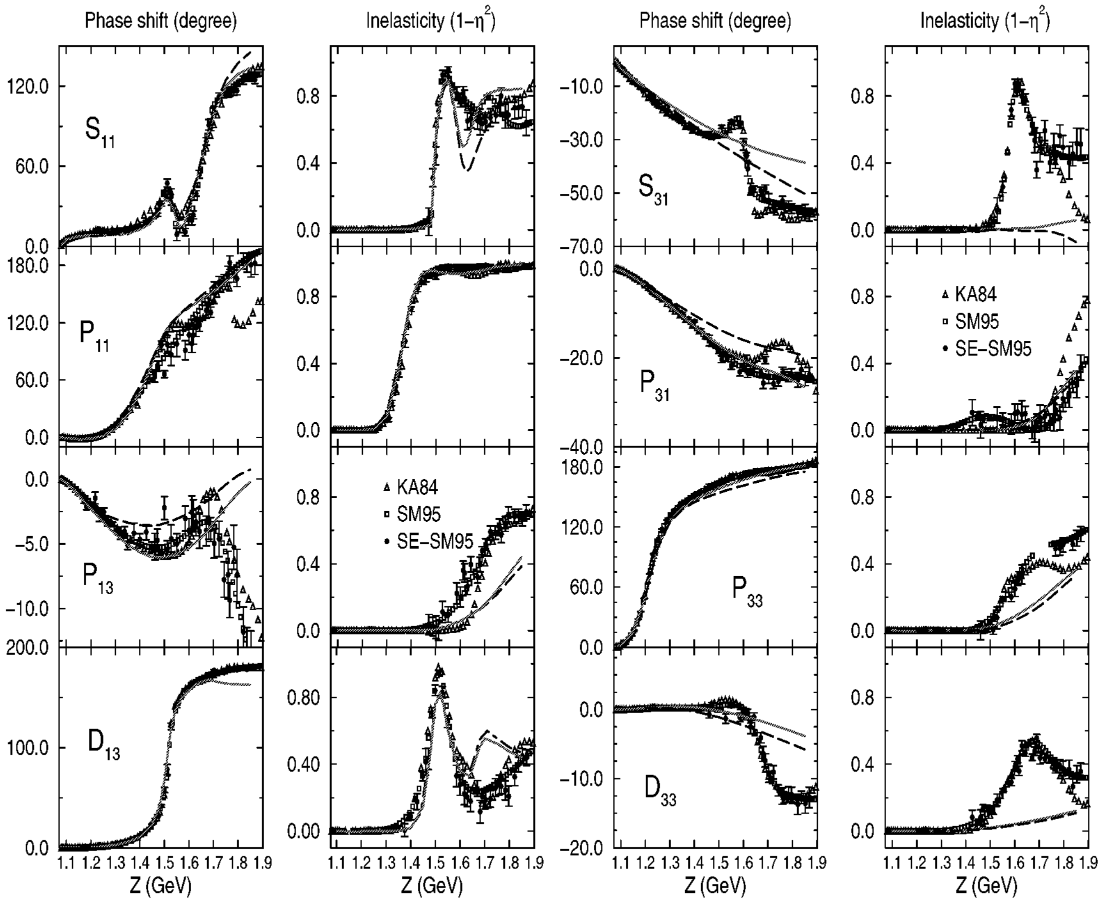

Figure 2.4: πN phase shifts and inelasticities calculated for different partial waves. The solid lines correspond to the full calculation, whereas the dashed ones were obtained using approximate form of propagators in the MN potentials (see text). The experimental data are taken from the phase shifts analyses KA84 [65, 66], SM95 [67] and SE-SM95 [67]

Specifically in the S_{11} partial wave, which is the most relevant one for the reaction $NN \to NN\eta$ close to threshold the agreement with the experimental data in a region of about 70 MeV above the η threshold (ηN threshold $\approx 1486MeV$) is very good as it is demonstrated in Fig. 2.5.

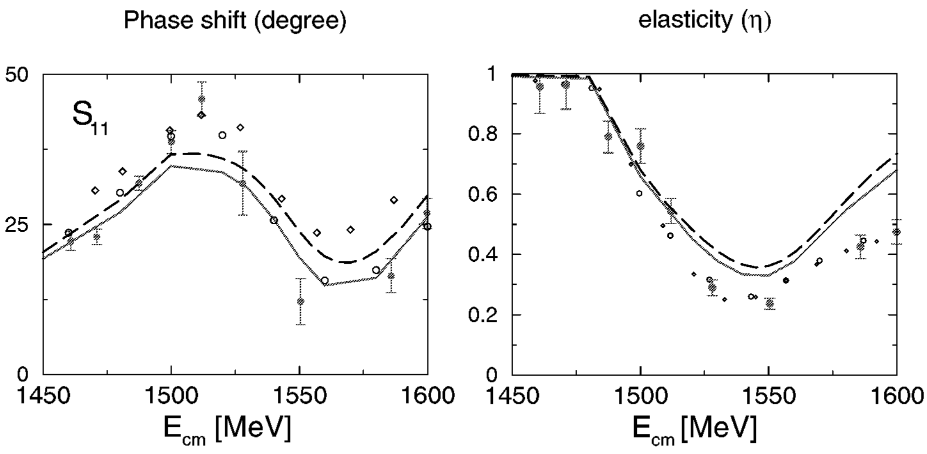

Figure 2.5: The πN phase shift and inelasticity in the S_{11} partial wave. The full and dashed lines are defined in caption to Fig. 2.4.

We should mention though that the $\pi N \to \eta N$ total and differential cross sections are slightly overestimated by the model (cf. Fig. 2.6). However, within the uncertainties of the experimental data the description is quite reasonable.

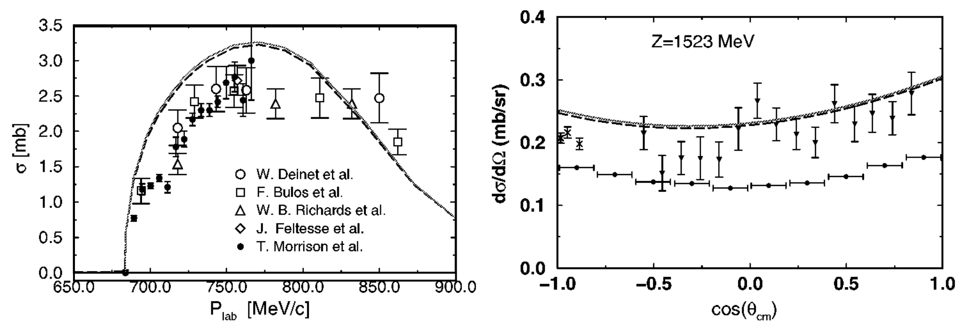

Figure 2.6: Total and differential cross sections for the reaction $\pi^- p \to \eta n$. The experimental data are taken from [30, 68–74]

We want to remind the reader, that in our calculation of the $NN \to NN\eta$ reaction the off shell $MN \to \eta N$ amplitudes are required. The calculation of the full off-shell T-matrices for the model developed by O.Krehl becomes difficult technically since the $MN \to MN$ potentials contain 3-body singularities. Thus, in our calculation some approximations in the propagator in the $MN \to MN$ potentials are applied in order to avoid these difficulties. We would like to concentrate on this in more detail.

Even in the case when we are interested in the on-shell T-matrix $T(\vec{k},\vec{k}')$ (where $\vec{k},\vec{k}'$ are on-shell momenta) the potential $V(\vec{q},\vec{p})$ in the Lippman-Schwinger equation

$$
\begin{aligned}
T(\vec{k},\vec{k}') &= V(\vec{k},\vec{k}') + \int V(\vec{k},\vec{q})G(q)T(\vec{q},\vec{k}')d\vec{q}, \\
T(\vec{q},\vec{k}') &= V(\vec{q},\vec{k}') + \int V(\vec{q},\vec{p})G(p)T(\vec{p},\vec{k}')d\vec{p}, \qquad (2.17)
\end{aligned}
$$

has singularity on the real axis. In order to demonstrate this we consider the propagator for a typical t-channel exchange potential.

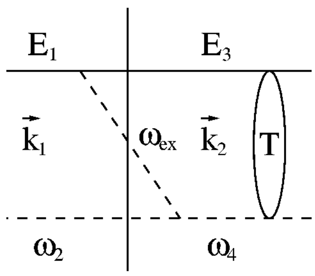

It is given by $\frac{1}{(Z-E_3-\omega_2-\omega_{ex})}\frac{1}{\omega_{ex}}$, where Z is the total energy. If $\vec{k}_1$ is on-shell then $Z = E_1 + \omega_2$ (this is the case of the potential $V(\vec{k},\vec{q})$ in the first equation in (2.17)). A singularity will appear for $E_1 - E_3 - \omega_{ex} = 0$ only under condition $m_1 > m_3 + m_{ex}$.

However, for the off-shell potential, i.e. when $\vec{k}_1, \vec{k}_2$ are off-shell (cf. potential $V(\vec{q},\vec{p})$ in eq. (2.17)), the propagator $Z - \sqrt{k_1^2 + m_2^2} - \sqrt{k_2^2 + m_3^2} - \sqrt{(\vec{k}_1 - \vec{k}_2)^2 + m_{ex}^2}$ will always have singularities (if $Z \geq m_2 + m_3 + m_{ex}$) on the real axis k_2 at some values of k_1 and angle between $\vec{k}_1$ and $\vec{k}_2$. To avoid those singularities the contour of the integration in [37] is shifted into the complex plane so that the equations (2.17) take the form:

$$
\begin{aligned}
T(\vec{k},\vec{k}') &= V(\vec{k},\vec{k}') + \int d\vec{q}e^{i\phi}V(\vec{k},\vec{q}e^{i\phi})G(\vec{q}e^{i\phi})T(\vec{q}e^{i\phi},\vec{k}') \\
T(\vec{q}e^{i\phi},\vec{k}') &= V(\vec{q}e^{i\phi},\vec{k}') + \int d\vec{p}e^{i\phi}V(\vec{q}e^{i\phi},\vec{p}e^{i\phi})G(\vec{p}e^{i\phi})T(\vec{p}e^{i\phi},\vec{k}') \qquad (2.18)
\end{aligned}
$$

The solution of the Lippman-Schwinger equation in the complex plane (second equation) is possible now since $V(qe^{i\phi}, pe^{i\phi})$ does not have singularities anymore. However we need the T-matrix on the real axis. In order to find the on-shell T-matrix an additional integration (not integral equation) has to be performed (cf. the first equation in (2.18)) along some complex contour C. When k is on-shell the poles of $V(k,q)$ are located in the complex plane as it is illustrated in Fig. 2.7 by the dashed line[5]. Therefore for some values of $\phi \in (0, \phi_{max})$ (ϕ_{max} is the maximal

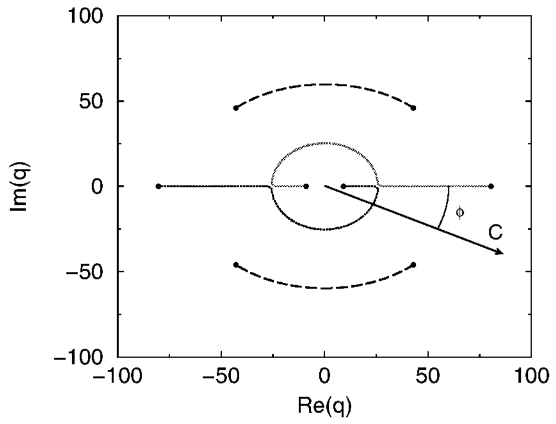

Figure 2.7: Location of singularities in the complex plane. The dashed line corresponds to the case where the rotation of the integration contour back to the real axis is possible.

angle for which the contour does not cross the trajectory of the singularities in the complex plane) the calculation can be done. The situation is different in the case when the full off-shell T-matrix is needed. Here the singularities of the off-shell potential $V(k,q)$ can be located in any place in the complex plane at some values of the off-shell momentum k, as it is shown in Fig. 2.7 by the dotted lines. Thus, a selection of the integration contour like in Fig. 2.7 is not applicable because it would always cross the trajectory of the singularities. Of course, the path of integration may be chosen in different way, e.g. like in Fig. 2.8 (see for details, e.g., Ref. [57]). However, this integration is actually rather complicated and constitutes a time consuming computational problem. Thus, in our case we want to avoid these difficulties and we remove the three body singularities by applying an approximate procedure. We are interested in the energy region near

[5] we discuss the $\pi N \to \pi N, \eta N$ on-shell T-matrices, i.e. when the condition that the mass of the initial particle is always smaller than the ones of its decay products is satisfied. For example for the $\pi\Delta \to MN$ (or $\rho N \to MN$) T-matrices the additional integration along the contour C can not be done since the potential $V(k, qe^{i\phi})$ has singularities (cf. dotted line in Fig. 2.7) which are crossed by this contour. These singularities appear because, e.g., Δ can decay into on-shell πN system ($m_\Delta > m_N + m_\pi$) so that in the u-channel nucleon exchange potential $\pi\Delta \to \pi\pi N \to \pi\Delta$ (or $\pi\Delta \to \pi\pi N \to \pi N$) the $\pi\pi N$ intermediate state may be on-shell.

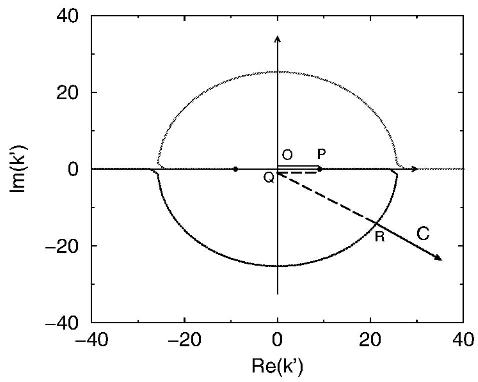

Figure 2.8: Some kind of contour deformation for the off-shell T-matrices. The dashed line corresponds to the integration contour on the second sheet.

the ηN threshold, i.e. in a region of $Z = m_\eta + M_N + Q$ where the excess energy Q is not more than 50 MeV. Therefore the singularities which can only occur below these energies are $2m_\pi + M_N$ and $2m_\pi + M_\Delta$. These singularities correspond to the $\pi\pi N$ and $\pi\pi\Delta$ intermediate states in the t-channel pion exchange diagrams for the $\pi N \to \rho N$ and $\pi N \to \sigma N$ potentials and in the u-channel N (or Δ) exchange diagrams for the $\pi N \to \pi\Delta$ and $\pi\Delta \to \pi\Delta$ potentials (cf. Fig. 2.3). The singularity for the $\pi\pi\Delta$ intermediate state appears at $Q \approx 20$ MeV above η threshold so that its impact should be small in this region. To avoid all these singularities in the calculation of the full off-shell MN T-matrices we replace Z in the propagator of the corresponding diagrams by $2m_\pi + M_B$ with $M_B = M_N, M_\Delta$, i.e.

$$\begin{aligned} Z &- \sqrt{m_\pi^2 + k^2} - \sqrt{m_\pi^2 + k'^2} - \sqrt{M_B^2 + (\vec{k} - \vec{k}')^2} \longrightarrow \\ 2m_\pi + M_B &- \sqrt{m_\pi^2 + k^2} - \sqrt{m_\pi^2 + k'^2} - \sqrt{M_B^2 + (\vec{k} - \vec{k}')^2}. \end{aligned} \tag{2.19}$$

The results for the πN phase shifts and inelasticities calculated using this approximation are given in Fig 2.4 by dashed lines. One can see that even for energies significantly above the ηN threshold this approximation works quite well.

At the end of this section we would like to draw attention to the fact that the model does not contain any direct $\rho N \to \eta N$ transition potentials which, in principle, should be present. In particular, there is no bare coupling of the ρN channel

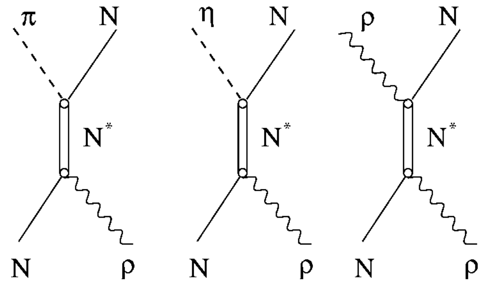

Figure 2.9: Additional diagrams containing the ρNN^* coupling which are included to the model.

to the $S_{11}N^*(1535)$ resonance. Of course the dressed ρNN^* coupling constant is present somehow due to coupled channel effects, e.g., by the process

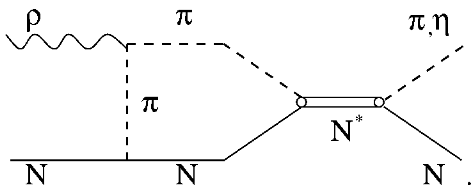

However, the tree level diagrams as shown in Fig 2.9 should be included as well. In order to investigate the relevance of these interactions for the $MN \to \eta N$ transition amplitudes we have created a variant of the MN model where these diagrams are included. We introduced some small negative bare coupling constant $g_{\rho NN^*}$[6]. The bare coupling constants $g_{\pi NN^*}$ and $g_{\eta NN^*}$ have been varied slightly to get better agreement for the πN inelasticity (while staying as close as possible to the experimental phase shift) compared to the results of the original model for the S_{11} partial wave (see Fig 2.10) in the region of about 60 MeV above ηN threshold.

[6]the sign of this resonance constant is not fixed. It turned out that choosing it to be negative allows to achieve better agreement for the η production in $NN \to NN\eta$ reactions.

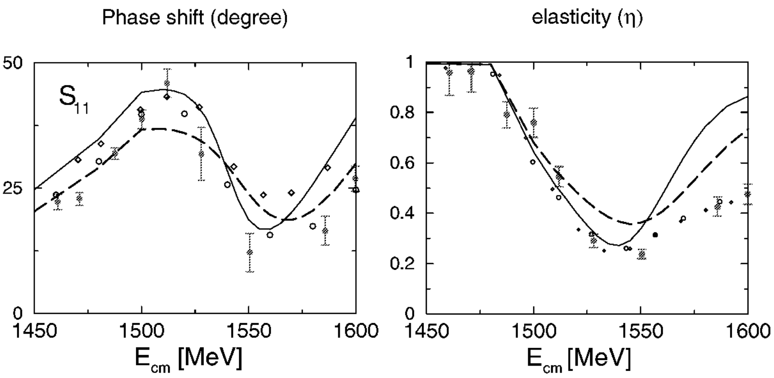

Figure 2.10: The πN phase shift and elasticity η for the S_{11} partial wave. The solid lines correspond to the results calculated with diagrams of Fig. 2.9 taken into account, whereas the dashed curves represent the results of the original model [36,37].

All other πN partial waves remain unchanged since the parameters of t- and u-channel exchange potentials were not varied. In chapter 3 we will present results for the η production with the original MN model and then we will discuss the influence of these additional graphs.

2.4 Models of nucleon-nucleon (NN) interaction

In this section we will discuss shortly the main features of the NN models which are utilized for treating the NN FSI and ISI. The effects of the FSI as well as the ISI will be investigated in detail in section 2.5 and chapter 4, respectively, so that the goal of this section is mainly to show that the NN models are realistic and hence good pre-requisites for our calculation.

There is a great number of NN models constructed on the basis of meson exchange theory which describe the low energy NN phase shifts quite well [35,59,75]. Let us discuss in more detail the full Bonn NN model presented in paper [35]. This model is derived in the framework of relativistic, time-ordered perturbation theory. The diagrams included in the model are presented in Fig. 2.11. They contain the well-known single meson exchange processes with $\pi, \rho, \sigma, \omega, \delta$ exchanges. We should mention that the σ meson is not considered as a genuine meson but stands for contributions from the correlated $\pi\pi$ interaction in the S wave. Uncorrelated $\pi\pi$ and even uncorrelated $\pi + boson$ exchanges (so-called crossed and stretched box diagrams) are included as well involving $NN, N\Delta$ and $\Delta\Delta$ intermediate states.

The model was built starting out from effective Lagrangians which in its interaction part consist of NN-meson and $N\Delta$-meson vertices. Taking into account effectively the extended quark structure of the hadrons these vertices were supplemented by form factors parameterized in the form:

$$F_\alpha(\vec{k}^2) = \left(\frac{\Lambda_\alpha^2 - m_\alpha^2}{\Lambda_\alpha^2 + \vec{k}^2}\right)^n, \quad n = 1, 2 \tag{2.20}$$

where $\vec{k}$ is the three momentum transfer and Λ_α is the cut off mass [7].

The on-shell NN amplitude $T_{NN}(Z)$ is determined by solving an integral equation of the Lippmann-Schwinger type:

$$T(Z) = V_{NN}(Z) + V_{NN}(Z)\frac{1}{Z - h_{NN}^{(0)} + i0}T(Z) \tag{2.21}$$

where Z is the initial energy and $h_{NN}^{(0)}$ is the free Hamiltonian for nucleons only.

The results of the Bonn model are in excellent agreement with the NN phase shifts and observables. For instance we would like to show the NN phase shifts in $^1S_0$ and $^3S_1$ partial waves (cf. Fig. 2.12). The off-shell NN T-matrices generated by the Bonn model for these partial waves will be used for the FSI in the reaction $NN \to NN\eta$.

[7] In the calculation of $NN \to NN\eta$ reaction we use the same type of effective Lagrangians and form factors as in the Bonn model. Moreover almost all coupling constants and cut off masses (except for ηNN) are taken from the full Bonn model [35] (see also the discussion in section 2.2 and in chapter 3)

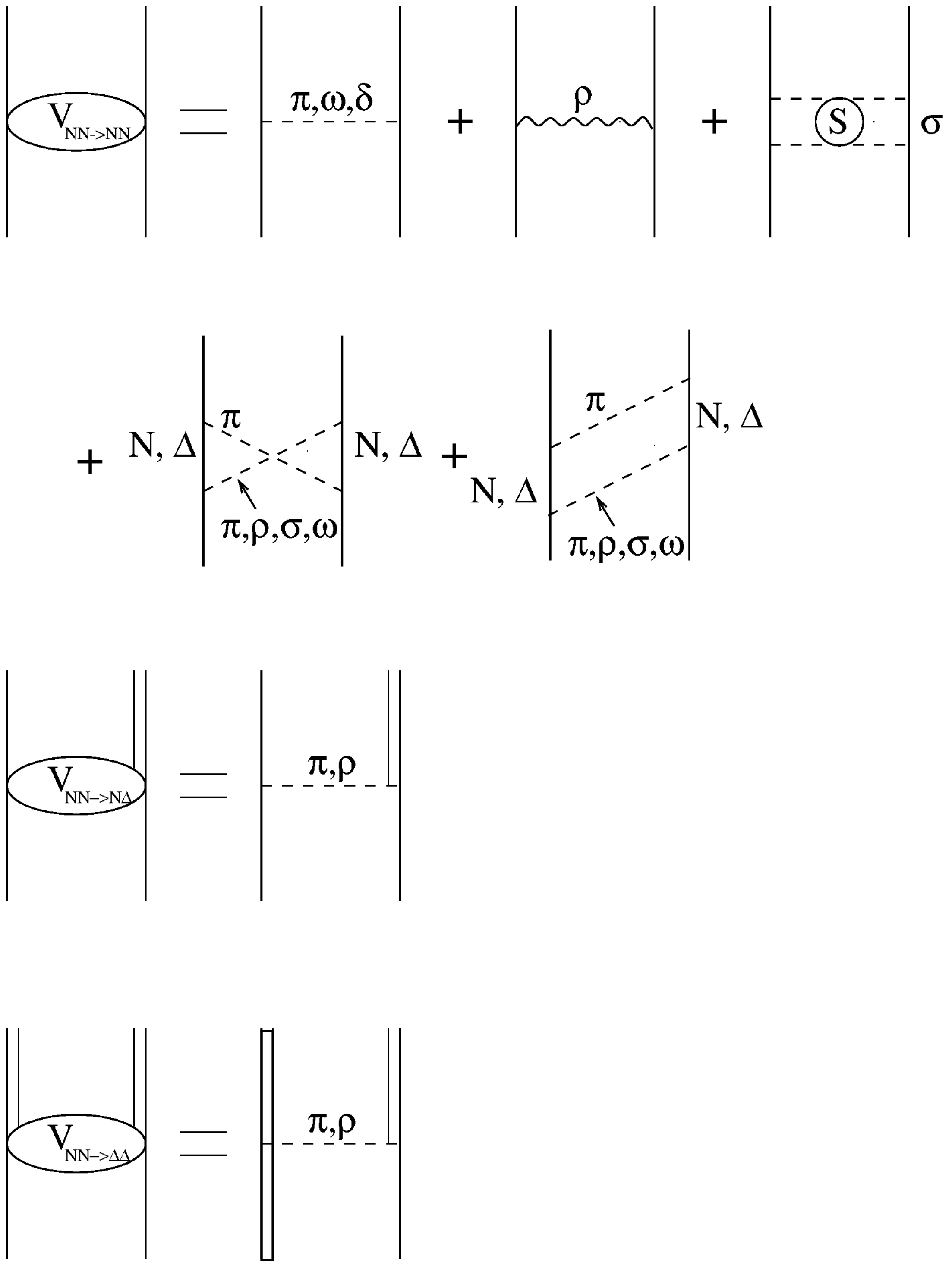

Figure 2.11: Diagrams corresponding to $NN \to NN, NN \to N\Delta$ and $NN \to \Delta\Delta$ potentials.

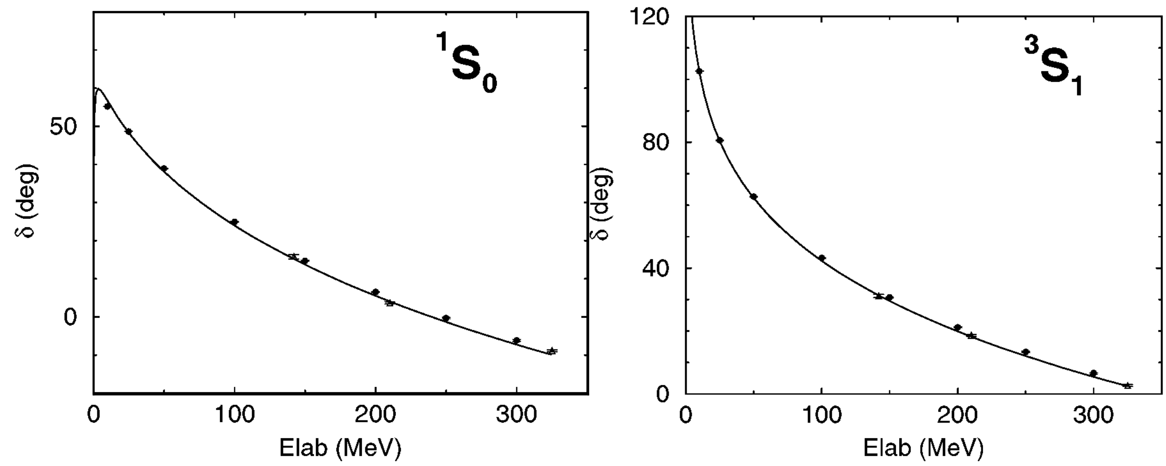

Figure 2.12: Phase shifts for the $^1S_0$ and $^3S_1$ partial waves calculated for the Bonn potential.

The region of applicability of the standard Bonn model [35] is limited by the π production threshold. Above the π threshold NN scattering becomes inelastic since the additional πNN intermediate state will contribute to two body NN T-matrix. The unitarity now requires

$$i(T_{22} - T_{22}^{+}) = T_{22}T_{22}^{+} + T_{23}T_{23}^{+} \tag{2.22}$$

where T_{22} is the elastic NN amplitude whereas T_{23} corresponds to the π production. Thus, the situation becomes very similar to that discussed in section 2.3 above πN threshold, where due to three body singularities on the real axis the integration in the Lippmann-Schwinger equation becomes technically much more difficult. Since the initial energy in the $NN \to NN\eta$ reaction is much higher than the one and even two pion production threshold some alternative NN model is required for the treatment of ISI effects.

Such an extended model was developed in [60] on the basis of the folded diagram formalism [76]. The dynamics included in this model is exactly the same as in the full Bonn model. Specifically the couplings to inelastic $N\Delta$ and $\Delta\Delta$ channels have been taken into account. The three body singularities in this model are removed due to an employement of the folded diagram formalism [60]. Like in the MN model, where the $\pi\pi N$ channel was taken into account effectively by $\rho N, \sigma N$ and $\pi\Delta$ channels, the πNN and $\pi\pi NN$ states are parametrized effectively by the two body $N\Delta$ and $\Delta\Delta$ channels. The width of the Δ-isobar is included by using a simple parameterization [77].

In such a model one has to solve a system of coupled channel equations

$$\begin{aligned}
T_{NN\to NN} &= V_{NN\to NN} + \sum_{\alpha=NN,N\Delta,\Delta\Delta} V_{NN\to\alpha} G_\alpha T_{\alpha\to NN} \\
T_{N\Delta\to NN} &= V_{N\Delta\to NN} + \sum_{\alpha=NN,N\Delta,\Delta\Delta} V_{N\Delta\to\alpha} G_\alpha T_{\alpha\to NN} \\
T_{N\Delta\to N\Delta} &= V_{N\Delta\to N\Delta} + \sum_{\alpha=NN,N\Delta,\Delta\Delta} V_{N\Delta\to\alpha} G_\alpha T_{\alpha\to N\Delta} \\
T_{\Delta\Delta\to\Delta\Delta} &= V_{\Delta\Delta\to\Delta\Delta} + \sum_{\alpha=NN,N\Delta,\Delta\Delta} V_{\Delta\Delta\to\alpha} G_\alpha T_{\alpha\to\Delta\Delta},
\end{aligned} \tag{2.23}$$

where the potentials $V_{N\Delta\to N\Delta}$ and $V_{\Delta\Delta\to\Delta\Delta}$ were assumed to be zero. These potentials may contribute only at the next to leading order of the NN T-matrix and hence their influence on the NN scattering is suggested to be of minor importance as compared to the $NN \to NN$ and $NN \to N\Delta$ transitions.

In Figures 2.13 and 2.14 we present the results of this model [60] for the NN phase shifts and inelasticities in the $^3P_0$ and $^1P_1$ partial waves which are subject of our interest in respect to the ISI. The agreement with experimental data is quite good so that this model may be considered as a good starting point for our calculation. In section 2.15 we will discuss the procedure of the calculation of the ISI loop and uncertainties associated with it.

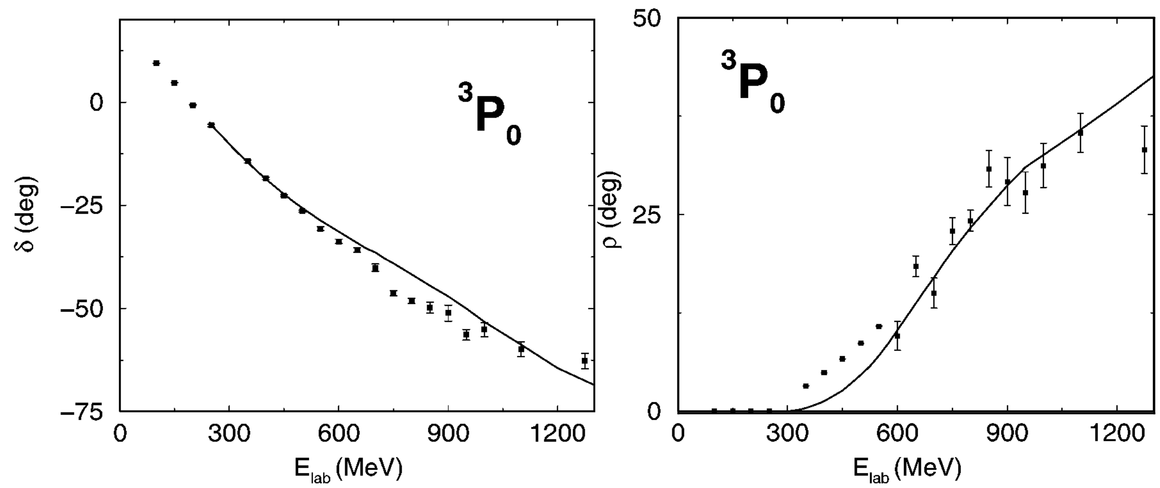

Figure 2.13: Phase shift δ and inelasticity $\eta = cos^2\rho$ calculated for the $^3P_0$ partial wave using the CCF model from Ref. [60]. The cquares represent experimental phase shifts, extracted from the SAID library and recalculated to satisfy the condition for the S-matrix: $S = \eta e^{2i\delta}$ (see also the discussion in section 2.5 about the definition of the S-matrix).

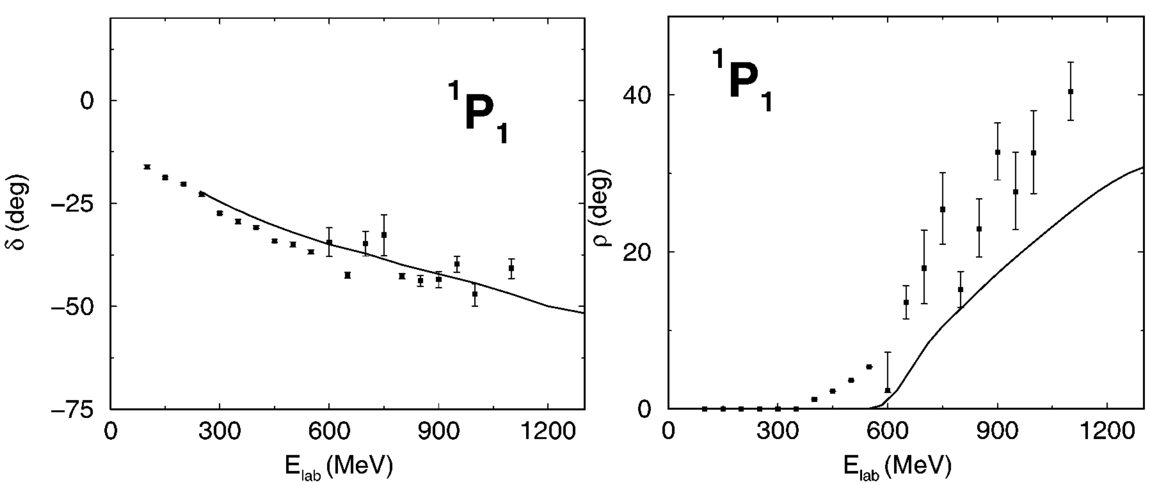

Figure 2.14: Phase shift δ and inelasticity $\eta = cos^2\rho$ calculated for the $^1P_1$ partial wave using the CCF model [60]. Same description of squares as in Fig. 2.13.

2.5 Initial state interaction (ISI) effects in the η production reactions.

In this section we would like to concentrate on effects of the nucleon-nucleon interaction in the initial state. The specific features of the ISI are:

- It takes place at rather high energy – at least compared to the FSI and to the energy region where standard NN potential models are valid. The laborotary energy corresponding to the η-threshold is $T_{lab} = 1250$ MeV.
- The ISI does not influence the energy dependence of η production near threshold since the initial protons are too fast and therefore feel only slightly the variation of the energy close to threshold[8].
- The NN scattering in the energy region in question is already strongly inelastic due to the fact that multiple pion production thresholds are open. In reference [40] it is shown that in such a case the ISI leads to the reduction of the cross section.

The relevant initial energy is so high that the well known realistic NN models such as the Bonn and the Paris potentials [35, 75] can not be applied anymore. This is connected with two different reasons: in case of the Paris or Bonn A,B,C etc. potentials no inelastic channels were included and therefore they are not valid for energies above π production threshold. In the full Bonn model such inelastic channels are, in principle, build in via couplings to the $N\Delta$ and $\Delta\Delta$ channels. However, since meson retardation effects are retained as well three body singularities occur for energies above π production threshold and therefore the calculation is technically much more difficult [78, 79]. In the following we will use some alternative NN model [60] which contains the same dynamic as the full Bonn model, specifically the coupling to $N\Delta$ and $\Delta\Delta$ channels, but where meson retardation effects are replaced by so-called folded diagrams and where the three body singularities are absent. Some details of this model are discussed in section 2.4.

[8] we are interested in the η production near the threshold, i.e. at excess energy $Q \leq 50$ MeV.

In this investigation we use two different methods of the calculation of ISI effects – an approximate approach introduced in [40] and the treatment which we will call full calculation. The difference between them is that in the former only the unitarity cut (U.C.) is calculated whereas in the latter the full loop integration is performed, i.e. the P.V. integral is taken into account as well. It will be shown in chapter 4 (cf. also [40,42]) that the P.V. integral in the FSI loop plays the leading role in the calculation. Arguing that in the initial state the colliding nucleons are very fast it is assumed in Ref. [40] that the contribution of P.V. integral is suppressed as compared to the on-shell "unitarity cut" term. Then the ISI loop integral takes the form (c.f. Appendix 7.5):

$$M^{ISI}_{1\,loop} = \int d\vec{p}\,'' \, \frac{M^{Born}(\vec{p}\,'';\vec{p})T^{ISI}_{NN}(\vec{p}_i,\vec{p}\,'')}{\sqrt{s}-2\sqrt{m^2+p''^2}+i0} \approx -i\pi\frac{p_i E(p_i)}{2}T_{NN}(\vec{p}_i)M^{Born}(\vec{p}_i;\vec{p}) \quad (2.24)$$

The ISI effect in this approach reduces to a factor, as defined in Figure 2.15. The

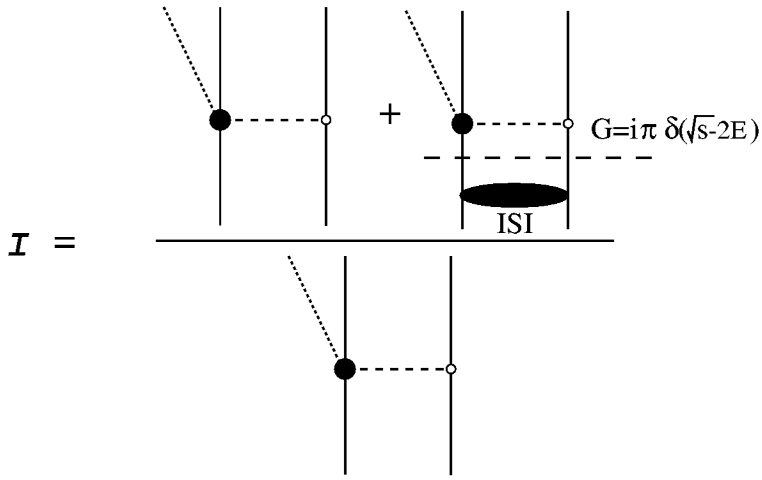

Figure 2.15: The definition of the ISI factor in the approximate approach.

main advantage of this treatment is that the effect of the ISI can be expressed only via on-shell NN data – phase shifts δ and inelasticity η which can be taken, e.g., from the SAID library [80]. This implies that the effect of the ISI reduces to a factor which is model independent at least as far as the NN on-shell data are uniquely determined:

$$|I|^2 = \big|1 - i\frac{\pi E(p_i)}{2} p_i T_{NN}\big|^2 = \frac{1}{4}\big|1 + \eta cos(2\delta) + i\eta sin(2\delta)\big|^2 \tag{2.25}$$

We should mention that the T-matrix in our calculation is defined by $T = -\frac{2}{\pi E}\frac{\eta e^{2i\delta} - 1}{2ip}$ and the S-matrix has the standard form, i.e. $S = \eta e^{2i\delta}$. One should be carefull in utilizing the NN phase shifts and inelasticities from SAID library since they are defined in a different way, namely by

$$S = \frac{1 - \tan^2 \rho_0 + i \tan \delta_0}{1 + \tan^2 \rho_0 - i \tan \delta_0} \tag{2.26}$$

and just the values of ρ_0 and δ_0 are specified in SAID [80] (this notation was introduced in reference [81]). When we discuss the data from SAID in this work we imply the standard values η and δ recalculated from the ones given by SAID by comparing the expressions for the S-matrices.

A trivial consequence of the expression (2.25) is $|I|^2 \leq \frac{1}{4}(1+\eta)^2$, i.e. using the prescription of [40] we get that the ISI factor is always less than unity and therefore reduces the magnitude of the cross section[9].

However, in such a simplified approach there are some uncertainties in the calculation of ISI effects:

i) This approach requires nucleon-nucleon phase shifts and inelasticities for different partial waves at the relevant energies. But these are not well known for the NN channels with I=0, because of the lack of the experimental data related to the measurement on the neutron target at high energies, i.e. for the pn scattering. For the $^1P_1$ partial wave of the initial nucleons which is relevant for $pn \to pn\eta$ and $pn \to d\eta$ reactions the experimental data are available only up to $T_{lab} = 1300\ MeV$ [82]. Therefore, the η meson production which starts from $T_{lab} = 1250\ MeV$ is just on the tail of measured data. It is worth noting that two independent analyses are performed by SAID collaboration in order to obtain phase shifts and inelasticities – the energy dependent solution is determined by fitting over the whole interval of energies, whereas the single-energy results are fitted to data within the specified range of energies. For the pn reaction an energy dependent solution exists up to

[9] The full consideration including P.V. integral, as will be seen later, does not change this conclusion.

1300 MeV [82], while the last single-energy point is only at 1100 MeV. Note, that using the SAID library [80] one can calculate NN phase shifts and inelasticities for any energies. However, as it is stressed in [82], these results indeed make sense only below 1300 MeV, since experimental observables are not available for higher energies[10].

Therefore in our calculation we use predictions of the CCF NN model [60] for the $^3P_0$ and $^1P_1$ partial waves. This model is in quite good agreement with the experimental NN phase shifts and inelasticities in the energy regime including the η threshold (cf. Fig 2.13 and 2.14) and therefore can be considered as a good pre-requisite for the calculation. Another advantage of using this model is the possibility to calculate the P.V. integral explicitly by utilizing its half off-shell NN T-matrix. However, the data from SAID library will be used as well in our calculation to stress the band of uncertainties.

ii) It turns out that ISI effects in the reaction $NN \to NN\eta$ are rather strong. This means that the ISI factor I in eq. (2.25) (cf. also Fig. 2.15) is rather small, i.e. $|I|^2 \ll 1$, and the cross section is strongly reduced. This smallness of I comes from a strong cancellation between the diagrams shown in the numerator of Fig. 2.15 or correspondingly between the terms 1 and $\eta cos(2\delta)$ in the expression (2.25). Therefore even small differences in δ and η can lead to large variations in the ISI factor. Compare, for instance, the results for the ISI factor in $^3P_0$ partial wave for the $pp \to pp\eta$ reaction utilizing the data from SAID library and results of the NN model [60] which deviate only by $10 - 20\%$ from the SAID values.

SAID	$\|I\|^2$	NN model	$\|I\|^2$
$\delta = -61.3$ $\eta = 0.71$	0.19	$\delta = -67.0$ $\eta = 0.55$	0.13

Obviously, the deviation of about $10 - 20\%$ for the δ and η results in ISI factors that differ by about 40% and that means also the corresponding predictions for the total cross section differ by 40%.

[10]Note, that for pp scattering (and in particular for $^3P_0$ partial wave) data exist up to 3 GeV.

Another consequence of the cancellation in the expression (2.25) is that the P.V. integral, which was neglected up to now, might influence ISI effects. As it was already mentioned before, the ISI factor calculated using the formula (2.25) is universal, i.e. it is independent of the production mechanism. Of course the P.V. integral breaks this universality since it depends on the characteristics of the specific exchanged meson like its mass and the MN T-matrix.

We have performed calculation of the diagrams presented in Fig 2.2 including the P.V. integral in the initial state both for one loop and for double loop diagrams. Now we are going to discuss the influence of the P.V. integral and approximations used in the calculation. Let us generalize the definition of the ISI factor introduced in Fig 2.15 by replacing the ISI loop with the 2 body unitarity cut by the full loop integral, i.e. by the U.C. and the P.V. integral. In the following we will call it I_G. Then the reaction amplitude for the re-scattering processes may be written down in the form

$M_{2\to 3} =$

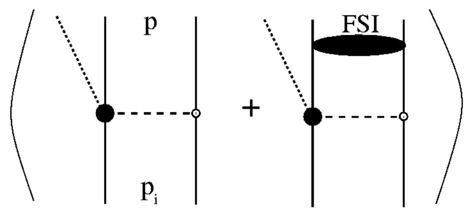

$\times I_G(\vec{p}_i^{\,thr}; \vec{p} = 0)$ (2.27)

Of course this is an approximate expression which assumes the factorization of the ISI and FSI loops in the double loop integral. However, this approximation is very convenient for the investigation of ISI effects and it is not far from reality. We would like to emphasize that in the final calculation we avoid this unnecessary simplification and calculate the double loop integral consistently.

Consider the expression for the ISI loop. According to formulae (7.38) and (7.41) in the appendices we have

$$
\begin{aligned}
M^{ISI}_{1\,loop} &= \int d\vec{p}\,'' \frac{M^{Born}(\vec{p}\,''; \vec{q}_\eta, \vec{p}) T^{ISI}_{NN}(\vec{p}_i, \vec{p}\,'')}{\sqrt{s} - 2\sqrt{m^2 + p''^2} + i0}, \\
M^{Born} &= \Gamma_{NNM} \frac{2\omega_{ex}}{q^2_{ex} - m^2_{ex}} T_{MN\to\eta N}
\end{aligned}
\qquad (2.28)
$$

The amplitude M^{ISI}_{1loop} has a three body singularity for exchanged mesons with $m_{ex} \leq m_\eta + Q$ ($m_{ex} = m_\pi, m_\eta, m_\sigma$ in the near threshold region) where Q is the excess energy of the reaction, i.e. denominator of the amplitude[11]

$$\begin{aligned} q_{ex}^2 - m_{ex}^2 + i0 &= E_{ex}^2 - \omega_{ex}^2 + i0 \\ &= (\sqrt{s} - E_2'' - E_3 - \omega_{ex} + i0)(\sqrt{s} - E_2'' - E_3 + \omega_{ex} + i0) \end{aligned} \tag{2.29}$$

can go to zero. Here $\sqrt{s} = 2m + m_\eta + Q$.

The first propagator in (2.29) has a singularity when all three intermediate particles are on mass shell, i.e.

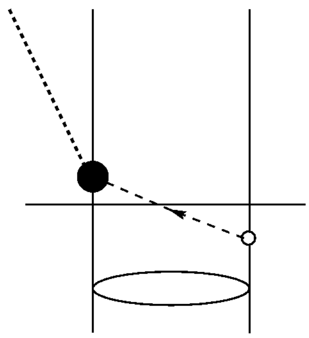

After the angular integration this 3 body propagator transforms into a logarithm which contains moving singularities, i.e. for each fixed momentum of the final particles the position of the singularity in the logarithm is different. In the present work we neglect this 3-body effect which is very complicated. Rather we will follow the approach which was already used in the work of Batinić et al. [23] and avoid the singularity in (2.29) by modifying the meson propagator, specifically by replacing the first term in (2.29) $(\sqrt{s} - E_2'' - E_3 - \omega_{ex} + i0)$ by $(E_2'' - E_3 - \omega_{ex} + i0)$. The discussed approximation is in line with a similar prescription utilized in the construction of the MN model. The MN model contains 3-body singularities in the VGT part of the Lippmann-Schwinger equation and they are removed in our calculation by using the static propagator. We want to emphasize that this approximation still provides the correct value for the contribution from the two body NN unitarity cut. This means that only the contribution from the P.V. integral can depend on the approximation discussed above. This is a very

[11] see notation in the appendix 7.5

important point because the two body unitarity cut contribution (δ-function term in the Green function) is significantly larger than the P.V. integral for almost all exchanged mesons.

In order to get a feeling for the reliability of this approximation we performed some test calculation for the P.V. integral on the basis of the ρ-meson exchange, where the mass is above $m_\eta + Q$ and therefore no singularities can occur. We want to explore the behaviour of the integrand of the amplitude (2.28) as a function of the momentum p'' for the approximate and exact ρ-meson propagators. For convenience (the integrand formally goes to infinity at $p'' = p_i$) let us write down the integrand of (2.28) in a suitable form:

$$\mathcal{P} = \frac{M^{Born}(p'')T_{NN}(p'')p''^2}{2(E(p_i) - E(p'') + i0)} = \frac{E(p_i)}{2p_i}\frac{p''^2 f(p'')h(p'')}{p_i - p'' + i0},$$
$$f(p'') \equiv M^{Born}(p'')T_{NN}(p''); \; h(p'') = \frac{2p_i}{E(p_i)}\frac{p_i - p''}{2(E(p_i) - E(p''))}, \quad (2.30)$$

where $h(p_i) = 1$. Then, subtracting and adding the same term, one gets

$$\mathcal{P} = \frac{E(p_i)}{2p_i}\left\{\frac{p''^2(p_i + p'')f(p'')h(p'') - 2p_i^3 f(p_i)}{p_i^2 - p''^2} + \frac{2p_i^3 f(p_i)}{p_i^2 - p''^2 + i0}\right\} \quad (2.31)$$

Note, that the integral from the last term in the brackets can be easily calculated analytically and it exactly corresponds to the contribution from the δ-function in (2.28). The first term in the brackets does not contain singularities at $p'' = p_i$ anymore and can be easy investigated. The integral from this term corresponds to the P.V. contribution and, therefore, is the piece which is interesting for us.

In Fig 2.16 we present the real and imaginary parts of the first term in the brackets of eq. (2.31) for the approximate and exact ρ-meson propagators. As one can see the difference is not large. Moreover, one can observe that both the real and imaginary parts of the integrand cross the zero line and change sign. Therefore significant cancellations between the positive and negative regions take place. We would like to mention that this cancellation is probably the main reason why the P.V. integral is smaller than the unitarity cut contribution. However, as it was already noted the P.V. integral is important since the U.C. contribution cancels with the Born term to a large extent.

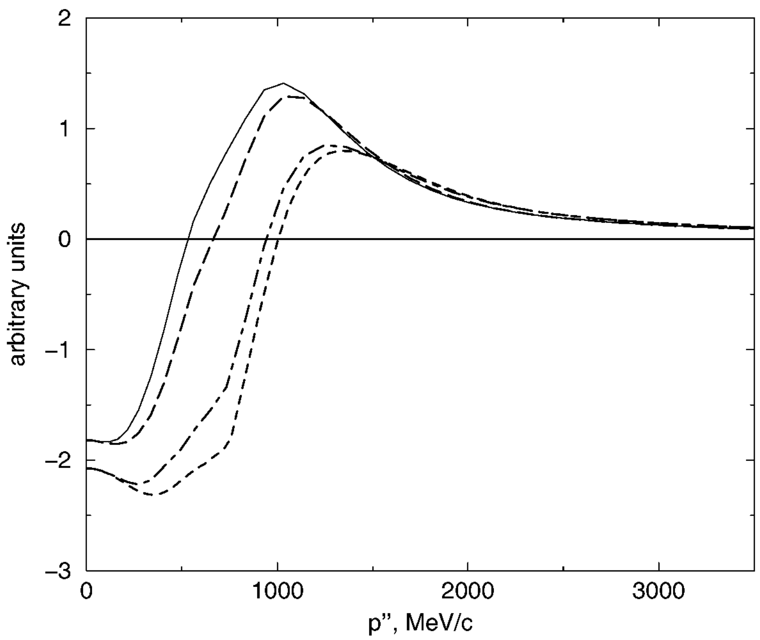

Figure 2.16: The first term in the brackets of eq. (2.31) (corresponding to the P.V. contribution) calculated for the ρ meson exchange, using the approximate (full curve for the real part and dot-dashed for the imaginary one) and exact (long dashed and dashed curves, respectively) ρ-meson propagators.

In table 2.3 we show the values of the ISI factor calculated near the η threshold for the $^3P_0$ partial wave of the pp pair, and also individual the component contributions, i.e. the Born term, P.V. integral and unitarity cut (U.C.).

As one can see from table 2.3 that the ISI suppresses the contribution of the ρ meson much more strongly compared to the pion. The origin of this phenomenon is twofold. First of all the masses of these mesons are completely different. The mass m_π = 140 MeV in the intermediate meson propagator leads to a much larger suppression of the high momentum contributions compared to the ρ case (m_ρ = 770 MeV). This means the cancellation between negative and positive regions shown in Fig.2.16 will be somewhat smaller in the case of pion and therefore the P.V. integral is larger! The second source of difference is the off-shell behavior of the $MN \to \eta N$ T-matrix. One can observe in Fig. 2.17 that the $\pi N \to \eta N$ off-shell T-matrix falls off much quicker with increasing initial c.m. momentum than

Q=1 MeV	Born	U.C.	P.V.	$\|I_G\|^2$	$\|I\|^2$ eq.(2.25)
π	0.88+0.57i	-0.5-0.56i	0.09-0.4i	0.35	↑
ρ	-0.46+0.7i	0.45-0.39i	0.06-0.18i	0.03	0.13
η	0.73+0.48i	-0.41-0.46i	-0.1-0.13i	0.08	↓
σ	-0.01-0.59i	-0.11+0.41i	-0.04+0.06i	0.11	

Table 2.3: Values of the ISI factor for the $^3P_0$ partial wave of the initial pp pair calculated at Q=1 MeV above the η threshold. $|I|^2$ corresponds to the ISI factor calculated using the approximate expression (2.25), whereas $|I_G|^2$ is the full ISI factor, i.e. including in addition the P.V. integral in the ISI loop. The contributions of the Born term, the P.V. integral and the unitarity cut (U.C.) are given as well.

the $\rho N \to \eta N$ amplitude. Again, this leads to a much larger P.V. contribution for π meson than for ρ. To confirm the above-mentioned hypothesis we performed a test calculation for the ρ-exchange replacing in the ISI loop the ρ mass in the propagator by $m_\pi = 140$ MeV and the $\rho N \to \eta N$ T-matrix by the one of $\pi N \to \eta N$. The results are summarized in table 2.4. Both effects, i.e. the ρ mass and the

	$m_\rho\!=\!770, T_{\rho N\to\eta N}$	$m_\rho\!=\!140, T_{\rho N\to\eta N}$	$m_\rho\!=\!770, T_{\pi N\to\eta N}$	$m_\rho\!=\!140, T_{\pi N\to\eta N}$
$\|I_\rho\|^2$	0.03	0.11	0.12	0.38

Table 2.4: Influence of the mass of the exchanged meson and of the $MN \to \eta N$ amplitudes ($M = \pi, \rho$) on the ISI factor. The vertex function is always ρNN.

$\rho N \to \eta N$ transition amplitudes cause a comparable reduction of I_ρ by a factor about 3 (9 in combination). The same tendency is observed in the case of other mesons, i.e. η and σ. But since the η-mass ($m_\eta = 545\ MeV$) and the $\eta N \to \eta N$ T-matrix are somewhere in between π and ρ the effect is not so pronounced.

Thus, we come to the conclusion that due to the cancellation occurring in eq. (2.25) the P.V. integral in the ISI loop plays numerically a very important role. It breaks the universality of the ISI predicted by eq. (2.25) leading to a strongly different reduction for various meson exchanges. It is interesting to mention that the authors of Ref. [23] came to a quite different conclusion. They claim that in

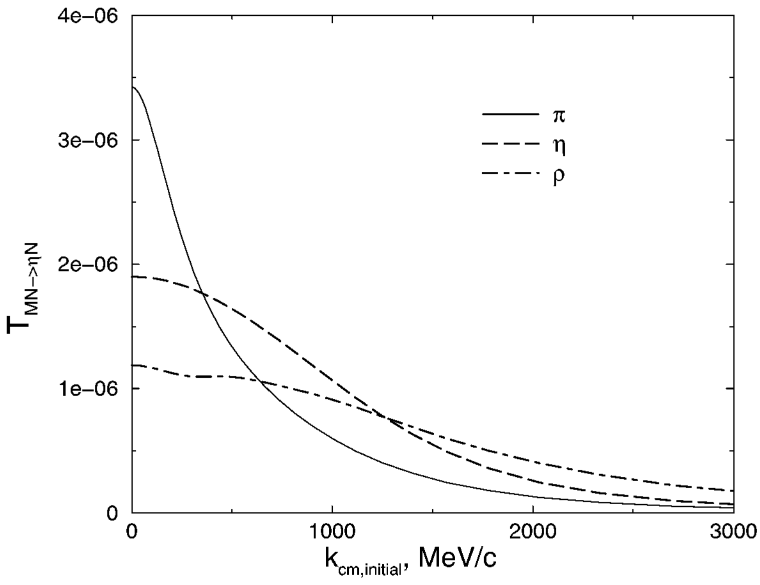

Figure 2.17: The off-shell behaviour of the $MN \to \eta N$ T-matrices as a function of the cm. initial momentum.

their analysis of η production it turned out that the combined distortions from the FSI and ISI are not sensitive to the dynamics of the production mechanism. This is hard to reconcile with our findings reported above where there is clear evidence that ISI effects are not universal for the different meson exchanges, i.e. that the ISI is very sensitive to the different production mechanisms.

For the $^1P_1$ partial wave contributing to the $pn \to pn\eta$ reaction the situation is slightly different because the cancellation in the on-shell approach (cf. eq. (2.25)) is not so strong – the on shell ISI factor is 0.3 instead of 0.1 in $^3P_0$. However, even in this case the influence of the P.V. integral is still significant, especially for the π meson exchange (see table 2.5).

$^1P_1$	on-shell		including P.V.			
	NN model	SAID	π	ρ	η	σ
$\lvert I\rvert^2$	0.3	0.28	0.4	0.2	0.23	0.31

Table 2.5: The pn ISI factor calculated for the $^1P_1$ partial wave for on-shell approximate and full approaches.

Chapter 3

Results

In this chapter we will present the results of our calculations for the reaction $NN \to NN\eta$ [83, 84].

The chapter is structured in the following way. First, in section 3.1, we specify the parameters utilized in the calculation, i.e. the coupling constants and the cut off masses in the form factors of the meson-baryon vertices. Then in section 3.2 we discuss the results of our full model. Finally, section 3.3 is devoted to the results of our calculation based on an approximate treatment of ISI effects (cf. eq. (2.25)).

3.1 Parameters utilized in the calculation.

The parameters which were used in the calculation are summarized in table 3.1.

All of them, except those involving the η meson, are taken from the full Bonn NN model. The η meson is not included in the full Bonn model. Its coupling constant with the nucleon varies rather strongly in the literature. Therefore we will consider different values for this coupling constant in our investigation and discuss its influence on the results. The value of about $\frac{g^2_{\eta NN}}{4\pi} = 1.8$ as it follows from SU(6) symmetry is utilized in the MN model [36] whereas OBE versions of the NN Bonn models [35, 59] use values between 3 and 7. In our full calculation the value of $\frac{g^2_{\eta NN}}{4\pi} = 1.8$ is employed in agreement with the MN model. As will

	$m_M(MeV)$	$\frac{g^2_{MNN}}{4\pi}$	$\Lambda_{MNN}(MEV)$
π	134.97	14.4	1300
ρ	769	0.84 ($\kappa_\rho = 6.1$)	1400
η	547.45	1.8-3 see text	1500
σ	550	5.689	1700

Table 3.1: Values of meson masses, coupling constants and cut off masses utilized in the calculation. The value of the η coupling constant, $g_{\eta NN}$, is discussed in the text. Monopole type form factors are used at all mesons-baryon vertices.

be discussed later, for the approximative approach the η meson exchange plays a more important role for the reaction $pp \to pp\eta$ and the value $\frac{g^2_{\eta NN}}{4\pi} = 3$, used in this case, leads to a slightly better agreement with the experimental data. The authors of references [25, 27] claim that only a very small value of this coupling constant allows to describe the experimental data on the reaction $pp \to pp\eta$. E.g., a value of only about $\frac{g^2_{\eta NN}}{4\pi} = 0.4$ was used in [27] while in [25] the η contribution was even completely neglected.

3.2 Results of the full calculation for η production.

3.2.1 Total cross sections for the reaction $NN \to NN\eta$.

The results of the full calculation for the reactions $pp \to pp\eta$, $pn \to pn\eta$ and $pn \to d\eta$ are presented in Fig. 3.1 by the dashed curves. The calculation utilizes the original MN model (cf. section 2.3) for the elementary η-production amplitude and the NN models the Bonn B [59] and the CCF [60] for the FSI and ISI, respectively.

As one can observe from this figure, for the $pp\eta$ case we get an overestimation by approximately 30% whereas for $pn \to pn\eta$ the calculation underestimates the experimental data by about 40-50%. Therefore, the ratio of the cross sections is underestimated by a factor of about 2 (cf. the dashed curve in Fig. 3.2).

Experimental information about this ratio is available from a measurement at Uppsala [13]. According to the Uppsala measurement the ratio is almost constant over a wide energy range $\sim 16 - 80$ MeV with a value of 6-6.5 units.

The situation for $pn \to d\eta$ is very similar to the reaction $pn \to pn\eta$ since both processes are determined by the $I = 0$ isospin channel (Note that for the latter reaction this is the case because the contribution of the $I = 1$ channel is much smaller than the one for $I = 0$).

Thus, our full calculation, based on the original Jülich MN model [36], allows us to describe qualitatively the experimental data on the total cross section for all channels of the reaction $NN \to NN\eta$. However, it is interesting to see whether our results can be improved if we slightly extend the MN model by introducing some additional graphs. We have mentioned in section 2.3 that the original MN model does not contain any tree-level contributions to the $\rho N \to \eta N$ transition. Certainly, the $\rho N \to \eta N$ transition T-matrix is not equal to zero due to coupled channel effects but, in principle, tree level Born diagrams should be included as well. Since we are interested in the η-production in NN collisions near threshold, which is characterized by a strong influence of the $S_{11}N^*(1535)$ resonance, it is a natural choice to add the $\rho N \to N^*(1535) \to \eta N, \rho N, \pi N$ potentials to the model (cf. Figure 2.9 in section 2.3). In fact, since the $\pi N \to N^*(1535) \to \eta N$ transition potential is included in the original MN model, the coupling of the $N^*(1535)$ to the other MN channels should be taken into account anyway, for consistency reasons. Thus, we have extended the model of Ref. [36] by including these diagrams, introducing a negative value for the $g_{\rho NN^*}$ coupling constant[1]. This choice allows us to achieve a better agreement for the πN inelasticity η (cf. Fig. 2.10) in the S_{11} partial wave while staying as close as possible to the results for the S_{11} phase shift and the $\pi N \to \eta N$ transition cross section as predicted by the original model.

Interestingly, the $\rho N \to \eta N$ and $\pi N \to \eta N$ transition T-matrices, and, in particular, their relative phase changed somewhat as well. In case of the original MN model the amplitudes of the π- and ρ-exchange contributions are almost orthogonal to each other. Thus, there is practically no interference between these

[1] The sign of meson-nucleon-resonance coupling constants is not fixed experimentally.

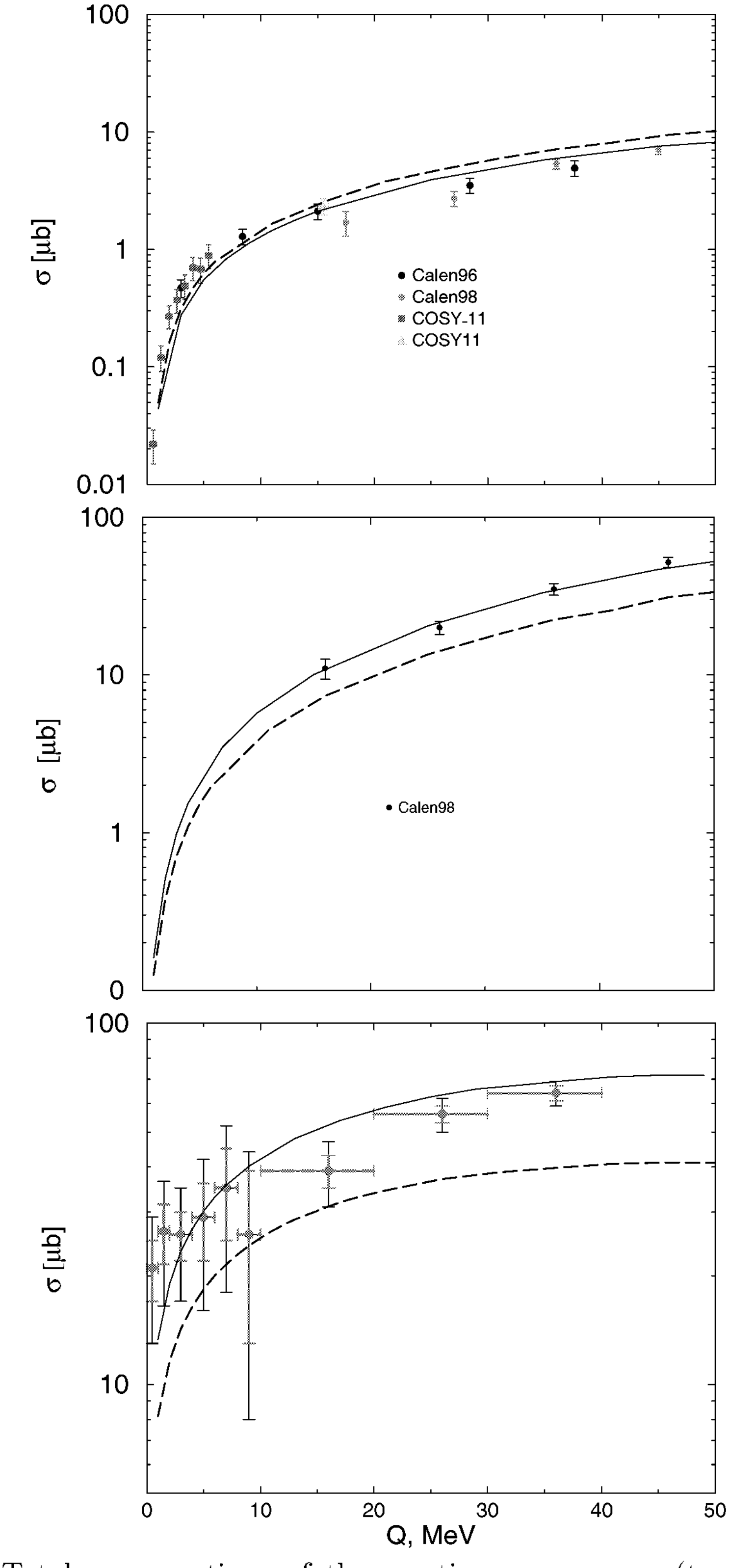

Figure 3.1: Total cross sections of the reactions $pp \to pp\eta$ (top), $pn \to pn\eta$ (middle) and $pn \to d\eta$ (bottom). The dashed lines represent the results of the full calculation with the original MN model of Ref. [36], whereas for the solid lines additional diagrams corresponding to the $\rho N \to N^*(1535) \to \eta N, \rho N, \pi N$ potentials are included in the MN model (see text). Data are from Ref. [9,11,13–15]

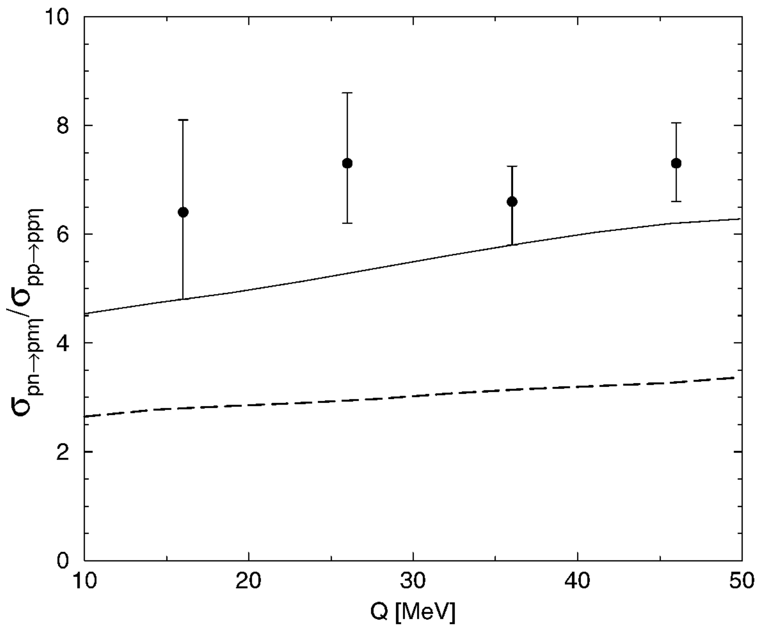

Figure 3.2: Cross-section ratio of the reactions $pp \to pp\eta$ and $pn \to pn\eta$ calculated in the full model. Notation is the same as in Fig.3.1. Data are from Ref. [13].

contributions. (I will come back to this point later when the contributions of different meson exchanges to the result will be discussed.) The additional diagrams which we introduced into the MN model yield a slight modification of the orientation of these amplitudes in the complex plane and, as a consequence, now interference effects do occur. Specifically, we observe a destructive interference for the isotriplet channel ($I = 1$) and a constructive interference for the $I = 0$ case leading to a very good agreement with the experimental data for all reaction channels. The results based on the extended MN model are presented in Figs. 3.1 and 3.2 by the solid lines.

It is worth mentioning that the interference between the π- and ρ-meson exchanges is also the key point in a recent paper of Fäldt and Wilkin [25]. We will discuss below that the cross section ratio $\sigma_{pn\to pn\eta}/\sigma_{pp\to pp\eta}$ for π- or ρ-meson exchange is approximately equal to 4.5 in Born approximation. This follows simply from isospin arguments. We also know that FSI effects can only reduce this ratio (see Fig. 3.9 in section 3.3.3). Thus, since the π- and ρ-meson exchanges are the dominant contributions in the model of Fäldt and Wilkin (the contribution from ω exchange is small), the only two mechanisms to increase this ratio are (i) strong interference effects between the π- and the ρ-meson exchanges and/or (ii) different ISI factors in the corresponding initial NN states ($^3P_0$ and $^1P_1$), respectively. However, the ISI factors are assumed to be almost identical in Ref. [25]: $I_{^3P_0} = 0.77$ and $I_{^1P_1} = 0.73$. Therefore the only way to achieve the large cross section ratio as required by the experiment is a strong interference effect between the π and the ρ exchanges. One should note that the relative sign between the π and the ρ contributions is not fixed and was chosen by hand in their publication.

In our model the interference effect between the π- and ρ-meson contribution is much less pronounced. It plays more the role of a fine-tuning effect. The cross sections for the reactions $NN \to NN\eta$ are already reasonably described on the basis of the original Jülich MN model with consistent inclusion of ISI effects. We would like to emphasize that ISI- as well as FSI effects are not universal but depend on the concrete meson production mechanism. A consistent treatment of these effects is very important for a simultaneous description of all available experimental data on the considered reactions.

3.2.2 Contributions of different meson exchanges.

Let us examine our model in more detail and analyze the contributions of the individual exchange diagrams. We do this for the calculation based on the original MN model. The differences between the results obtained utilizing the original MN model and its extended version (with some additional diagrams discussed in the previous subsection) are presented in table 3.2 at the end of this subsection.

As can be seen in table 2.3, for the reaction $pp \to pp\eta$ the effect of the ISI[2] for π exchange is almost a factor of 10 larger than the one for ρ exchange and about three times larger than the ones for η and σ, respectively. This means that ISI effects reduce the contributions from π exchange much less than those

[2] We would like to remind the reader that in our full calculation the ISI and the FSI in the double loop integral (cf. Fig. 2.2) are not factorized! Therefore, the values of the ISI factors presented in tables 2.3 and 2.5 give just a feeling about the effect of the ISI for the various meson exchanges.

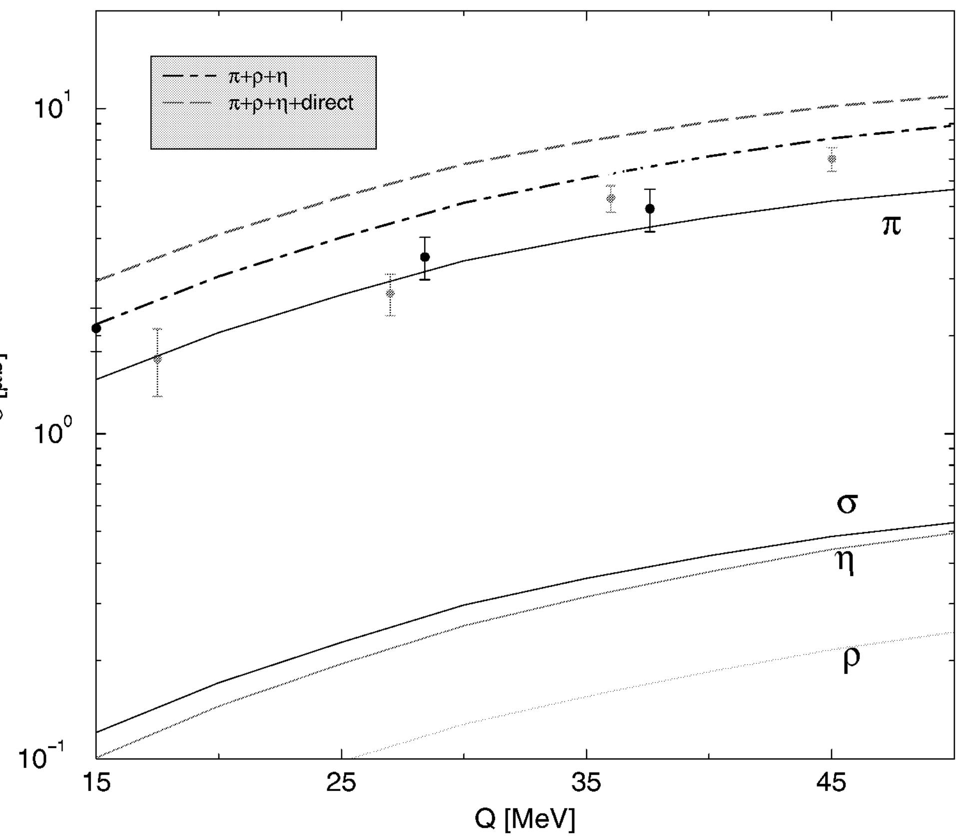

Figure 3.3: Contributions of different meson exchanges to the reaction $pp \to pp\eta$ in the full model. The presented results are based on the original MN model.

from the other mesons. Therefore, it is not surprising that the π exchange plays the dominant role in our calculation of the reaction $pp \to pp\eta$ (see Figure 3.3). Nevertheless, the contributions of the other mesons, especially of the η exchange and of the direct term are still significant. We should remark, however, that their importance is mainly due to interference effect with the amplitude of the π exchange. The η exchange and the direct term contribute constructively to the reaction $pp \to pp\eta$ whereas the interferences from the σ and the ρ mesons are destructive. However, as it was already mentioned, the contributions of the π and the ρ meson exchanges are practically orthogonal to each other (cf. table 3.2). Note, that the value $g^2_{\eta NN}/(4\pi) = 1.8$, taken from the MN model, was used in our full calculation.

Let us discuss the contributions to the reaction $pn \to pn\eta$. In the appendix 7.8 it is shown (cf. eq. (7.90)) that the production amplitude for isovector particles like π and ρ is 3 times larger in the $I = 0$ channel as compared to the $I = 1$ case whereas the contributions of isoscalar particles remain the same. As a consequence, in Born approximation the cross sections resulting from the π and ρ contributions in the $I = 0$ case are almost by a factor 10 larger than in the I=1 case whereas the ones for the η meson and other terms remain the same. Therefore the reaction $pn \to pn\eta$ is dominated by the π and ρ meson contributions from the $I = 0$ channel. However, let us not forget about the influence of the ISI and the FSI! For the relevant NN partial wave in the initial state, the $^1P_1$, the cancellation effect in the ISI loop, discussed in section 2.5, is not so pronounced as in the $I = 1$ ($^3P_0$) case (cf. the on-shell ISI factors in table 3.3 for $^3P_0$ and $^1P_1$ partial waves). Consequently, for the reaction $pn \to pn\eta$ the difference between the ISI for the various mesons is much smaller (cf. table 2.5). The FSI increases the total cross section. However, it effects the relative strength of the different meson exchange contributions only rather weakly[3]. The relative contributions to the reaction $pn \to pn\eta$ in the dominant channel with I=0 are shown in Fig. 3.4.

The dominant role belongs again to the pion exchange. The contributions of the η and the ρ mesons exhibit opposite features as in the $pp \to pp\eta$ case, i.e. the η is destructive while the ρ is constructive. The direct term again adds constructively and its contribution nearly cancels with the one resulting from η exchange. The contribution from σ exchange turns out to be negligible.

At the end of this subsection we would like to present a table which illustrates the interference effects between the π and the ρ mesons for the original as well as the extended MN models and for both isospin channels I=0 and I=1. It is obvious that the interference in the extended model is much more pronounced.

[3]FSI effects calculated for the different meson exchange processes in the reaction $pp \to pp\eta$ are disscused in detail in section 4.4. Similar conclusions hold also for the reaction $pn \to pn\eta$.

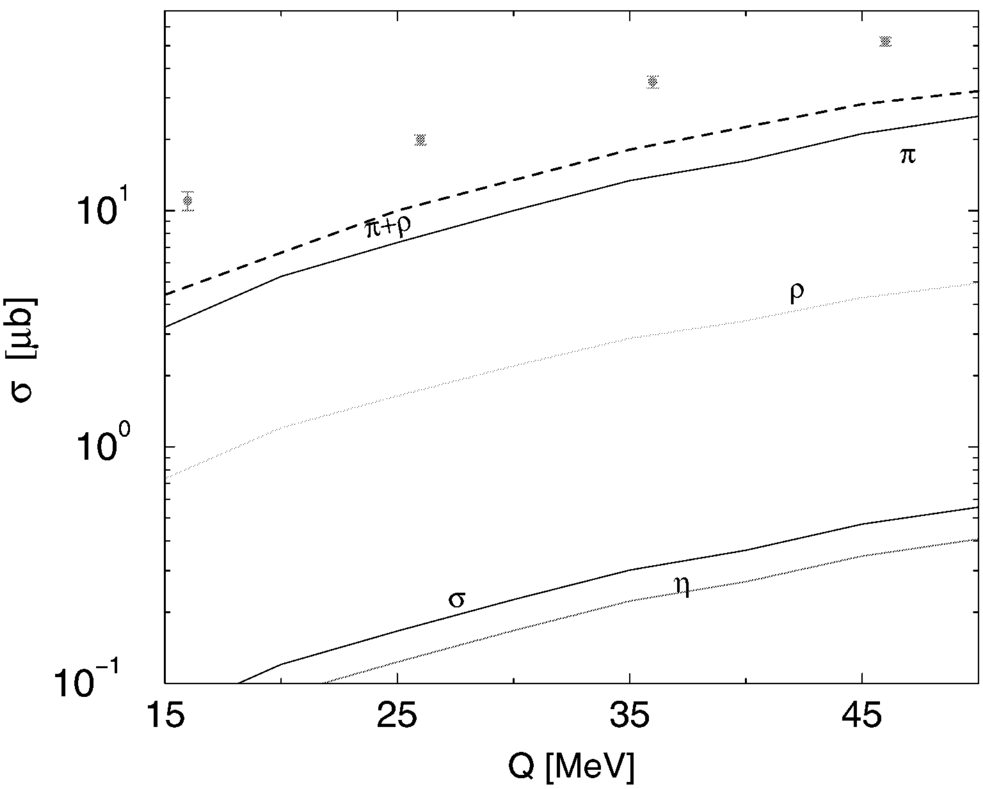

Figure 3.4: Contributions of different meson exchanges to the reaction $pn \to pn\eta$ (I=0) in the full model. The presented results are based on the original MN model.

	Original model	Extended model
	$\frac{\|M_\pi+M_\rho\|^2}{\|M_\pi\|^2+\|M_\rho\|^2}$	$\frac{\|M_\pi+M_\rho\|^2}{\|M_\pi\|^2+\|M_\rho\|^2}$
I=1	0.88	0.66
I=0	1.13	1.45

Table 3.2: Illustration of interference effects for the reaction amplitudes corresponding to contributions from the π and the ρ mesons (excess energy Q=35 MeV).

3.2.3 Role of the ηNN coupling constant.

Now we would like to analyze the influence of the ηNN coupling constant, $g_{\eta NN}$, on the results of our model. It follows from the discussion in subsection 3.2.2 that the contribution of η exchange leads to a reduction of the cross section ratio. This fact is also mentioned by Fäldt and Wilkin [25]. Clearly, in view of this, the contribution from η exchange is counter-productive for reproducing the experimentally observed large cross section ratio and, consequently, phenomenological approaches like the one in Ref. [25] tend to neglect its contribution altogether (or, technically speaking, assume that $g_{\eta NN}$=0). However, we would like to stress that in more elaborate model calculations like in ours $g_{\eta NN}$ enters not only via the η exchange contribution but also in the direct term, which is not negligible, and interferes constructively in both isospin channels of the reaction $NN \to NN\eta$. Therefore, the influence of the ηNN coupling constant is more complicated. As it was already noted, in the reaction $pp \to pp\eta$ the η exchange and the direct term are both constructive while in $pn \to pn\eta$ $(I = 0)$ their joined contribution is small because the two mechanisms cancel each other. Therefore, we expect that also in our model the cross section ratio will increase if $g_{\eta NN}$ is reduced. For instance for $Q = 35$ MeV the ratio increases by approximately 20% (from 5.75 to 6.87) when $g^2_{\eta NN}/(4\pi)$ is reduced from 1.8 to 1.0. However, due to cancellation effects in the dominant isospin I=0 channel of the reaction $pn \to pn\eta$, the ηNN coupling constant influences primarily the cross section of the $pp \to pp\eta$ reaction, and therefore, leads only to a mild dependence of the cross section ratio on this coupling constant.

3.2.4 Differential cross section for the reaction $pp \to pp\eta$

At the end of this chapter we would like to say some words about the differential cross section $d\sigma/d\Omega_\eta$, i.e. the angular distribution of the produced η mesons, for the reaction $pp \to pp\eta$. For the first time this cross section was measured in Uppsala [16] at the excess energies Q = 16 and Q = 37 MeV. Being nearly flat for the lower energy the differential cross section shows a clear anisotropy at Q = 37 MeV. Since the lowest possible partial waves for the η with respect to the final proton pair are s and d (a p wave is not allowed due to selection rules) the anisotropy was associated with large d wave contributions. However, it seems that new data of a measurement performed by the TOF collaboration at the COSY accelerator in Jülich with much higher statistics do not confirm this strong anisotropy. These data exhibit basically the same flat behavior for both measured excess energies, Q = 15 MeV and Q = 41 MeV [17], suggesting that the d-wave contribution is negligible. Preliminary data exist also due to recent measurement by COSY 11 collaboration [12]. They also measured $d\sigma/d\Omega_\eta$ at Q = 15 MeV and found that it is totally flat.

The amplitude for this process may be schematically presented in the following form

$$M = M_{^3P_0\to^1S_0s}\ \phi_f^+(\vec{p}_i\cdot\vec{\epsilon}_i) + M_{^3L_2\to^1S_0d}\ \phi_f^+\left\{(\vec{q}_\eta\cdot\vec{\epsilon}_i)(\vec{q}_\eta\cdot\vec{p}_i) - \frac{1}{3}q_\eta^2(\vec{p}_i\cdot\vec{\epsilon}_i)\right\}, \quad (3.1)$$

where $\vec{p}_i$ and $\vec{q}_\eta$ are the c.m. momenta of the initial protons and the produced η meson, respectively, whereas $\vec{\epsilon}_i$ is the spin one polarization vector of the initial protons and ϕ_f is the spin zero function of the final protons. For the d-wave amplitude the corresponding initial states are denoted by $^3L_2$, where $^3L_2 = ^3P_2, ^3F_2$ and the sum over these states is implied in (3.1).

Unfortunately the predictions of the CCF NN model [60] for the $^3P_2$ partial wave, for energies around the η-production threshold, deviate rather strongly from Arndt's phase shift analysis, and therefore the corresponding T-matrices cannot be considered to be realistic anymore. Hence we refrain from using it in our investigation. However, we can obtain an estimation of the cross section on the basis of a somewhat mixed approach, namely by calculating the s-wave amplitude from our full analysis and resorting to the approximative treatment without the P.V. integral in the ISI loop for the d-wave. This procedure is not so unreasonable since in the combined ISI factor for the $^3L_2 \to ^3L_2'$ transitions (including nondiagonal amplitudes) the cancellation effect between the Born amplitude and the unitarity cut contribution, described in detail in section 2.15, which leads to the importance of the P.V. integral is much less pronounced. The result of this estimation as well as the experimental data from Uppsala and Jülich are shown in Fig. 3.5.

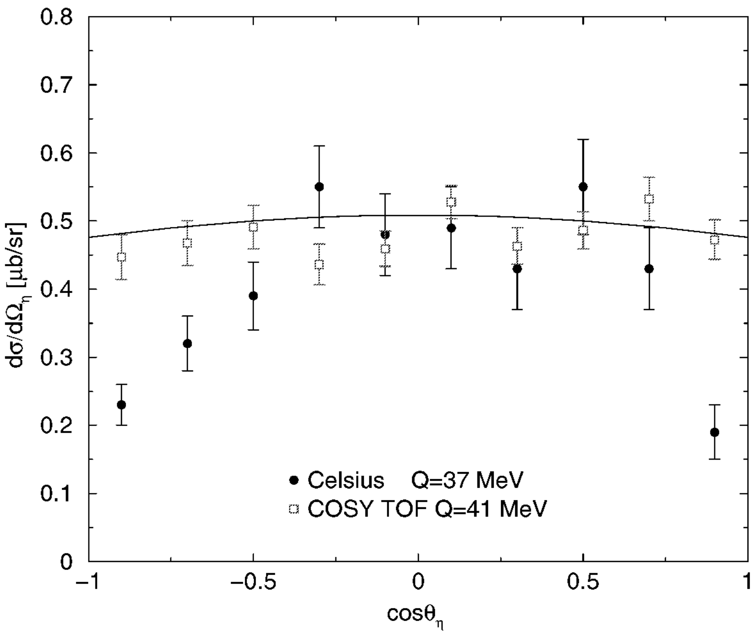

Figure 3.5: Angular distribution of the η for the reaction $pp \to pp\eta$. The data are taken from Refs. [16] and [17]. The data from COSY TOF collaboration are normilized to the value of 6 μb for the total cross section which is expected at Q=41 MeV (cf. tendency for the behaviour of the total cross section in Fig. 3.1).

3.3 Results for the η production within the approximative ISI approach.

In this section we want to present calculations based on the assumption that the ISI factor is given by on-shell information alone, i.e. by Eq. (2.25). We do this in order to examine and to document the reliability and the quality of this approximative treatment of ISI effects .

3.3.1 Total cross sections

Results for all reaction channels $pp \to pp\eta$, $pn \to pn\eta$, $pn \to d\eta$, obtained within the approximative treatment of the ISI, are shown in figure 3.6. We employ ISI factors evaluated from phase shifts taken from the SAID NN database (with

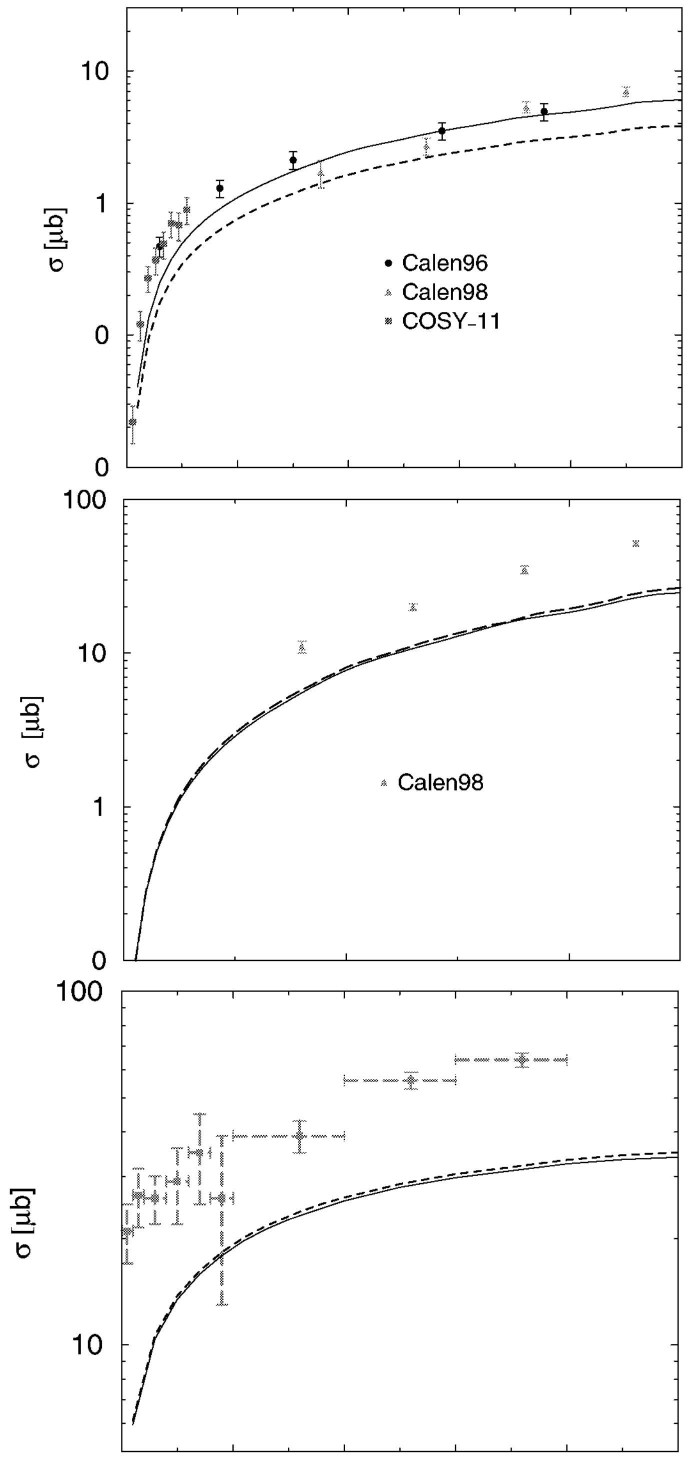

Figure 3.6: Total cross sections for the reactions $pp \to pp\eta$, $pn \to pn\eta$ and $pn \to d\eta$ calculated with the approximative approach for the ISI (Eq. (2.25)). The solid lines are based on NN phase shifts from SAID whereas for the dashed lines those of the CCF NN model [60] were used (cf. table 3.3).

reservation discussed in the ISI section) and from predictions of the CCF NN model [60] (see table 3.3).

	$\|I\|^2$: SAID	NN model
$^3P_0$	0.19	0.13
$^1P_1$	0.28	0.3

Table 3.3: ISI factors evaluated from on-shell NN data taken from the SAID database and from the CCF NN model [60].

This calculation has been done using the NN potential Bonn B [59] for the FSI. The value $g^2_{\eta NN}/4\pi = 3$ is employed in the calculation.

Comparing the results in Fig. 3.6 with those from the full calculation (cf. Fig. 3.1) clearly demonstrates that the approximative treatment of ISI effects leads to significant differences.

3.3.2 Role of different meson exchanges.

The goal of this subsection is to illustrate that the approximative treatment of ISI effects would even lead to different conclusions about the dominant mechanisms for the η-meson production as those given in chapter 3.2. Since the ISI factor is uniform constant in this approximative approach and the FSI are nearly the same for the various meson exchanges (cf. Fig. 4.8) the relative strength of the different contributions is determined predominantly by the corresponding Born terms. For the reaction $pp \to pp\eta$ the Born terms for the π, ρ, and η mesons are of similar magnitude whereas the one for the σ is by about a factor 2 smaller. The relative contributions to the cross section with ISI and FSI effects taken into account are shown in Fig. 3.7. As one can observe in this figure the contributions from π, η and ρ are indeed comparable.

The situation is different in the $I = 0$ channel. It was already mentioned in subsection 3.2.2 and in the appendix 7.8 that the production amplitude for isovector particles is 3 times larger in the $I = 0$ channel as compared to the $I = 1$ case whereas the contributions of isoscalar particles remain the same. This feature is

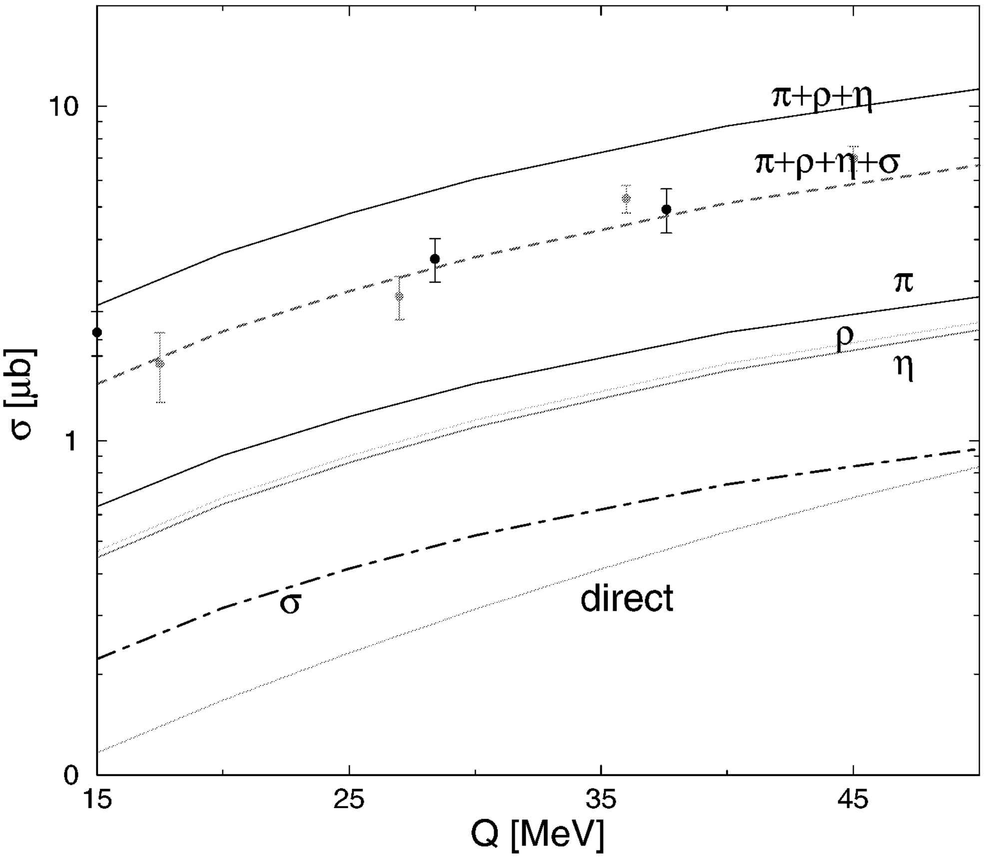

Figure 3.7: Contributions of different meson exchanges to the reaction $pp \to pp\eta$ within the approximative approach to ISI effects.

independent of the ISI treatment, so that $pn \to pn\eta$ ($I = 0$) reaction is qualitatively described just by π and ρ exchanges both for the full and approximative approaches. However the influence of the ρ exchange in the full calculation is much weaker.

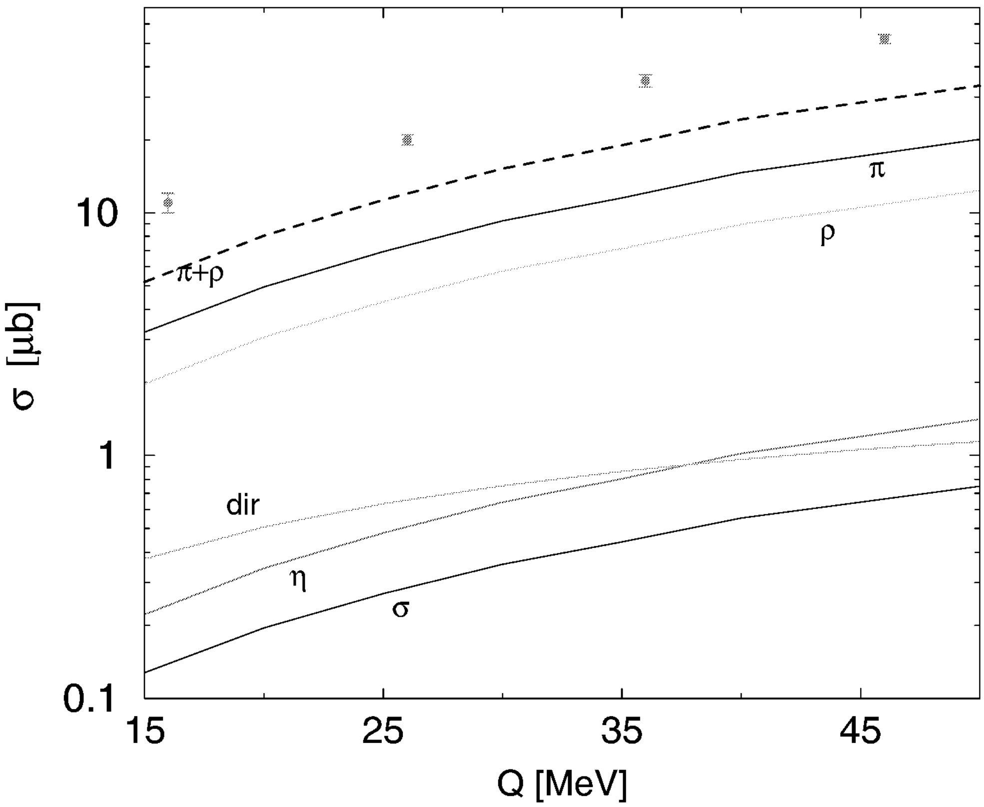

Figure 3.8: Contributions of different meson exchanges to the reaction $pn \to pn\eta$ (I=0) within the approximative approach to ISI effects.

3.3.3 Cross section ratio $\sigma_{pn\eta}/\sigma_{pp\eta}$

In this subsection we are going to discuss the cross section ratio with emphasis on the role played by ISI effects, FSI effects and the Born amplitudes. We do this for the case when the ISI is determined by the on-shell prescription Eq. (2.25). Since the ratio of ISI effects is the same constant for the different meson exchanges in the approximate approach, it is more convenient to analyze the role of other ingredients such as production amplitude and FSI effects for the cross section ratio in this case than in the full calculation.

Due to the favorable isospin coefficient the cross section of the reaction $pn \to pn\eta$ is primarily determined by the $I = 0$ channel. Indeed, in Born approximation the cross section ratio $\sigma_{pn\to pn\eta}/\sigma_{pp\to pp\eta}$ for isovector meson exchange (i.e. for π- or ρ exchange) is approximately equal to 9/2. This estimation 9/2 was obtained by neglecting the contribution of the channel with $I = 1$ in the reaction $pn \to pn\eta$. The exact value of the cross section ratio is equal to 5. However, considering only the pure $I = 0$ channel, it is more convenient to analyze the contributions of different constituents to the cross section ratio. The factor 1/2 results from differences in the isospin coefficients for these reactions in conjunction with a statistical factor for identical particles required for the pp case (cf. eq. (7.27) and eqs. (7.78 - 7.79)).

We have already mentioned that the contributions of π and ρ exchange practically do not interfere with each other for the original MN model. This is true both for the full calculation as well as for the case with the approximate ISI. Therefore, the cross sections ratio for the sum of these two mesons is basically the same as the one for the individual contributions, i.e. $R_{\pi+\rho} \approx R_\pi \approx R_\rho \approx 4.5$. The contributions of the η and σ mesons to the reaction $pp \to pp\eta$ in the approximative approach are constructive which leads to a reduction of the ratio to a value of about 3.7. The ISI effects (which are different for the different initial NN states, cf. table 3.3!) increase the ratio again yielding values of around 5.5 to 8.5 (the first value corresponds to the ISI taken from the SAID data whereas the second one was obtained utilizing the CCF model for the ISI). However, effects from the FSI are much stronger for the $I = 1$ channel as it is seen in Fig. 3.9. They enhance the cross section for $pp \to pp\eta$ much more than the one for $pn \to pn\eta$ and, accordingly the cross section ratio is finally reduced to a factor of around 1.5 - 2, depending on the energy. Because of differences in the energy dependence of the FSI for the I=0 and I=1 channels one gets a cross section ratio which is not a constant.

In Fig. 3.10 we present the total ratio $\sigma_{pn\to pn\eta}/\sigma_{pp\to pp\eta}$ with inclusion of both isospin channels in the $pn\eta$ case.

It is obvious from the above discussion that in a realistic model calculation like

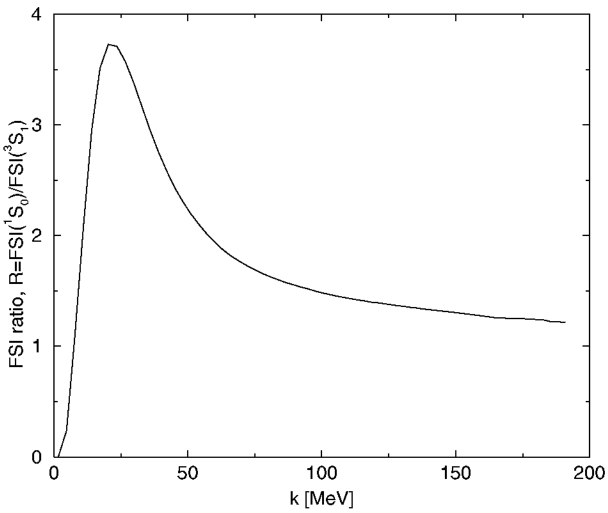

Figure 3.9: Ratio of FSI factors $R = F_{pp\eta}/F_{pn\eta,I=0}$

ours the cross section ratio results from a rather delicate interplay between several ingredients, in particular, the actual production mechanism and effects from the FSI as well as from the ISI. This means that one should be very cautious with drawing conclusions on the cross section ratio from simple model analyses when only one or two of those ingredients are considered explicitly.

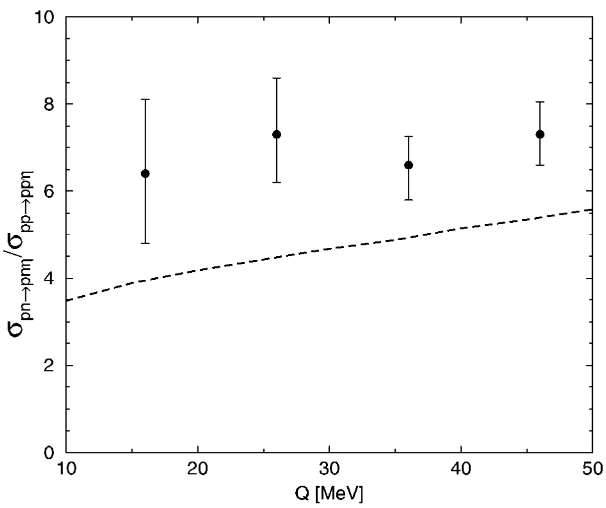

Figure 3.10: Ratio of the $pn \to pn\eta$ and $pp \to pp\eta$ cross sections calculated with the approximative ISI factors utilizing the CCF NN model [60].

Chapter 4

Final state interaction effects in meson production in NN collisions

4.1 Introduction

Already in the 1950's K. Watson [38] and A. Migdal [39] have shown that the energy dependence for meson production reactions $NN \to NNx$ near threshold is predominantly determined by the strong NN interaction in the final state. Their arguments have been used for justifying a rather simple treatment of effects from the final state interaction (FSI) (see, e.g., Refs. [20–22, 85]). It consists in simply multiplying the basic production amplitude with the on-shell NN T-matrix, i. e.

$$\mathcal{M} = -NA_{prod}^{on} \cdot \frac{e^{i\delta} \sin\delta}{ka_{NN}}, \tag{4.1}$$

where $\delta = \delta(k)$ is the S-wave NN phase shift, a_{NN} the NN scattering length, A_{prod}^{on} the on-shell meson production amplitude and N a normalization factor. This expression suggests that the FSI effect is universal, i. e. does not depend on the specific meson emitted.

Recently, some aspects of FSI effects in the reaction $NN \to NNx$ were investigated by Hanhart and Nakayama [40], Niskanen [41] and Uzikov and Wilkin [86].

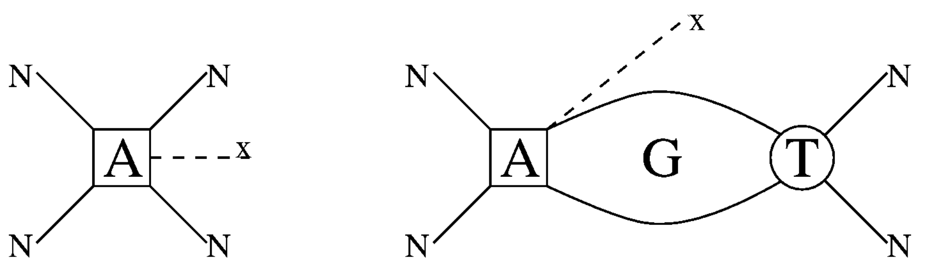

Figure 4.1: Diagrammatic representation of the DWBA expression Eq. (4.2). A is the elementary meson-production amplitude and T the NN T-matrix.

In particular, the authors of [40, 41] pointed out that the evaluation of the total reaction amplitude by just multiplying the production amplitude by the on-shell NN T-matrix is not acceptable for obtaining quantitative predictions. In the present work we want to study those FSI effects in more detail. Specifically, we want to shed some light on the validity of the multiplication prescription Eq. (4.1). We examine the influence of the NN FSI on the absolute value of the reaction amplitude by employing realistic models of the NN interaction. Furthermore we investigate the dependence of the FSI effects on the mass of the produced meson. For that purpose we will vary the mass of x and adopt values corresponding to those of the π, η, and η' mesons.

In general the total amplitude for the reaction $pp \to ppx$ can be determined from the DWBA expression

$$\mathcal{M} = A^{on}_{prod} + A^{off}_{prod} G_0 T_{NN}. \tag{4.2}$$

where the term on the very right side implies an integration over the off-shell production amplitude and the off-shell NN T-matrix. Eq. (4.2) corresponds to the sum of the two diagrams shown in Fig. 4.1. Meson production in NN collisions requires a large momentum transfer between the initial and final nucleons which is typically of the order of $\sqrt{mm_x}$, where m is the nucleon mass and m_x the mass of produced meson. Thus the range of the production interaction will be much smaller than the characteristic range of the NN interaction in the final state.

Goldberger and Watson argued that in such a case the meson can be considered to be produced practically from a point like region so that the production amplitude can be factored out of the integral [46], i.e.

$$\mathcal{M} = A^{on}_{prod} + A^{off}_{prod} G_0 T_{NN} \;\approx\; A^{on}_{prod}[1 + G_0 T_{NN}] \;=\; A^{on}_{prod} \psi_k^{(-)^*}(\vec{r} = 0). \quad (4.3)$$

Here $\psi_k^{(-)}(\vec{r})$ is the (suitably normalized) NN wave function in the continuum [46], where $\psi_k^{(-)}(0)$ is related to the Jost function $\mathcal{J}$ via $\psi_k^{(-)^*}(0) \;= \mathcal{J}^{-1}(-k)$ [46]. Clearly also in this case one arrives at results where the FSI effects are reduced to a mere multiplicative factor $\mid \psi_k^{(-)^*}(0) \mid^2$ (commonly referred to as enhancement factor).

The prescription Eq. (4.3) has been utilized by several authors, e.g., [87–91] in their studies of meson production. To be concrete using the relation between the Jost function and the NN phase shift $\delta(k)$

$$\mathcal{J}(k) = \prod_{n=1} (1 + \frac{\alpha_n^2}{k^2}) exp\Bigg(-\frac{1}{\pi}\int\limits_{-\infty}^{\infty} \frac{dk' \delta_l(k')}{k' - k + i0}\Bigg), \quad (4.4)$$

(where $\alpha_n^2 = m\varepsilon_n$ with ε_n being the energies of possible bound states) and assuming that those phase shifts are given by the effective range approximation

$$S = e^{2i\delta_l} = \frac{-1/a + rk^2/2 + ik}{-1/a + rk^2/2 - ik} \quad (4.5)$$

one can easily get

$$\mathcal{J} = \frac{k + i\beta}{k + i\alpha}, \quad (4.6)$$

for the $^1S_0$ partial wave, where

$$\alpha = \frac{1}{r}\Bigg(1 + \sqrt{1 - \frac{2r}{a}}\Bigg), \quad \beta = \frac{1}{r}\Bigg(-1 + \sqrt{1 - \frac{2r}{a}}\Bigg). \quad (4.7)$$

In the papers [89–91] exactly this particular Jost function (Eq. (4.6)) has been utilized. In principle the effective range approximation is applicable only at small momentum k whereas the integration in (4.4) has to be performed over the whole region $k \in (-\infty, \infty)$. However, some potentials, specifically the Eckart potential,

$$V = \frac{-8\alpha^2}{\alpha^2 - \beta^2}\left(\frac{e^{-\alpha r}}{\alpha - \beta} + \frac{e^{\alpha r}}{\alpha + \beta}\right)^2,$$

are constructed in such a way that the corresponding S-matrix is identical to the effective range expansion, Eq. (4.5), for any value of k. This particular feature was exploited in [91].

A different type of Jost functions has been employed in the papers [87, 92–94] for investigating the energy dependence of the reactions $pp \to pp\eta$ and $pp \to pp\eta'$. The authors of [87, 92–94] aimed at taking into account Coulomb effects as well and this can be done by using a Jost function that is the solution of the scattering problem with Coulomb + Yamaguchi potential, i.e.

$$\mathcal{J} = \frac{e^{-\pi/2ka_B}}{\Gamma(1+\frac{i}{ka_B})} \frac{\lambda^{-1}(\beta^2+k^2) - (2\beta)^{-1}BF^{(\nu)}(B^2)}{\lambda^{-1}(\beta^2+k^2) - (2\beta)^{-1}BF^{(\nu)}(B^2) + (\beta - ik)^{-1}B^{-\nu}F^{(\nu)}(B)}. \quad (4.8)$$

Here $\nu = i/ka_B$, $B = (\beta+ik)/(\beta-ik)$, and $\Gamma(z)$ is the gamma function. $F^{\nu}(z) = (\nu+1)^{-1}F(1,\nu,\nu+2,z)$ and a_B is the Bohr radius of the proton. This analytical expression has been derived by H.van Haeringen (see [95, 96]).

The validity of the Jost function approach (4.3) has been examined by an explicit calculation of the loop diagram in Ref. [87] employing an OBE model for the production amplitude. However, one has to keep in mind that this investigation is based on a simple, Yamaguchi-type, separable potential for the NN FSI. It is well-known that the off-shell behavior of the T-matrix for the Yamaguchi potential is rather different from the one resulting from realistic models of the NN force. This can be seen from Fig. 4.2 where we compare the off-shell properties of the Paris [75] and (one version of) the Bonn [35] NN models with the one of the Yamaguchi potential for the $^1S_0$ partial wave. The most striking difference is definitely the zero crossing of the T-matrix that occurs for realistic potential models at off-shell momenta $q \approx 350$ MeV/c whereas the T-matrix resulting from the Yamaguchi potential never changes sign. As we will show below, this specific feature has a strong and important influence on the result for the FSI effects. In the following we will present calculations for the effects of the FSI considering different NN models and the production of mesons with different masses. Furthermore we take a look at the energy dependence of the FSI effects and examine the validity of some commonly used approximations.

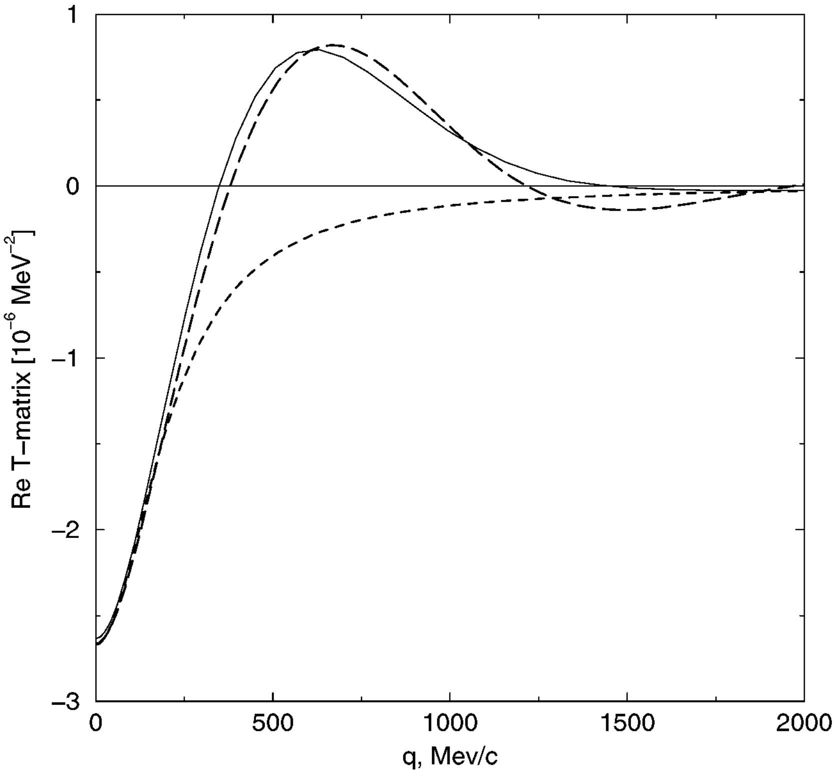

Figure 4.2: Real part of the NN $^1S_0$ T-matrix as a function of the off-shell momentum q calculated at the fixed on-shell momentum $k = 10$ MeV/c. The solid, long-dashed, and short-dashed lines are the results for the Paris [75], Bonn [35,60], and Yamaguchi potentials, respectively.

4.2 Loop diagram calculus

For the calculation of the loop diagram of Fig. 4.1 with off-shell amplitudes of realistic NN interactions we need to specify a model for the production amplitude. We assume that it has the form

$$A_{prod} = \frac{g \cdot A_{\mu N \to xN}}{t - m_\mu^2} \ , \tag{4.9}$$

which corresponds to the exchange of a scalar meson μ of mass m_μ in the t-channel followed by the production of a meson x in a re-scattering process $A_{\mu N \to xN}$.

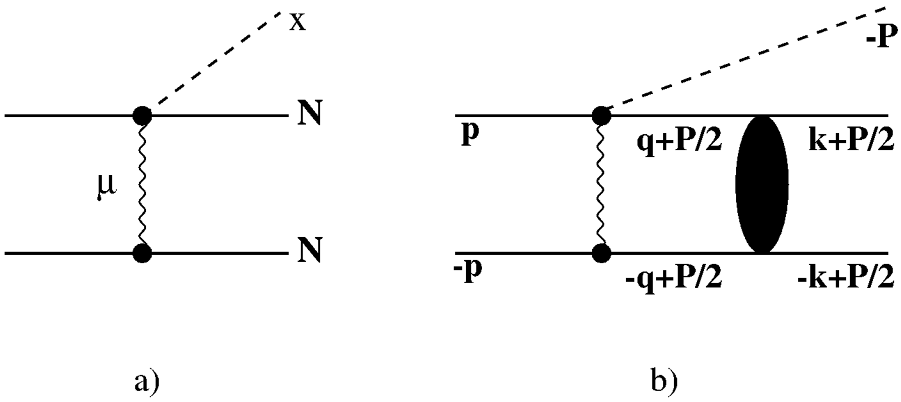

Figure 4.3: Contributions to the total reaction amplitude $\mathcal{M}$: (a) Born term A; (b) loop diagram including the final state interaction.

The corresponding diagram is shown in Fig. 4.3a. The coupling g at the $NN\mu$ vertex and the amplitude $A_{\mu N\to xN}$ are assumed to be constants. For the mass m_μ of the exchange particle we take the value of the pion mass, i.e. $m_\mu = 135$ MeV. Furthermore, for simplicity reasons, we use non-relativistic kinematics for the intermediate nucleons[1]. The total reaction amplitude for this production model is then given by the sum of the two diagrams of Fig. 4.3, i.e.

$$\mathcal{M} = A^{on}_{prod}\left(1 + \frac{A^{off}_{prod}}{A^{on}_{prod}} G T_{NN}\right) = A^{on}_{prod}\Psi(k). \tag{4.10}$$

For the sake of clarity we have rewritten the result for the reaction amplitude in a form similar to Eq. (4.3). The on-shell production amplitude in the last equation is

$$A^{on}_{prod} = -\frac{mg}{E}\frac{A_{\mu N\to xN}}{[(\vec{k} - \vec{P}/2 + \frac{m}{E}\vec{p})^2 + \lambda^2]} \tag{4.11}$$

where $E = \sqrt{m^2 + p^2}$ and $\lambda^2 = \frac{m}{E}m_\mu^2 + \frac{m^2}{E^2}\tau^2$ with $\tau = E - m$. $\Psi(\vec{k})$ is given by the expression

$$\Psi(\vec{k}) = 1 - \frac{m\pi[(\vec{k} - \vec{P}/2 + \frac{m}{E}\vec{p})^2 + \lambda^2]}{4\pi r}\int_0^\infty \frac{dqq\ T_{NN}(q,k)}{[q^2 - k^2 - i0]}\ ln[\frac{(q+r)^2 + \lambda^2}{(q-r)^2 + \lambda^2}]\ , \tag{4.12}$$

[1]However we would like to stress that all these simplifications do not change the general conclusion of this chapter

where $r =| \frac{m}{E}\vec{p} - \vec{P}/2 |$. The logarithm in (4.12) results from the angular integration of $\frac{1}{t(q') - \mu^2}$ term over $d\Omega_q$. $T_{NN}(q,k)$ is the NN half-off-shell T-matrix in the $^1S_0$ partial wave. It is related to the standard scattering amplitude $f(k)$ by

$$T_{NN}(k,k) = -f(k)/2\pi^2 m; \quad f(k) = \frac{e^{i\delta} sin(\delta)}{2ik}. \tag{4.13}$$

The function $F_{NN}(k) =| \Psi(\vec{k}) |^2$ can be considered as a generalization of the FSI enhancement factor $| \psi^{(-)*}_{k}(0) |^2$ that follows from the factorization assumption Eq. (4.3). We would like to emphasize, however, that (contrary to $\psi^{(-)*}_{k}(0)$ in Eq. (4.3)) $\Psi(\vec{k})$ does contain also information on the production mechanism and not only on the NN FSI.

In the actual calculations we want to include the Coulomb interaction between the outgoing protons. Therefore we have to replace the NN half-off-shell T-matrix in Eq. (4.12) by the quantity T^{cs}_{NN}, i.e. the Coulomb-distorted hadronic T-matrix. This quantity is obtained by the prescription introduced in Ref. [97], namely via

$$T^{cs}_{NN}(q,k) = \frac{C(\gamma_q)}{C(\gamma_k)} \frac{T_{NN}(q,k)}{T_{NN}(k,k)} T^{cs}_{NN}(k,k) \ , \tag{4.14}$$

where k and q denote the on-shell and off-shell momentum, respectively. $T_{NN}(k,k)$ and $T_{NN}(q,k)$ are the on-shell and half-off-shell T-matrices for the strong interaction alone. The Coulomb penetration factor C is given by

$$C^2(\gamma_q) = \frac{2\pi\gamma_k}{e^{2\pi\gamma_k} - 1}; \quad \gamma_k = \frac{m}{2}\frac{1}{\alpha k} \ , \tag{4.15}$$

with α being the fine-structure constant. Furthermore, the first term on the l.h.s. of Eq. (4.12) (the “1”) has to be replaced by $C(\gamma_k)$.

4.3 Discussion

First we want to discuss the dependence of $\Psi(k)$ on the mass of the produced meson. For that purpose we start out from a somewhat simpler expression for Ψ which follows from Eq. (4.12) for the kinematics at the production threshold:

$$\Psi(k) = C(\gamma_k) - \frac{m\pi[mm_x + m_\mu^2]}{4\pi\sqrt{mm_x + m_x^2/4}} \int_0^\infty \frac{dqq \ T^{cs}_{NN}(q,k)}{[q^2 - k^2 - i0]} \ ln[\frac{(q+\tilde{r})^2 + \tilde{\lambda}^2}{(q-\tilde{r})^2 + \tilde{\lambda}^2}] \ , \tag{4.16}$$

where

$$\tilde{r} = \frac{m}{m + m_x/2}\sqrt{mm_x + m_x^2/4}, \ \tilde{\lambda}^2 = \frac{m^2}{(m + m_x/2)^2}\frac{m_x^2}{4} + \frac{m}{m + m_x/2}m_\mu^2 \ .$$

For the production of a light meson, $m_x \ll m$, we get $\tilde{r} \approx \sqrt{mm_x}$, $\tilde{\lambda}^2 = m_\mu^2 + m_x^2/4$, so that there is a dependence of the integral on the r.h.s. of Eq. (4.16) on m_x. In the case of a heavy meson, $m_x \gg m$, it follows that $\tilde{r} \approx m$, $\tilde{\lambda}^2 \approx m^2$ and consequently $\Psi(k)$ does not depend on the mass of the emitted meson x. In other words, we expect that FSI effects are getting universal for the production of heavy mesons via an OBE-type production mechanism Eq. (4.9).

Let us now come to the results for the FSI factor $F_{NN} =\mid \Psi(k) \mid^2$. In Fig. 4.4 we show calculations for different NN models and for some typical masses of the emitted meson x. It can be seen from those figures that the magnitudes of F_{NN} resulting for the Bonn and the Paris potentials are fairly similar whereas the one for the separable Yamaguchi potential is quite different. (Note that different scales are used for each NN model!) This result can be understood qualitatively from the features of the corresponding off-shell T-matrices shown in Fig. 4.2. The T-matrices for the Bonn and Paris potentials are very similar. In particular, for both models there is a change of sign at an off-shell momentum of $q \approx 350$ MeV/c. Because of this change of sign cancellations occur in the integral for $\Psi(k)$ (cf. Eq. 4.12). The off-shell T-matrix of the Yamaguchi potential does not change sign. Therefore, no such cancellations take place in the integration and as a consequence the FSI factor F_{NN} is significantly larger than the ones for the realistic interaction models, cf. Fig. 4.4.

There is also a striking difference in the results with regard to the mass of the emitted meson. For the Paris and Bonn potentials the FSI factor decreases with increasing mass of the produced meson. However, for the Yamaguchi potential we observe the opposite effect. Here $F_{NN}(k)$ becomes larger with the mass of the produced meson. These features can again be understood in terms of the NN off-shell properties. However, now the off-shell behavior of the production amplitude, that enters into the integral (4.12) as well, becomes also relevant. With increasing mass of the produced meson the required momentum transfer t increases as well and, accordingly, the production mechanism gets more and more

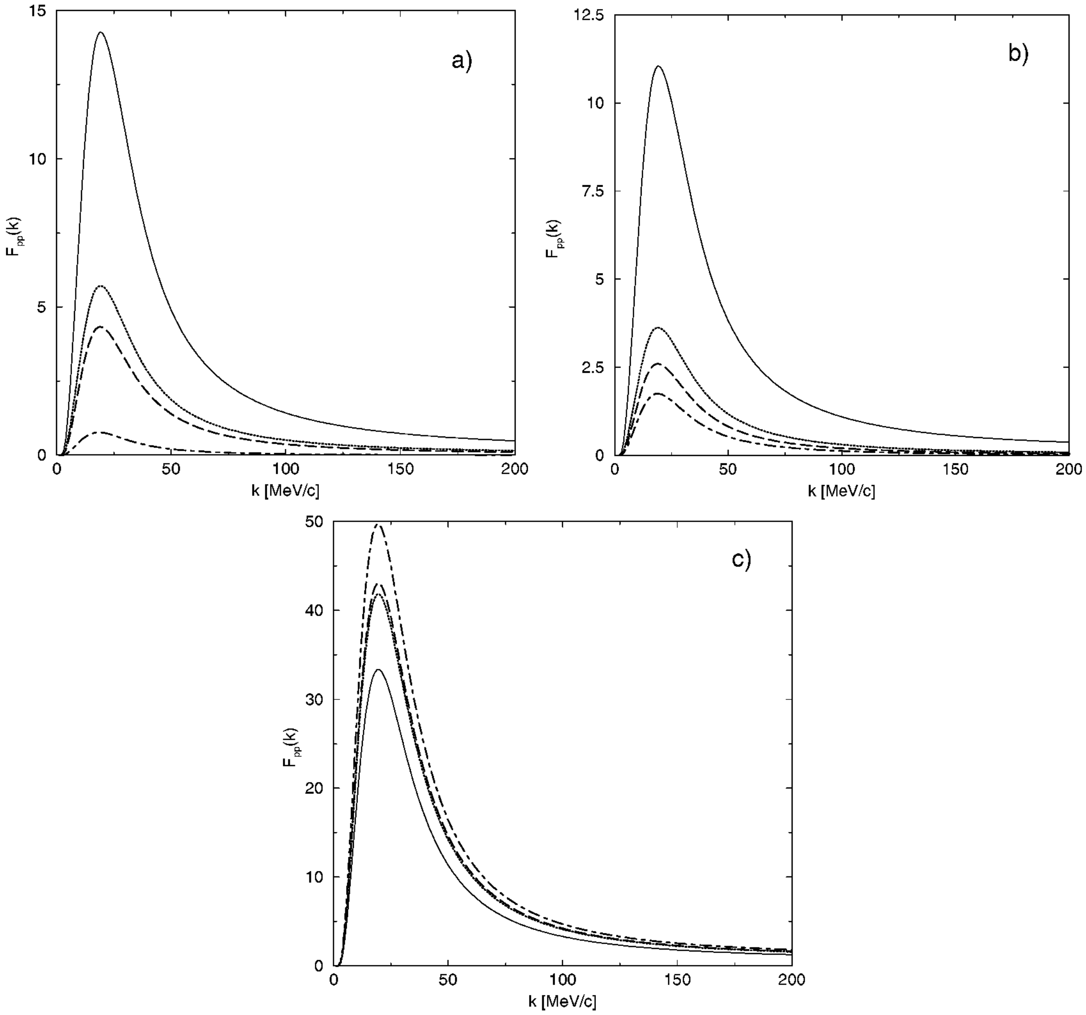

Figure 4.4: The FSI factor $F_{pp} = |\Psi(k)|^2$ (cf. Eq. (4.16)) for the Paris (a), Bonn (b), and the Yamaguchi (c) potentials and the production of the π (solid curve), η (dotted curve), and η' (dashed curve) mesons. The dash-dotted lines are the results based on the factorization assumption Eq. (4.3), i.e. $F_{pp}(k) = |\mathcal{J}(k)|^{-2}$. Note that different scales are used for each NN model!

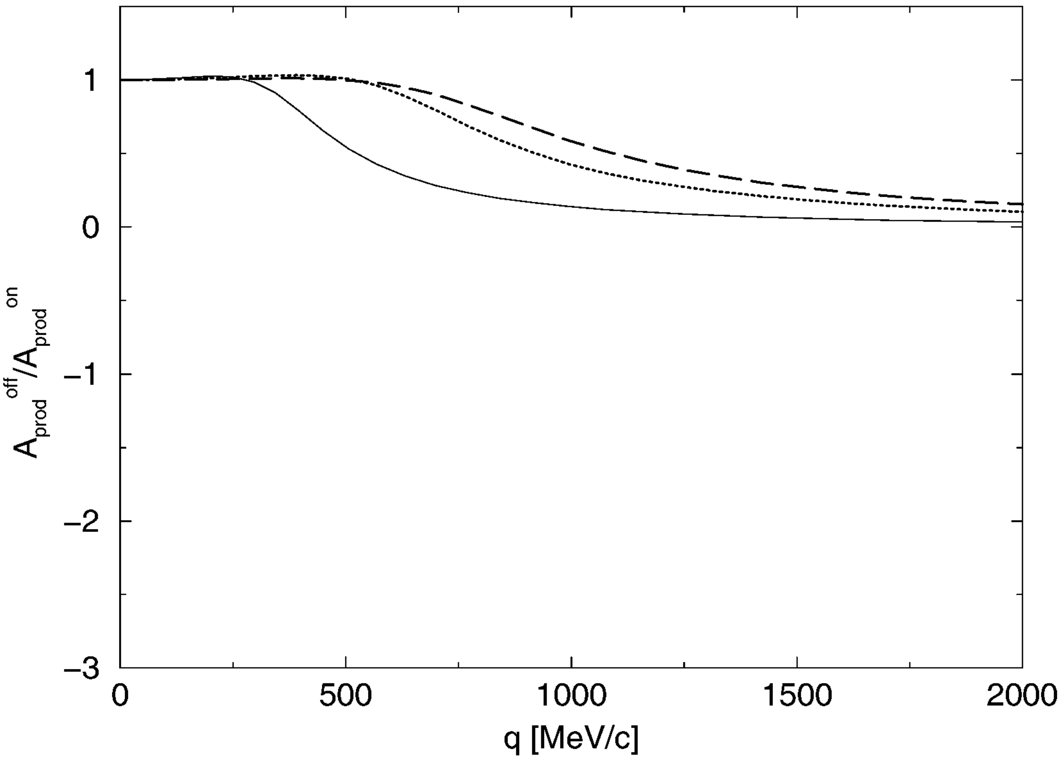

Figure 4.5: Ratio $A^{off}_{prod}/A^{on}_{prod}$ of the production amplitude as a function of the off-shell momentum q calculated at the fixed on-shell momentum $k = 0$ MeV/c. The solid, dotted and dashed curves correspond to the production of the π, η, and η' mesons, respectively.

short-ranged. As a consequence the production amplitude remains a constant over a larger (off-shell) momentum range, as can be seen in Fig. 4.5. This feature enhances the cancellation effects for the Bonn and Paris NN T-matrices, discussed above, and therefore leads to a reduction of F_{NN} for larger meson masses. In case of the Yamaguchi potential no such cancellations can occur and therefore the FSI factor turns out to be almost independent of the mass of the produced meson. Nevertheless, we see that also for realistic NN potentials the FSI factors become more and more similar with increasing mass of the produced meson, i.e. for high momentum transfers. This is expected. It simply reflects the universality of FSI effects for the production of heavy mesons as discussed above. We would like to emphasize that the universality of FSI effects at large t should set in not only for the particular production amplitude used in the present investigation (cf. Eq.

(4.9)), but is expected to occur in general. Actually, we examined the behavior of F_{NN} for the OBE-type production amplitude Eq. (4.9) with inclusion of form factors of monopole and dipole type

$$F(q) = \left(\frac{\Lambda^2 - \mu_{ex}^2}{\Lambda^2 + \vec{q}_{ex}^2}\right)^{\alpha}, \quad \alpha = 1, 2 \tag{4.17}$$

at the $NN\mu$ vertex. Corresponding numerical calculations clearly indicate that the qualitative behavior of the FSI factors remains basically unchanged.

However, it is important to realize that the actual values for the FSI factors do, of course, depend on the particular production amplitude. Thus, the results presented in Figs. 4.4 are *by not means* absolute predictions that can be taken from here and used blindly for FSI corrections in any other study of meson production. Rather our results demonstrate that FSI effects have to be calculated always explicitly, utilizing the respective production amplitudes and a proper NN off-shell T-matrix, if one wants to obtain reliable quantitative predictions. Specifically, this means that the apparent universality of the FSI effects for large meson masses *does not* imply that one can use the prescription applied in the studies [87, 89–91], i.e. take the production amplitude out of the integral in Eq. (4.16). Even though the factor $\Psi(k)$ becomes independent of the mass of the produced meson its actual magnitude is still determined by the off-shell properties of the NN T-matrix as well as by the production amplitude. In order to demonstrate this we show also results based on the factorization assumption Eq. (4.3) (dash-dotted curves). In this case the FSI factor is simply given by the enhancement factor $F_{NN}(k) = \mid \mathcal{J}(k) \mid^{-2}$. It is really startling how strongly the results for the Yamaguchi potential and for realistic NN interaction models differ. For the former potential the enhancement factor based on the Jost function is larger than the FSI factor obtained from Eq. (4.2) whereas for the latter models it turns out to be much smaller than the DWBA values. Clearly, these results suggest that it is rather questionable to use the Jost function of some arbitrary potentials for the evaluation of FSI effects in meson-production reactions [87, 89–91].

Finally a remark on the differences between the results for realistic NN models. Obviously these are small (about 20 %) for the pion-production case. But for the η' meson the Paris result is almost a factor 2 larger then the one for the

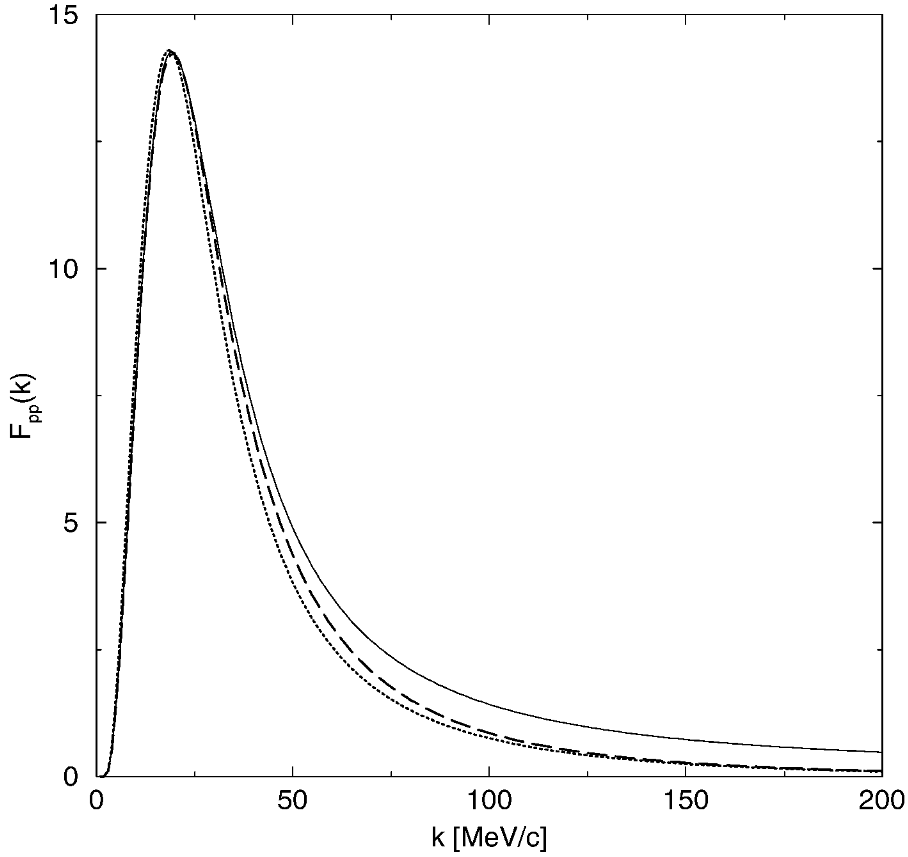

Figure 4.6: The FSI factor $F_{pp} = |\ \Psi(k)\ |^2$ for the Paris NN potential and for pion production (solid line) in comparison to results based on the approximations Eqs. (4.1) (dashed line) and (4.3) (dotted line). The latter two curves are normalized to the one of the Paris potential at the peak ($k \approx 20$ MeV/c).

Bonn model. This is not too surprising because for the production of heavier mesons a larger momentum transfer is required and therefore the features of the NN interaction at shorter distances (or larger off-shell momenta) become more and more important in the actual calculations. As we can see in Fig. 4.2 there are fairly large differences in the off-shell properties of these two models for large off-shell momenta.

By all the variations we see in the magnitudes of the FSI factors presented in Fig. 4.4 we would like to point out that their energy dependence is basically the same for all the different potentials and for the different meson masses. If we normalize them to the same value for small k (e. g., at the peak of F_{NN} at $k \approx 20$ MeV/c) all curves would lie essentially on top of each other. This means that the energy dependence of the FSI factors is really primarily determined by the on-shell NN T-matrix. Consequently, the on-shell prescription Eq. (4.1) is indeed a fairly good approximation, at least for energies near the production threshold. In order to demonstrate this let us compare one of the curves based on the Paris potential with the result corresponding to Eq. (4.1) (normalized to the Paris curve at $k \approx 20$ MeV/c), cf. Fig. 4.6. None-the-less, we do observe an increasing difference between these two curves for $k \geq 50$ MeV/c, which corresponds to excess (cms) energies $Q \geq 3$ MeV. For $k = 100$ MeV/c ($Q \approx 10$ MeV) the curves differ already by a factor of around 2. It is interesting to see that the Jost function approach (Eq. (4.3)) deviates even more strongly from the correct results than the on-shell approximation in the energy range $k \leq 100$ MeV/c.

Let us now investigate the origin of those discrepancies in more detail. For that purpose we re-write the amplitude $\mathcal{M}$ of Eq. (4.2) in the form given in Ref. [40]

$$\begin{aligned}
\mathcal{M} &= -A^{on}_{prod}\frac{e^{i\delta}\sin\delta}{ka_{pp}} \cdot [P(k) - a_{pp}\ k\ \cot\delta] \\
&= -A^{on}_{prod}\frac{e^{i\delta}\sin\delta}{ka_{pp}} \cdot [P(k) + 1 - 1/2 a_{pp} r_0 k^2 + O(k^4) + ...] \qquad (4.18)
\end{aligned}$$

Here $P(k)$ is proportional to the principal value of the loop integral (cf. Fig. 4.3b) and contains the information on the off-shell behavior of both A_{prod} and T_{NN}. (Note that we have neglected corrections coming from the Coulomb interaction in Eq. (4.18) for simplicity reasons. Those terms don't play a role anymore at the energies were the discrepancies discussed above occur.)

Evidently corrections to the simple on-shell prescription Eq. (4.1) come from the energy dependence of the function $P(k)$ as well as from the $\cot\delta$ term. Actual calculations with the NN potentials utilized in the present study revealed that the value of $P(k)$ at $k = 0$ is positive and about 3 to 5 units large which makes it to be the dominant piece of the terms in the bracket of Eq. (4.18). Furthermore, $P(k)$ is slowly decreasing with k. The k^2 term is slowly increasing with k (Note that a_{pp} is negative for the $^1S_0$ partial wave!) so that there is a compensation in the energy dependence of the terms in the brackets of Eq. (4.18). This circumstance is certainly partly responsible for the fact that Eq. (4.1) works relatively well.

As already mentioned above, the value at $P(k = 0)$ is positive and fairly large (cf. also the comments in Ref. [40]). Note that in order to get Eq. (4.1) with the normalization N set to one, as chosen in Refs. [22, 85], we have to assume that $P(k) \equiv 0$ and omit all the terms proportional to k^2, k^4, etc., in the square brackets on the r.h.s. of Eq. (4.18). Therefore, this particular normalization can be only obtained under very specific conditions, cf. the discussion in the Appendix of Ref. [98].

4.4 FSI in the reactions with the $\eta(\eta')$-meson production. Influence of the mass of the exchanged meson.

Besides the dependence of the FSI effects on the mass of the produced meson and the features of the NN interaction it is also interesting to examine the influence of the production mechanism, specifically of the mass of the exchanged meson. Therefore, in this subsection we want to consider the production of a meson with a fixed mass m_x and present some results for the dependence of the FSI factor on the mass of the exchanged meson. For the production of heavier mesons (for instance for η, η', ...) we find that the absolute magnitude of the FSI factor depends rather weakly on the mass of the exchanged meson m_μ, cf. Fig. 4.7. It may be understood qualitatively from an analysis of Eq. (4.16). The mass m_μ of the exchange particle enters in the coefficient in front of the integral and also in $\tilde{\lambda}^2$. The latter is responsible for cutting off the integral in Eq. (4.16) at higher momenta. When m_μ is increased the integral obtains more contributions from higher momenta. Due to this the cancellation of negative and positive regions is increased and, consequently, the magnitude of the integral is reduced. However, at the same time the coefficient in front of the integral increases with growing of m_μ. The numerical calculation shows that these opposite effects basically cancel each other. Anyway, the limiting case when $m_x \gg m$, which was already discussed above, also demonstrates the independence of the FSI factor on the mass m_μ.

In principle, the observations discussed so far in this subsection have only quali-

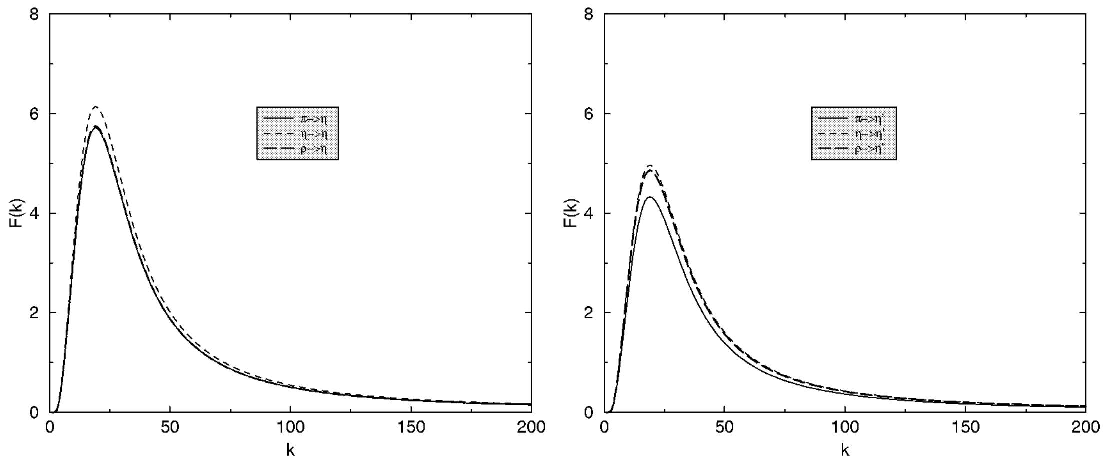

Figure 4.7: The FSI factor $F_{pp} = \mid \Psi(k) \mid^2$ (cf. Eq. (4.16)) for the Paris potential and the production of the η and η' mesons calculated with the different meson exchanges (see notation in the figure).

tative character because the full dynamics of the meson-nucleon amplitudes and the specific structure of the involved meson-baryon vertices were not taken into account. However, a realistic calculation of the η-meson production involving microscopic NN and MN models confirms that the results discussed above are not far from the reality. Let us consider FSI factors calculated for the reaction $pp \to pp\eta$ for different meson-exchange contributions (see Fig.4.8), and utilizing the Bonn B NN potential [59] and the Jülich MN model [36]. As one can see from Fig.4.8 the full dynamical calculation of the η-production process yields values of the FSI factors for the different meson exchanges that are close to each other. This is in line with a conclusion made on the basis of a qualitative analysis. We would like to emphasize, however, that the main reason for this are the very similar off-shell properties of the different $MN \to \eta N$ T-matrices ($M = \pi$, ρ, η, σ) as is illustrated in Fig. 4.9. Finally, note that the absolute magnitude of the FSI effect in the dynamical calculation increases compared to the curves in Fig. 4.7 because the off-shell MN T-matrix reduces the cancellation effect discussed in section 4.3.

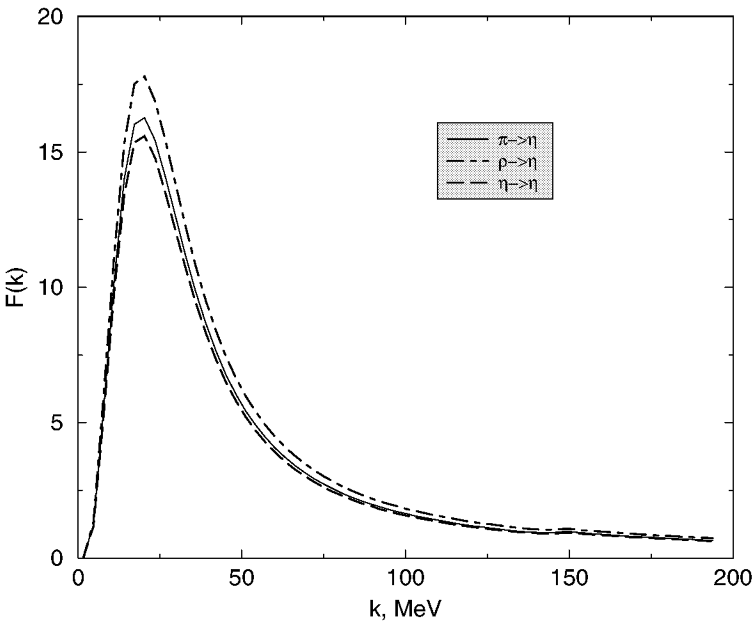

Figure 4.8: FSI factors calculated for our η-production model for the different meson exchanges. The full curve corresponds to the π exchange, the dot-dashed one to the ρ and the dashed one to the η. The curve for the σ meson lies just on the top of the one for the ρ and is not shown.

4.5 Conclusions

In the present chapter we have studied some aspects of effects from the final state interaction in the meson-production reaction $NN \to NNx$ near threshold. Specifically, we have demonstrated that the NN FSI cannot be factorized from the production amplitude if one wants to obtain reliable quantitative predictions. This conclusion confirms the arguments given in the paper [40]. Furthermore, we have demonstrated that the absolute value of the FSI factor depends on the momentum transfer, i.e. on the mass of the produced meson. It is not universal! Only for large momentum transfers, i.e. for the production of heavy mesons, the FSI factor is getting independent of the mass of the produced meson. We have shown that the use of the Jost function of both realistic and some arbitrary potentials for the evaluation of FSI effects is rather questionable and may lead to the results considerably different from the ones of correct calculation. In particular, the use of

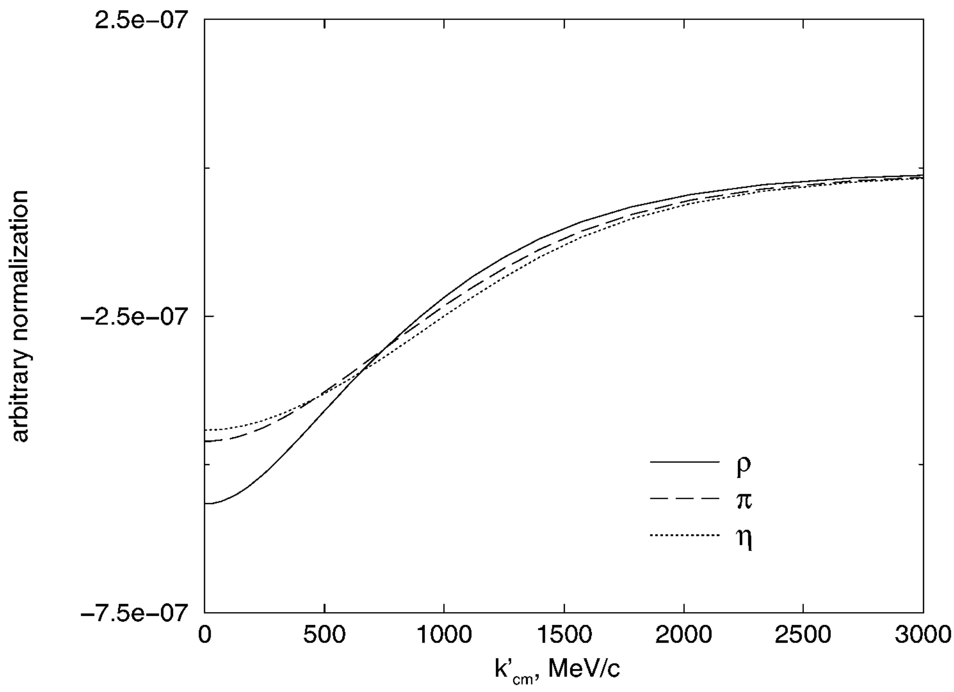

Figure 4.9: Off-shell behavior of the $MN \to \eta N$ T-matrices as a function of final cm momentum k'.

the Jost function of the Bonn and the Paris NN potentials leads to a considerable underestimation of FSI effects. We also would like to point out that the energy dependence of FSI effects looks very similar for all considered NN potentials and for the different meson masses. The classical approach of Migdal and Watson also works, however, only for a limited energy range near the threshold. Finally, it was noted that for the production of heavier mesons (like η, η' etc.) in the reaction $pp \to ppx$ the absolute magnitude of the FSI factors is almost independent of the type of the exchanged meson. This phenomenon was first observed in a simple model but then also confirmed in a realistic calculation involving all dynamical ingredients such as the NN and MN T-matrices as well as MNN vertices.

Chapter 5

$a_0^-(980)$ production in the reaction $pd \to ppa_0^- p_s$ close to threshold

5.1 Introduction

In this chapter we would like to concentrate on the production of a_0^- mesons in NN collisions. We will present a qualitative estimation of the a_0^- cross section in the reaction $pn \to ppa_0^-$ and discuss the importance of an experimental measurement of this reaction.

The understanding of the structure of the lightest scalar mesons $f_0(980)I^G(J^{PC}) = 0^+(0^{++})$ and $a_0(980)1^-(0^{++})$ poses one of the most fundamental problems in physics of hadrons. Both these mesons are strongly coupled to the $K\bar{K}$-channel and have practically equal masses.

The standard interpretation consists in viewing these mesons as $q\bar{q}$-states [99,100]. The authors of paper [100] have suggested, that the $f_0(980)$ is a mixture of $u\bar{u}$, $d\bar{d}$ and $s\bar{s}$-states. At the same time the $a_0(980)$ was build from non-strange quarks only. There exist also attempts to build the $f_0(980)$ from $s\bar{s}$-component only [101,102], in analogy to the nearby almost $s\bar{s}$ meson $\phi(1020)$. The coupling of the $f_0(980)$ to the non-strange sector in this model is due to nonperturbative QCD effects. Note that in line with the models [99–102] it is difficult to explain the practical coincidence of the masses for the $f_0(980)$- and $a_0(980)$-mesons. Another possibility is the four-quarks $qq\bar{q}\bar{q}$ model for the lightest scalar mesons proposed in Ref. [103]. This model could explain the mass degeneration for these mesons and their large branching into the $K\bar{K}$-channel.

In Gribov's confinement model [104] the a_0 and f_0 are rather exceptional mesons and their properties should differ from the predictions of more standard quark models like [99–101, 103]. In particular, in Gribov's model the interaction cross sections of the a_0- and f_0-mesons with hadrons should be small.

There is also a "hadron molecular" model, in which both mesons are build from a K and $\bar{K}$ state [105]. The authors of the papers [106, 107] have developed a meson-exchange model to describe the $f_0(980)$- and $a_0(980)$-mesons. In their approach both these mesons originate from the coupling of the $\pi\pi$-channel to the $K\bar{K}$-channel. But in contrast with the $f_0(980)$, the $a_0(980)$ would not appear to be a $K\bar{K}$ bound state but a dynamically generated threshold effect with a relatively broad structure ($\Gamma_{a_0} \approx 200 MeV, \bar{m}_{a_0} \approx 990 MeV$). Note, that different approaches give different predictions for the properties of the a_0- and f_0-mesons. So, a precision measurement of the parameters for the lightest scalar mesons may solve the problem of their nature.

Note, that the proposal to study properties of the a_0^+-meson in the reaction $pp \to da_0^+$ at the ANKE spectrometer of COSY was discussed already in detail in ref. [108]. Here we discuss the possibility to study the reaction $pd \to ppa_0^- p_s$ to get informations on the properties of the negative a_0^--meson. The investigation of the neutral a_0 is more complicated since it is strongly mixed with $f_0(980)$ due to coupling with $K\bar{K}$ state. Therefore it is much more interesting to study the charged a_0 mesons to investigate their genuine quark content.

The resonance $a_0^-(980)$ was observed for the first time in the reaction $K^-p \to \Sigma^+(1385)\eta\pi^-$ [109]. This meson manifests itself as a sharp peak in the $\pi^-\eta$-effective mass distribution. The mass of the a_0^- was found to be $\bar{m} = 981$ MeV and the visible width of the peak to be around 50 MeV. The experimental data of the paper [109] were analyzed in ref. [110]. In that paper a two-channel parameterization for the S-matrix was used to get information on the parameters of the a_0^- meson. It was found, that the visible width of the peak $\Gamma_{vis} \approx 50$ MeV is smaller than the bare width $\Gamma_{\pi\eta}$ for the decay of the a_0 into the $\pi\eta$-channel ($\Gamma_{\pi\eta} \approx$

80 MeV). The inequality $\Gamma_{vis} < \Gamma_{\pi\eta}$ is a consequence of the $K\bar{K}$-threshold. The $a_0(980)$ meson is strongly coupled to the $K\bar{K}$ system and the $K\bar{K}$ threshold is located only 10 MeV above the position of the peak. Because of this the form of the peak is not of Breit-Wigner type but is strongly affected by the $K\bar{K}$-threshold. Note, that in the four-quark model [103] the bare width $\Gamma_{\pi\eta}$ should be much larger, namely of the order of 300 MeV, see in this context also ref. [111]. That is why the form of the peak is sensitive to the quark content of the $a_0(980)$-meson.

Note, that the experimental data [109] are not in contradiction to the following ratio for the coupling constants:

$$d = \frac{g^2_{a_0^- K^- K^0}}{g^2_{a_0^- \pi^- \eta}} = \frac{3}{2}. \tag{5.1}$$

This value for d corresponds to the assumption that the a_0 belongs to the lowest $SU(3)$ octet of scalar mesons and that the $\eta - \eta'$ mixing angle is zero, $\theta_{\eta\eta'} = 0$. Note, that in the 1^3P_0 $q\bar{q}$-nonet interpretation of the a_0 [100] the ratio d is:

$$d = \frac{\lambda}{2cos^2(\theta_{\eta\eta'})},$$

where $\lambda \approx 0.6$. That is why the branching ratio of the a_0-meson into the $K\bar{K}$-channel is relatively suppressed in this model in comparison to the predictions of the $SU(3)$-octet approach ($d \approx 0.8$ in [100]). Recent experimental data on a_0-production in the $\pi^- p$-collisions [112] give evidence for the ratio d to be close to unity. In particular, it follows from the analysis of ref. [112], that the charged a_0^+ has a slightly larger mass than the neutral one, namely $\bar{m} = (998 \pm 4) MeV/c^2$. Its width is $\Gamma(a_0^+) = (69 \pm 11) MeV/c^2$ and the ratio $d = 0.91 \pm 0.11$. Note, that from the analysis of the paper [113] this ratio d is larger, $d = 1.16 \pm 0.18$. In the four-quark approach [103] the coupling to the $K\bar{K}$-channel has to be large. We conclude, that the ratio of the coupling constants is also very sensitive to the quark content of the $a_0(980)$ meson. Note, that in both experiments [109] and [112] only the $\pi\eta$ decay mode of a_0 was investigated whereas the branching ratio for charged a_0's was never measured directly.

In this investigation we suggest to extract the parameters of the $a_0^-(980)$ meson from measuring its production in nucleon-nucleon collisions [114][1]. To be more

[1]The a_0-meson production in pp and pn reactions is also studied in recent work [115].

concrete, we suggest to study the reaction $pn \to ppa_0^-$ using a deuterium target. To reconstruct the kinematics, one needs to measure all final protons for the reaction $pd \to ppa_0^- p_s$, where p_s is the proton-spectator momentum. At the same time both decay channels of the a_0^- contain negative particles and/or could be easily identified through the photons from η-decay. In the case of identification of both leading decay channels for the a_0^--meson the study of this reaction at the ANKE spectrometer of COSY should provide unique information on fundamental characteristics of this meson.

5.2 Total cross section for the reaction $pn \to ppa_0^-$.

Consider the process for exclusive production of a resonance meson[2] in NN collisions, i.e. the reaction

$$NN \to NNR.$$

As we will demonstrate, the results for the absolute value of the total cross section depend very drastically on the measured interval of mass for the resonance. The explanation is simple: in case of a threshold reaction $2 \to 3$ and under the constraint that the production amplitude is constant, the total cross section is proportional to Q^2, where Q is the excess energy. Therefore the production of a meson with mass lighter than the nominal mass is getting more preferable. Let us illustrate this by some concrete formulae. In the case of the production of a stable particle of mass m in the pp-collision ($pp \to pp$ + "stable particle") we get the following expression for the diproton mass spectrum near threshold (the production amplitude is suggested to be constant!):

$$\frac{d\sigma}{dm_{pp}} \propto F(k)k\sqrt{Qm_p - k^2} \tag{5.2}$$

Here $F(k)$ is the pp enhancement factor [40, 87, 88], k is the relative momentum of the final protons, and $m_{pp} = 2m_p + k^2/m_p$. If we consider the production of a meson with finite width Γ, we should convolute the expression (5.2) with the

[2]By "resonance" mesons we mean mesons with relatively large width

spectral density $\rho(m,\Gamma)$. For a narrow resonance it can be parameterized by a Breit-Wigner (BW) function

$$\rho(m,\Gamma) = \frac{\Gamma/2\pi}{(m-\bar{m})^2 + \Gamma^2/4}, \tag{5.3}$$

where $\bar{m}$ is the averaged (nominal) mass of the unstable particle. Thus, instead of (5.2) we get

$$\frac{d\sigma}{dm_{pp}} \propto F(k)k \int_{m_{min}}^{m_{max}} dm \frac{\Gamma/2\pi}{(m-\bar{m})^2 + \Gamma^2/4} \sqrt{m_p(Q+\bar{m}-m-k^2/m_p)}, \tag{5.4}$$

where $Q = \sqrt{s} - 2m_p - \bar{m}$ is the nominal excess energy, $m_{max} = Q + \bar{m} - k^2/m_p$ and the value of the minimal mass m_{min} should be discussed more attentively. Since the absolute value of the cross section for the production of resonance mesons depends on the interval of measured a_0 mass in the concrete experiment, we introduce this lower limit m_{min} which should be fixed by experimental setup. From our point of view it seems to be more preferable to perform this measurement in the rather narrow interval of mass not far from the peak of the resonance, $\bar{m}$, i.e. choosing, for instance, $m_{min} \sim \bar{m} - \Gamma$. This specific choice is related with the fact that experimental observables like $\frac{d\sigma}{dm_{pp}}$ from eq.(5.4) should strongly depend on the region of large momenta k (or light mass m). Really, the lighter mass of a_0 contributing to the square root of eq.(5.4) the larger momentum k is taken into account. However, the cross section in the region of large momenta depends significantly on the dynamical properties of the production mechanism (on the A_{prod} as a function of k) and is therefore model-dependent.

Let us illustrate the dependence of the integral in eq.(5.4) on the m_{min} a little bit more concretely. Rewriting the integral in (5.4) in dimensionless variables we get

$$\frac{d\sigma}{dm_{pp}} \propto F(k)kI(x_0); \tag{5.5}$$

where

$$I(x_0) = \frac{1}{\pi} \int_0^{x_{max}} \frac{\sqrt{x}dx}{(x-x_0)^2+1}. \tag{5.6}$$

Here we introduced the notations

$$x_0 = \frac{Q-k^2/m_p}{\Gamma/2}, \qquad x_{max} = \frac{Q+\bar{m}-m_{min}-k^2/m_p}{\Gamma/2}.$$

As is seen from the BW-formula (5.3), the probability to find a very light a_0 is small. So it seems, that the diproton mass spectrum should not be sensitive to the choice of m_{min}. But this is not a correct statement. Indeed, in view of the fact that the leading decay channel for a_0^--meson is $a_0^- \to \pi^-\eta$, let us choose $m_{min} = m_\pi + m_\eta$. Doing so, we obtain that $I(x_0)$ is a smoothly decreasing function for large negative x_0. Thus, the distribution (5.5) for $\frac{d\sigma}{dm_{pp}}$ has a long tail in the

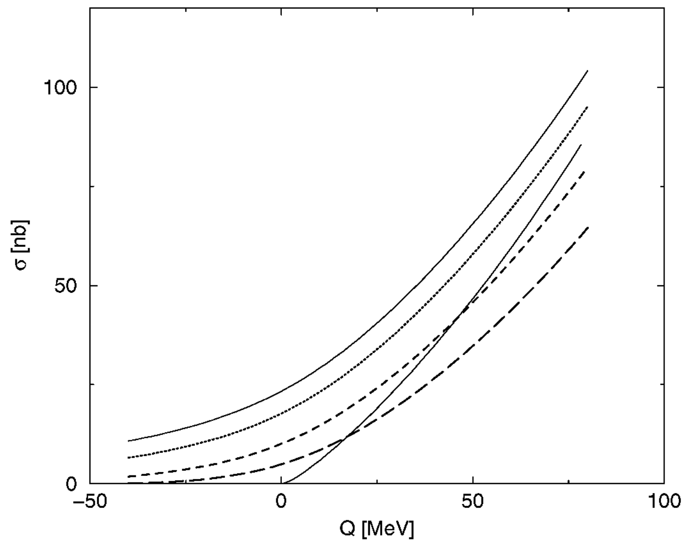

Figure 5.1: Total cross section for the reaction $pn \to ppa_0^-$ versus excess energy Q for different values of $m_{min} = \bar{m} - C$. Solid line $C = 290$ MeV; dotted line $C = 200$ MeV; dashed line $C = 100$ MeV; long-dashed line $C = 50$ MeV. $\Gamma = 50$ MeV for all curves. The curve for the production cross section in the case of a stable a_0-meson is also shown.

region of large momenta k ($k^2 \gg m_p Q$ (i.e. for $m \ll \bar{m}$)) and the total cross section depends essentially on the chosen value of m_{min}. In Figure 5.1 we give the dependence of the total cross section for the reaction $pn \to ppa_0^-$ for some specific values of the minimal mass $m_{min} = \bar{m} - C$. The production amplitude is calculated in a simple fusion model and is discussed in the next Section. Fig. 5.1 demonstrates the drastic dependence of the production cross section on the value of the parameter C, i.e. on the minimial mass of a_0 measured in the concrete experiment. Again, the contribution from the region of the resonance peak with $\mid m - \bar{m} \mid \leq \Gamma/2$ to this cross section corresponds to the choice of the parameter

$C \leq \Gamma$.

5.3 Production amplitude for the reaction $pn \to ppa_0^-$

For estimating the production amplitude for the reaction $pn \to ppa_0^-$ close to threshold we use a simple fusion model with intermediate η- and π-mesons. The advantage of this approach is that the result can be expressed in terms of the experimental observables so that the model does not contain free parameters. The corresponding Feynman diagram is shown in Fig. 5.2. We use the following values

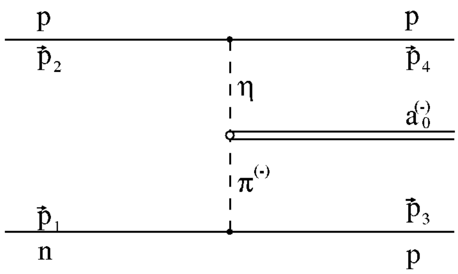

Figure 5.2: Feynman diagram for the production amplitude of the reaction $pn \to ppa_0^-$.

for the πNN and ηNN coupling constants [35]: $g^2_{\pi NN}/4\pi = 14.6$, $g^2_{\eta NN}/4\pi = 3.0$. The $a_0\eta\pi$ coupling constant is determined from the relation

$$\Gamma_{\pi\eta} = \frac{g^2_{a_0\pi\eta}}{8\pi} q_{\pi\eta}, \tag{5.7}$$

where $q_{\pi\eta}$ is the relative $\eta\pi$ momentum. For the bare partial width $\Gamma_{\pi\eta}$= 80 MeV we obtain from (5.7) that $g_{a_0\eta\pi} = 2.5$.

The amplitude M_{34} which corresponds to the Feynman graph of Fig. 5.2 is

$$M_{34} = \sqrt{2}\frac{g_{\eta NN} F_\eta(q_1^2)}{2m_p}\frac{g_{\pi NN} F_\pi(q^2)}{2m_p} g_{\pi\eta a_0} \bar{m} \frac{\bar{u}(p_3)\gamma^5 \hat{q} u(p_1)\bar{u}(p_4)\gamma^5 \hat{q}_1 u(p_2)}{(q^2 - m_\pi^2)(q_1^2 - m_\eta^2)}. \tag{5.8}$$

Here $\bar{m}$ =983.4 MeV is the nominal mass of the a_0 meson and $F_{\pi,\eta}$ are form factors which are assumed to be given by

$$F_i(q^2) = \frac{\Lambda_i^2 - m_i^2}{\Lambda_i^2 - q^2}, \quad i = \pi, \eta. \tag{5.9}$$

We take $\Lambda_\pi = 1300$ MeV and $\Lambda_\eta = 1500$ MeV, in accordance with the Bonn B potential model [59]. The total production amplitude has to be antisymmetrized with respect to spin and space variables of the final protons ($34 \to 43$). Finally, for the averaged production matrix element we get

$$\mid \bar{M} \mid^2 = g_{\pi NN}^2 g_{\eta NN}^2 g_{a_0\pi\eta}^2 \frac{F_\pi^2(q^2) F_\eta^2(q_1^2) m_p^2 \bar{m}^4}{(q^2 - m_\pi^2)^2 (q_1^2 - m_\eta^2)^2}, \tag{5.10}$$

where $q^2 = q_1^2 = -m_p\bar{m}$. Taking into account the strong final state interaction between the final protons (via the enhancement factor $F(k)$), we get the following expression for the production cross section

$$\sigma_{pn\to ppa_0} = \frac{\mid \bar{M} \mid^2}{4I} \frac{1}{8\pi^3(2m_p + \bar{m})} \sqrt{\frac{2\mu_3}{m_p^3}}\, \Phi(Q, \Gamma), \tag{5.11}$$

where

$$\Phi(Q,\Gamma) = \int_0^{k_{max}} dk F(k) k^2 \int_{m_{min}}^{m_{max}} \frac{dm\ \Gamma/2\pi}{(m - \bar{m})^2 + \Gamma^2/4} \sqrt{m_p(Q + \bar{m} - m - k^2/m_p)},$$

$m_{min} = \bar{m} - C$, $m_{max} = Q + \bar{m} - k^2/m_p$, $k_{max} = \sqrt{m_p(Q + \bar{m} - m_{min})}$,
$\mu_3 = 2m_p\bar{m}/(2m_p + \bar{m})$, $I = 2E_1 \mid \vec{p}_1 \mid = (2m_p + \bar{m})\sqrt{\bar{m}(\bar{m} + 4m_p)}/2$.

The momentum dependence of the *pp* enhancement factor $F(k)$ was discussed in detail in chapter 4. For reactions with high momentum transfer like $NN \to NN\pi, NN\eta, NN\eta'$, etc. its momentum dependence is practically not sensitive to any concrete form of production amplitude. At the same time the absolute value of the enhancement factor depends on the features of the production amplitude and also on the mass of the emitted particle, as was recently clarified in refs. [40, 42] (see also chapter 4). In our treatment we use the *pp* enhancement factor $F_{Ya}(k)$ calculated with a separable Yamaguchi potential [87]. The absolute value of the enhancement factor is obtained by introducing a rescaling factor ξ, so that

$$F(k) = \xi F_{Ya}(k).$$

The factor ξ is chosen in such a way that the absolute value of the enhancement factor $F(k)$ agrees with those obtained for realistic NN models such as the Bonn or Paris potentials. In line with our estimations in chapter 4 we take $\xi = 1/5$.

The resulting cross section versus the excess energy Q is shown in Fig. 5.1 for different values of C. The expression (5.11) for the cross section ignores the influence of the $K\bar{K}$ threshold. To get the expressions for the partial cross sections $pn \to ppK^-K^0$ and $pn \to pp\pi^-\eta$ we substitute the spectral density in Eq. (5.3) by

$$\rho(m, \Gamma(m)) = \frac{1}{2\pi} \frac{\Gamma_{\pi\eta} + \Gamma_{K\bar{K}}(m)}{\mid m - \bar{m} + i(\Gamma_{\pi\eta} + \Gamma_{K\bar{K}}(m))/2 \mid^2} \,. \tag{5.12}$$

In this formula we put again $\Gamma_{\pi\eta}$ to be constant, but include the dependence of $\Gamma_{K\bar{K}}$ on the mass, i.e.

$$\Gamma_{K\bar{K}} = \frac{g^2_{a_0 K\bar{K}}}{8\pi} \sqrt{2m_{K^-K^0}(m - m_{K^0} - m_{K^-})} \,, \tag{5.13}$$

where $m_{K^-K^0} = m_{K^-} m_{K^0}/(m_{K^-} + m_{K^0})$.

Results within this two-channel approach for the total and partial cross sections for the reaction $pn \to ppa_0^-$ are shown in Figs. 5.3 and 5.4, respectively, for different values of the ratio $d = g^2_{a_0^- K^- K^0}/g^2_{a_0^- \pi^- \eta} = 0,\ 3/2$ and 3. As can be seen from Fig. 5.3, the total cross section is getting smaller when $g_{a_0^- K^0 K^-}$ increases. This decrease of the cross section is a consequence of a destructive interference between the direct decay amplitude $a_0 \to \pi\eta$ and the amplitude for the decay $a_0 \to \pi\eta$ through the intermediate $K\bar{K}$-state.

5.4 How to extract parameters of the a_0^--meson from the experiment

We want to extract the following parameters for the a_0^--meson: Its average mass $\bar{m}$ and the coupling constants $g_{a_0\pi\eta}$ and $g_{a_0 K\bar{K}}$. These are the parameters which determine the form of the resonance peak.

The ratio of the coupling constants d (5.1) may be extracted from the direct

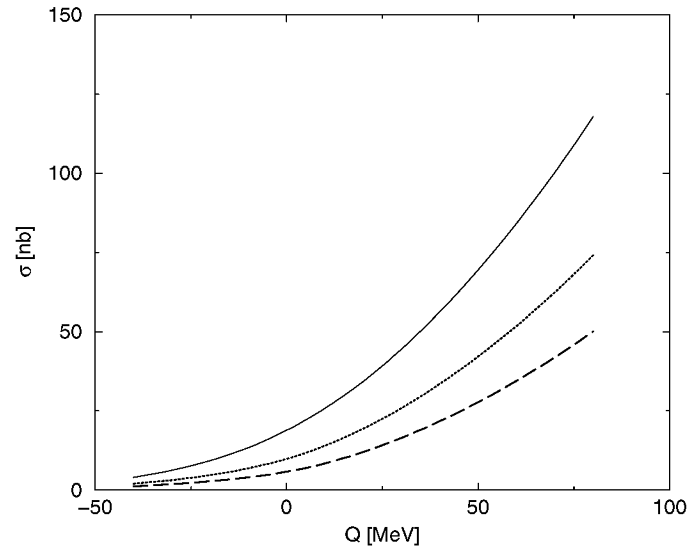

Figure 5.3: Total cross section for the reaction $pn \to ppa_0^-$ for different values of $d = g^2_{a_0^- K^- K^0}/g^2_{a_0^- \pi^- \eta}$. Solid line $d = 0$; dotted line $d = 1.5$; dashed line $d = 3.0$. $\Gamma_{\pi\eta} = 80$ MeV, $C = 100$ MeV for all considered cases.

measurement of the ratio for branchings at a fixed mass of a_0-meson:

$$\frac{Br(a_0 \to K\bar{K})}{Br(a_0 \to \pi\eta)} = \frac{g^2_{a_0 K\bar{K}}}{g^2_{a_0\pi\eta}} \frac{\sqrt{2m_{K^-K^0}(m - m_{K^0} - m_{K^-})}}{q_{\pi\eta}} \tag{5.14}$$

After getting the experimental information on the ratio (5.14) we have still to determine the two parameters $\bar{m}$ and $g_{a_0\pi\eta}$. We see two alternative ways how to extract these parameters.

i) Study of the effective mass spectrum. The distribution over the effective $\pi\eta$ mass is given by the following expression

$$\frac{d\sigma}{dm_{\pi\eta}} = \frac{|M|^2}{4I} \frac{\Gamma_{\pi\eta}}{8\pi^4 m_p \sqrt{s}} \sqrt{\frac{\bar{m}}{2m_p + \bar{m}}} \frac{1}{|m - \bar{m} + i\Gamma/2|^2} \int_0^{k_{max}} F(k) \sqrt{k^2_{max} - k^2}\, k^2 dk \tag{5.15}$$

where $k_{max} = \sqrt{m_p(Q - m + \bar{m})}$. In addition to the phase volume the dependence of expression (5.15) on the mass m comes from the enhancement factor $F(k)$ in the integral

$$\int_0^{k_{max}} F(k) \sqrt{k^2_{max} - k^2}\, k^2 dk \ . \tag{5.16}$$

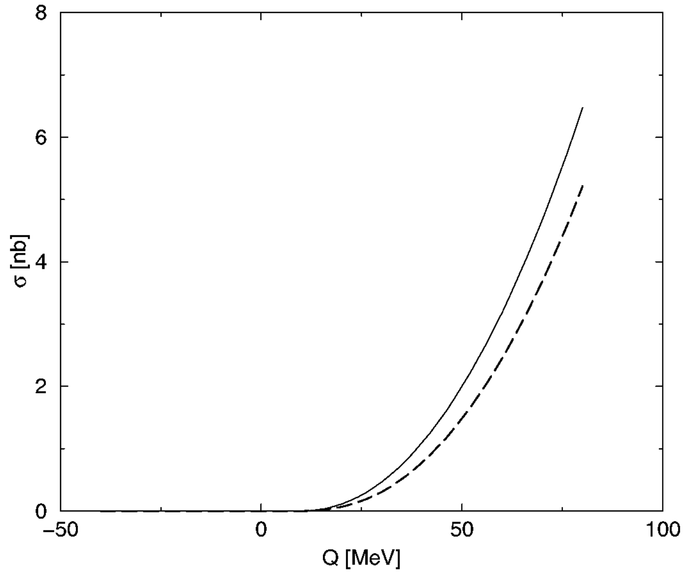

Figure 5.4: Partial cross sections $pn \to ppK^-K^0$ for different values of d. Solid line $d = 3.0$; dashed line $d = 1.0$. The values of Γ and C are the same as in Fig. 5.3.

The form of the resonance mass spectrum given by expression (5.15) is presented in Figs. 5.5 and 5.6 for different values of $\Gamma_{\pi\eta}$, the ratio d and the mass $\bar{m}$ of a_0. These figures illustrate the sensitivity of the mass spectrum to these parameters. Corresponding results for $d\sigma/dm_{K\bar{K}}$ for different values of d and $\Gamma_{\pi\eta}$ are presented in Fig. 5.7.

ii) Binnie's method. This method was introduced by Binnie et al. [116] to investigate the production of ω-, η- and η'-mesons in the reaction $\pi^- p \to nX$. It consists in studying the resonance excitation curve versus beam momentum under the condition that the momentum of the final neutron is kept fixed.

Considering the case of the reaction $pn \to ppa_0^-$, let us look at the expression for the following differential cross section:

$$\frac{d^6\sigma}{d^3k d^3P} = \frac{|M(E,\vec{P},\vec{k})|^2}{4I} \frac{F(k)}{(16\pi)^2 m_p \mu_3 \sqrt{s}} \frac{\Gamma_{\pi\eta}}{|Q - \vec{P}^2/2\mu_3 - \vec{k}^2/m_p + i\Gamma/2|^2} \quad (5.17)$$

where $\vec{P} = \vec{p}_3 + \vec{p}_4$, $2\vec{k} = \vec{p}_3 - \vec{p}_4$ and $\vec{p}_3$ and $\vec{p}_4$ are defined in Fig. (5.2). Let us also fix the absolute values of the momenta P and k in some small intervals ΔP^*

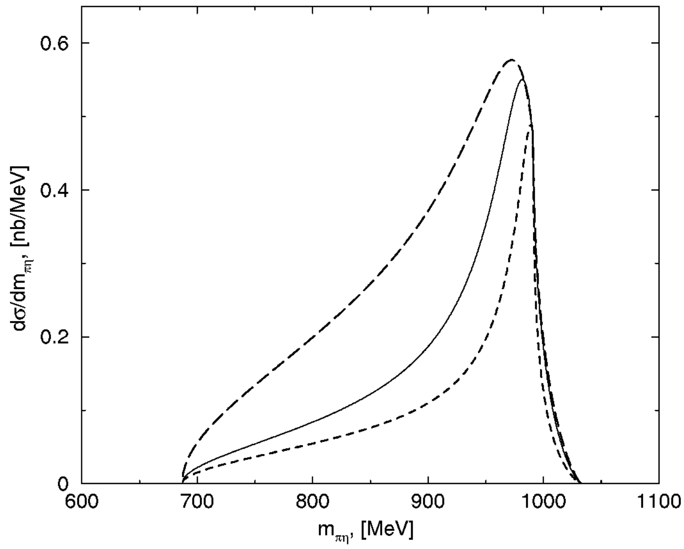

Figure 5.5: Differential cross section $d\sigma/dm_{\pi\eta}$ for different values of d and Γ. m_{a_0} is equal to 983.5 MeV. Solid line $\Gamma = 80$ MeV, $d = 1.5$; long-dashed line $\Gamma = 150$ MeV, $d = 1.5$; dashed line $\Gamma = 80$ MeV, $d = 3.0$. All curves correspond to $T_{lab} = 2636$ MeV.

and Δk^*.

In this case the dependence of the double differential cross section $d^2\sigma/dP^*dk^*$ is determined by the following equation:

$$d^2\sigma\,|_{P^*,k^*} = \frac{|M|^2}{4I}\frac{F(k^*)\Gamma_{\pi\eta}}{|Q - P^{*2}/2\mu_3 - k^{*2}/m_p + i\Gamma/2|^2}\frac{P^{*2}k^{*2}\Delta P^*\Delta k^*}{(2\pi)^4 m_p\mu_3\sqrt{s}} \tag{5.18}$$

As can be seen, the energy dependence of expression (5.18) is the same as the one of the cross section for a BW resonance. In order to apply this method for the production of a_0-meson, one needs to vary the beam energy and to study the curve of resonance excitation for the a_0-meson.

5.5 Some remarks on kinematics

In order to measure the reaction $pn \to ppa_0^-$ one needs to use a deuteron target, i.e. one has to study the reaction $pd \to ppa_0^- p_s$. We suggest to investigate this reaction for small momenta of the proton-spectator, $p_s \leq 200 MeV/c$. In Table

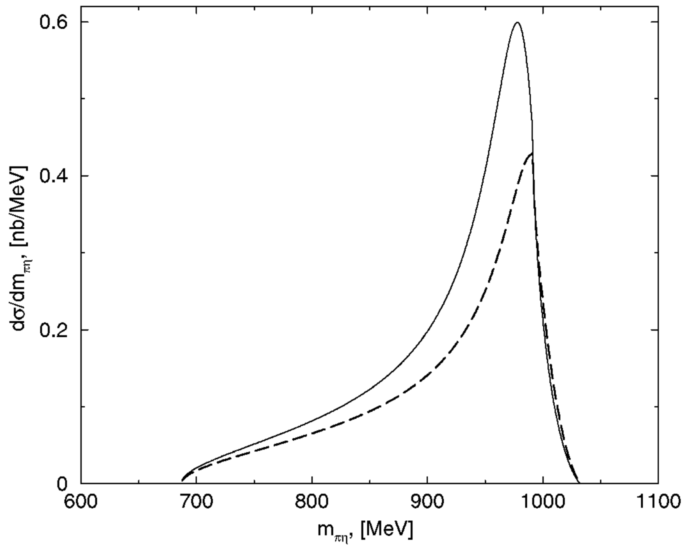

Figure 5.6: Differential cross section $d\sigma/dm_{\pi\eta}$ at different masses of a_0-meson but at fixed d and Γ (d= 0.91, Γ = 80 MeV). Solid line – m_{a_0} = 983.5 MeV, dashed line – m_{a_0} = 999 MeV.

5.1 we give the threshold energies for this reaction for some typical values of the spectator momentum. To estimate the production cross section on the deuteron, we assume a simple pole mechanism for this reaction. The corresponding Feynman diagram is shown in Fig. 5.8. Usually such a pole approximation works well up to spectator momenta of $p_s \leq 150 - 200 MeV$. In this region all re-scattering diagrams give negligible corrections to the leading pole term. The distribution over the spectator momentum corresponding to the pole mechanism of Fig. 5.8, is given by the expression

$$\frac{d\sigma}{d\vec{p}_s} = \mid \psi_d(\vec{p}_s) \mid^2 \sigma_{np \to ppa_0^-}(\sqrt{s'}) \ , \tag{5.19}$$

where $\psi_d(\vec{p}_s)$ is the deuteron wave function in the momentum space and the invariants s and s' are introduced for the reactions $pd \to ppa_0^- p_s$ and $pn \to ppa_0^-$, respectively. The relation between s and s' is determined by kinematics. The distribution over the proton spectator-momenta for $\sqrt{s'}$ being fixed is shown in Fig. 5.9. Note, that near the threshold the production cross section for the reaction $pn \to ppa_0^-$ is a rather sharp function of $\sqrt{s'}$. Therefore, the expression (5.19) at a fixed beam energy may be used to study the energy dependence of the cross

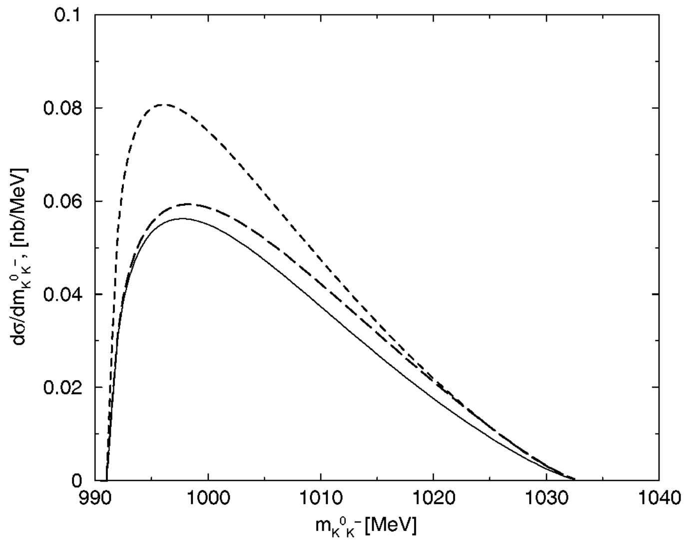

Figure 5.7: Differential cross section $d\sigma/dm_{K\bar{K}}$ at different values of d and Γ. m_{a_0} is equal to 983.5 MeV. The notation of the curves is given in the caption to Fig. 5.5.

section $pn \to ppa_0^-$.

$p_s(MeV/c)$	$\cos\vec{p}\vec{p}_s$	$T_p(MeV)$	$\sqrt{s_{a_0p_s}}(MeV)$
0	—	2454	2159
100	-1	2884	2268
100	0	2484	2169
100	1	2165	2080
200	-1	3538	2434
200	0	2577	2198
200	1	1971	2025
300	-1	4581	2678
300	0	2738	2248
300	1	1846	1987

Table 5.1: Some values of threshold energies T_p and $\sqrt{s_{a_0p_s}}$ are given for different momenta of proton-spectator.

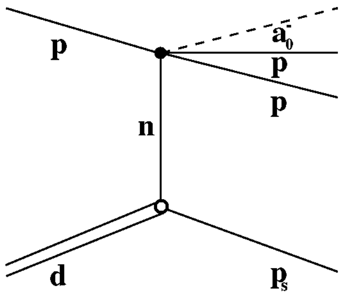

Figure 5.8: Feynman diagram for the reaction $pd \to ppa_0^- p_s$.

5.6 Is it possible to extract the a_0N-amplitude from the reaction $pd \to ppa_0p_s$?

The produced a_0^- interacts with the fast protons as well as with the slowly moving spectator. However, the interaction of the a_0 with the spectator should be evidently negligibly small in this kinematics. The main reason for this is that the produced a_0^- moves in forward direction with high momentum. Consequently, the total energy in the system "a_0 + spectator" is also large. In Table 5.1 we present values for the invariant energy $\sqrt{s_{a_0p_s}}$ for some typical values of the momenta and angles of the spectator. As can be seen from the Table, the typical values of $\sqrt{s_{a_0p_s}}$ are large, in particular much larger than $m_{a_0} + m_{p_s} = 1922$ MeV. That is why the interaction of the produced meson with the proton-spectator should have only a small influence on the reaction amplitude. A signal of this interaction may be found only in the case when the spectator moves along the direction of beam and has momenta > 300 MeV/c. Unfortunately, the number of events in this geometry is seriously limited because of the small probability to find a proton with a large momentum in the deuteron, see also Fig. 5.9. At the same time the interaction of the a_0 with a fast proton may be observed (provided that it is not negligibly small; in Gribov's approach it is small, see [104]). Near the threshold both the protons and the a_0 move slowly (in their rest frame). That is why the interaction between the a_0 and the proton can have an influence on the a_0p- and pp effective mass distributions. In the papers [87, 93] we gave some examples of

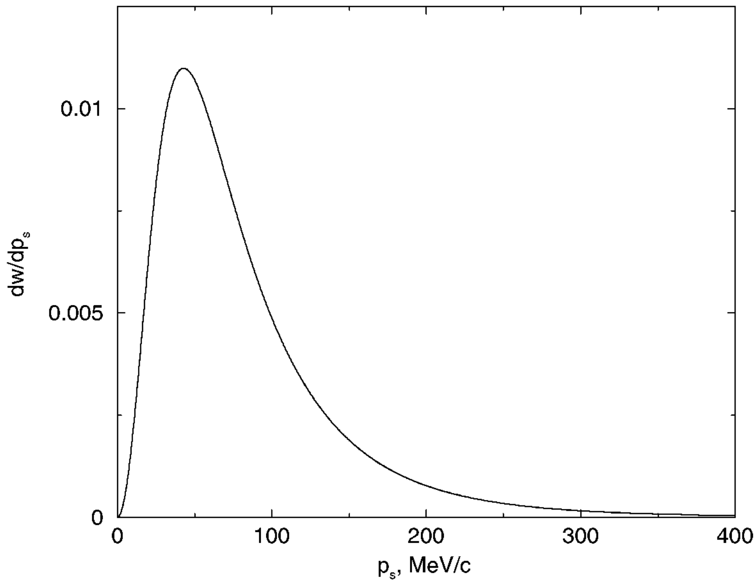

Figure 5.9: The distribution over the proton spectator-momentum for $\sqrt{s'}$ being fixed.

these distributions for the cases of η- and η' production in the pp collisions. In the case of a_0-production these distributions have to be corrected because of the (presumably) large width of the produced a_0 in comparison to those for η and η' cases.

In conclusion we would like to emphasize that the measurement of the momentum for fast protons simulteneously with the spectator momentum opens the possibility to reconstruct the effective mass of the $a_0^-(980)$ and identify the process. Additional measurements of the final states for the a_0^--meson should provide the opportunity to find the mass and the coupling constants for this lightest negative scalar meson. A similar idea for measuring the reaction $pn \to pp\pi^-$ on deuteron target at 2 GeV was proposed in ref. [117]. Recently the reaction $pd \to pp\pi^- p_s$ was also studied in the ref. [118].

From the theoretical point of view the results presented in this chapter should be considered as first rough estimation of the effect. Obviousely, in order to get more reliable predictions some improvement is needed in the treatment of FSI and ISI effects as well as of the primary production mechanism. Concerning the production process the model developed in Jülich by Janssen et al. [106] could be applied for the calculation in order to check the hypothesis that the a_0 is a dynamically generated threshold effect.

Chapter 6

Summary

In conclusion we would like to present a short list of the main results obtained in the thesis.

- A detailed theoretical analysis of the different channels of the reaction $NN \to NN\eta$, i.e. $pp \to pp\eta$, $pn \to pn\eta$ and $pn \to d\eta$, has been performed in the near-threshold region, i.e. for the energy not more than 50 MeV above threshold. The production mechanisms which have been included consist of re-scattering terms with $M = \pi, \rho, \eta, \sigma$ meson exchanges and the direct η production. Effects of the final and initial state interaction between the nucleons are fully taken into account. The calculation utilizes the Bonn B and the CCF NN models for the treatment of the FSI and ISI, respectively, and a realistic coupled-channel model of the πN system developed in Jülich, which was used for the calculation of the $MN \to \eta N$ transition amplitudes. A quantitative agreement of calculated cross sections with the experimental data is achieved for all channels of this reaction.

- It is found that the leading role in the process of the η-meson production near threshold belongs to the re-scattering mechanism with the intermediate pion exchange. The contributions from other meson exchanges, specifically from ρ and η as well as from the direct η production are smaller. However, they are still important and have to be taken into account because of their influence on the cross sections due to the interference with the amplitude corresponding to the π exchange.

- NN FSI effects in the reactions $NN \to NNM$ with production of meson M but with different masses are studied in detail. It is demonstrated that the full reaction amplitude can not be factorized on the pieces corresponding the production process and independently the NN FSI if one is interested in the quantitative predictions for the cross sections. It is shown that the use of the Jost function for the evaluation of NN FSI effects leads to the results considerably different from the ones of correct calculation. It is shown also that NN FSI effects are not universal with respect to the different produced mesons, i.e. their absolute values definitely depend on the mass of the produced meson (momentum transfer).

- It is found that ISI effects in the reaction $NN \to NN\eta$ are not universal with respect to the different meson exchanges, i.e. to the different production mechanisms. It is emphasized that taking into account NN ISI effects affects the magnitude of the cross sections significantly leading to a reduction of a factor 10 (or even more) in some cases.

- The total and differential cross sections of the a_0-meson production in the reaction $pn \to ppa_0^{(-)}$ have been evaluated. The dependence of these cross sections on the specific parameters of the a_0 meson such as position of the resonance, its width, branching ratio is investigated.

Chapter 7

Appendices

7.1 Kinematics of the reaction $NN \to NNx$

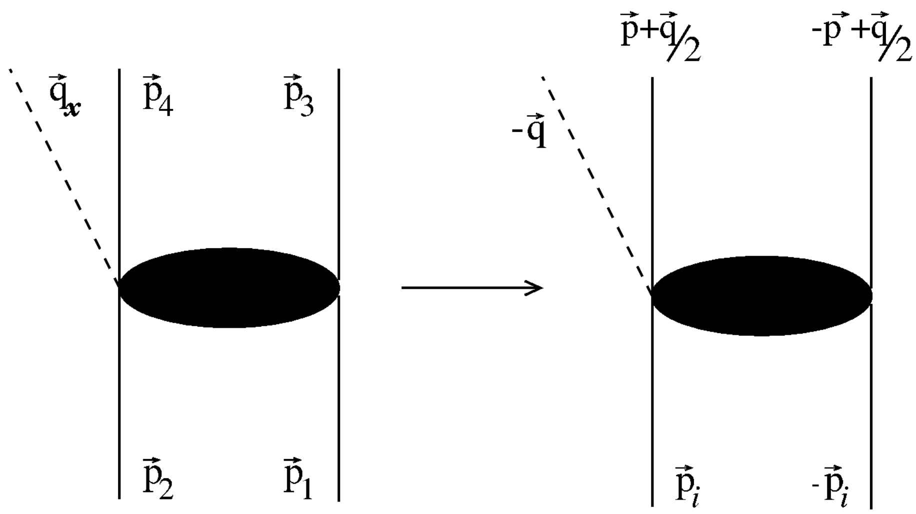

It is convenient to describe three particle kinematics by means of Jacobi coordinates

$$
\begin{aligned}
\vec{P} &= \vec{p}_3 + \vec{p}_4 + \vec{q}_x && - \quad \text{total momentum} \\
\vec{p} &= \frac{m_3\vec{p}_4 - m_4\vec{p}_3}{m_3 + m_4} && - \quad \text{relative momentum of final nucleons} \\
\vec{q} &= \frac{m_x(\vec{p}_3 + \vec{p}_4) - (m_3 + m_4)\vec{q}_x}{m_3 + m_4 + m_x} && - \quad \text{relative momentum of the produced meson x} \\
& && \quad\;\; \text{with respect to the c.m. system of the final nucleons.}
\end{aligned}
\tag{7.1}
$$

In the center of mass (c.m.) system of the reaction $NN \to NNx$

$$\vec{P} = 0; \qquad \vec{p} = \frac{\vec{p}_4 - \vec{p}_3}{2}; \qquad \vec{q} = -\vec{q}_x \tag{7.2}$$

and all momenta of the final particles are defined in terms of $\vec{p}$ and $\vec{q}$ (see figure). The energy of the reaction in such a case is

$$\begin{aligned} \sqrt{s} = Z &= \sqrt{q^2 + m_x^2} + \sqrt{(\vec{p} + \vec{q}/2)^2 + m^2} + \sqrt{(\vec{p} - \vec{q}/2)^2 + m^2} \\ &\overset{|\vec{p}|,|\vec{q}| \ll m}{\approx} 2m + \frac{p^2}{m} + \frac{q^2}{4m} + \sqrt{q^2 + m_x^2} \end{aligned} \tag{7.3}$$

For $|\vec{q}| \ll m_x$ the energy takes the non-relativistic form

$$Z = 2m + m_x + Q, \quad \text{where } Q = \frac{p^2}{m} + \frac{q^2}{2\mu}; \quad \mu = \frac{2mm_x}{2m + m_x} \tag{7.4}$$

For the initial energy E_i and momentum p_i in the c.m. system one gets

$$Z = 2E_i = 2\sqrt{m^2 + p_i^2} \implies p_i = \sqrt{\frac{Z^2 - 4m^2}{4}} \tag{7.5}$$

Sometimes it is useful to know the kinetic energy E_{lab} (beam momentum p_{lab}) of the initial particle in the laboratory system

$$E_{lab} = \frac{Z^2}{2m} - 2m; \quad p_{lab} = \sqrt{\left(\frac{Z^2}{2m} - m\right)^2 - m^2} \tag{7.6}$$

At the η threshold the kinematical variables have the values shown in table 7.1.

Z	E_i	p_i	E_{lab}	p_{lab}
2423.8	1211.9	767	1254.2	1981.6

Table 7.1: The values of different kinematical variables at the η threshold in the reaction $pp \to pp\eta$. The values of the energies and momenta are given in MeV and MeV/c, respectively.

7.2 Conventional notation

In this appendix we introduce conventional notation which will be used in the calculation.

Metrical tensor

$$g_{\mu\nu} = g^{\mu\nu} = \begin{pmatrix} 1 & 0 & 0 & 0 \\ 0 & -1 & 0 & 0 \\ 0 & 0 & -1 & 0 \\ 0 & 0 & 0 & -1 \end{pmatrix}. \tag{7.7}$$

Pauli matrices

$$\sigma_x = \begin{pmatrix} 0 & 1 \\ 1 & 0 \end{pmatrix}, \sigma_y = \begin{pmatrix} 0 & -i \\ i & 0 \end{pmatrix}, \sigma_z = \begin{pmatrix} 1 & 0 \\ 0 & -1 \end{pmatrix}$$

Dirac matrices

For Dirac matrices $\gamma^\mu = (\ \gamma^0, \gamma^1, \gamma^2, \gamma^3\ )$ the standard presentation is used, i.e.

$$\gamma^0 = \begin{pmatrix} I & 0 \\ 0 & -I \end{pmatrix}, \ \vec{\gamma} = \begin{pmatrix} 0 & \vec{\sigma} \\ -\vec{\sigma} & 0 \end{pmatrix}, \ \gamma^5 = \begin{pmatrix} 0 & I \\ I & 0 \end{pmatrix},$$

$$\sigma^{\mu\nu} = \frac{i}{2}\left[\gamma^\mu \gamma^\nu\right] = \frac{i}{2}(\gamma^\mu\gamma^\nu - \gamma^\nu\gamma^\mu). \tag{7.8}$$

Definition of fields

For the scalar and pseudoscalar mesons:

$$\phi(x) = \frac{1}{(2\pi)^{\frac{3}{2}}} \int d^3k \frac{1}{\sqrt{2\omega_k}} [a(\vec{k})e^{-ik\cdot x} + a^\dagger(\vec{k})e^{ik\cdot x}]\ , \tag{7.9}$$

For the vector mesons:

$$\phi^\mu(x) = \frac{1}{(2\pi)^{\frac{3}{2}}} \int d^3k \frac{1}{\sqrt{2\omega_k}} \sum_{\lambda=-1}^{1} [a_\lambda(\vec{k})\epsilon^\mu(\vec{k},\lambda)e^{-ik\cdot x} + a_\lambda^\dagger(\vec{k})\epsilon^{*\mu}(\vec{k},\lambda)e^{ik\cdot x}]\ , \tag{7.10}$$

where $\omega_k = \sqrt{\vec{k}^2 + m_M^2}$ and the commutation relation for the operators a and $a^\dagger$ has Bose form

$$[a(\vec{k}), a^\dagger(\vec{k}\,')] = \delta^{(3)}(\vec{k} - \vec{k}\,') \ ; \ [a(\vec{k}), a(\vec{k}\,')] = 0 \ ; [a^\dagger(\vec{k}), a^\dagger(\vec{k}\,')] = 0 \qquad (7.11)$$

The state $\left|\vec{k}\right\rangle$ is built using the relation

$$\left|\vec{k}\right\rangle = a^\dagger(\vec{k})\,|0\rangle. \qquad (7.12)$$

Normalization of this state is defined by

$$\left\langle\, \vec{k}\,|\,\vec{k}'\,\right\rangle = \delta^{(3)}(\vec{k} - \vec{k}\,'). \qquad (7.13)$$

The nucleon field has the form

$$\Psi_N(x) = \frac{1}{(2\pi)^{\frac{3}{2}}} \int d^3k \sum_{\lambda=-1/2,1/2} [u(\vec{k},\lambda) b_N(\vec{k},\lambda) e^{-ik\cdot x} + v(\vec{k},\lambda) c^\dagger_{\bar{N}}(\vec{k},\lambda) e^{ik\cdot x}] \qquad (7.14)$$

The following anticommutators are not equal to zero:

$$\{b_N(\vec{k}), b^\dagger_N(\vec{k}\,')\} = \{c_{\bar{N}}(\vec{k}), c^\dagger_{\bar{N}}(\vec{k}\,')\} = \delta^{(3)}(\vec{k} - \vec{k}\,') \qquad (7.15)$$

The 4-component spinors u and v are solutions of the Dirac equation. They are defined by

$$\begin{aligned} u(\vec{k},\lambda) &= \sqrt{\frac{E_k + m}{2E_k}} \begin{pmatrix} I \\ \frac{\vec{\sigma}\cdot\vec{k}}{E_k + m} \end{pmatrix} \chi_\lambda \\ v(\vec{k},\lambda) &= \sqrt{\frac{E_k + m}{2E_k}} \begin{pmatrix} \frac{\vec{\sigma}\cdot\vec{k}}{E_k + m} \\ I \end{pmatrix} \chi_{-\lambda}, \end{aligned} \qquad (7.16)$$

where I is the unit matrix and χ_λ are the states with spin projection equal to $1/2$ and $-1/2$

$$\chi_{1/2} = \begin{pmatrix} 1 \\ 0 \end{pmatrix} \quad \text{and} \quad \chi_{-1/2} = \begin{pmatrix} 0 \\ 1 \end{pmatrix}$$

The orthogonality condition requires

$$\bar{u}(\vec{k},\lambda) u(\vec{k},\lambda') = \bar{v}(\vec{k},\lambda) v(\vec{k},\lambda') = \sqrt{\frac{m}{E_k}} \delta_{\lambda\lambda'} \qquad (7.17)$$

7.3 Γ_{MNN} vertices

On the basis of the MNN Lagrangians introduced in section 2.2 and of the fields defined in the previous section one can write down expressions for the MNN vertices. For the pseudoscalar (π, η) productions the vertices are

$$\langle \lambda_3 \,|\, \Gamma_P \,| \lambda_1 \rangle = \frac{1}{(2\pi)^{\frac{3}{2}}} \frac{1}{\sqrt{2\omega_q}} \frac{f_{PNN}}{m_P} \bar{u}_{\lambda_3} \gamma_5 \gamma_\mu u_{\lambda_1} i q^\mu$$
$$= i \frac{1}{(2\pi)^{\frac{3}{2}}} \frac{1}{\sqrt{2\omega_q}} \frac{f_{PNN}}{m_P} N_1 N_3 \chi^\dagger_{\lambda_3} \vec{\sigma} \vec{l} \chi_{\lambda_1}, \qquad (7.18)$$

where $\vec{l} = \vec{q} - \epsilon_q \left(\frac{\vec{p}_1}{\epsilon_1 + m} + \frac{\vec{p}_3}{\epsilon_3 + m} \right) + \frac{1}{(\epsilon_1 + m)(\epsilon_3 + m)} (\vec{p}^{\,2}_1 \vec{p}_3 - \vec{p}^{\,2}_3 \vec{p}_1)$.
Here P means π and η, $N_i = \sqrt{\frac{\epsilon_i + m}{2\epsilon_i}}$ and ϵ_q and ω_q are the zeroth component of 4-vector q and its energy respectively, i.e. $\epsilon_q = \epsilon_1 - \epsilon_3$, $\omega_q = \sqrt{m_P^2 + \vec{q}^{\,2}}$. For the numerical calculation it is convenient to introduce the vector $\vec{l}$ in the spherical basis, i.e.

$$l_\mu = |\vec{l}| \sqrt{\frac{4\pi}{3}} Y_{1\mu}(\hat{l}).$$

Then the matrix element in (7.18) is simply equal to

$$\chi^\dagger_{\lambda_3} \vec{\sigma} \vec{l} \chi_{\lambda_1} = \sqrt{3} l_{\lambda_1 - \lambda_3} C^{\frac{1}{2}\lambda_1}_{\frac{1}{2}\lambda_3 1 \lambda_1 - \lambda_3}. \qquad (7.19)$$

For the scalar and vector products in spherical coordinates there are useful relations which are utilized in the calculation of σNN and ρNN vertices below, namely

$$\vec{A}\vec{B} = \sum_\mu (-1)^\mu A_\mu B_{-\mu}$$
$$(\vec{A} \times \vec{B})_\alpha = \sum_{\mu_1 \mu_2} -i\sqrt{2} C^{1\alpha}_{1\mu_1 1\mu_2} A_{\mu_1} B_{-\mu_2} \qquad (7.20)$$

The σNN vertex is

$$\langle \lambda_3 \,|\, \Gamma_\sigma \,| \lambda_1 \rangle = \frac{1}{(2\pi)^{\frac{3}{2}}} \frac{1}{\sqrt{2\omega_q}} g_{\sigma NN} \bar{u}_{\lambda_3} u_{\lambda_1}, \qquad (7.21)$$

where the product $\bar{u}_{\lambda_3} u_{\lambda_1}$ is expressed in terms of two component spinors χ by

$$\bar{u}_{\lambda_3} u_{\lambda_1} = N_1 N_3 \left\{ \delta_{\lambda_1 \lambda_3} (1 - \frac{\vec{p}_1 \vec{p}_3}{(\epsilon_1 + m)(\epsilon_3 + m)}) - \frac{i}{(\epsilon_1 + m)(\epsilon_3 + m)} \chi^\dagger_{\lambda_3} \vec{\sigma} [\vec{p}_3 x \vec{p}_1] \chi_{\lambda_1} \right\} (7.22)$$

with

$$\chi^{\dagger}_{\lambda_3}\vec{\sigma}[\vec{p}_3\vec{p}_1]\chi_{\lambda_1} = -i\sqrt{6}\left(\sum_{\mu_1\mu_2=-1}^{1} C^{1\lambda_1-\lambda_3}_{1\mu_1 1\mu_2} p_{3\mu_1} p_{1\mu_2}\right) C^{\frac{1}{2}\lambda_1}_{\frac{1}{2}\lambda_3 1\lambda_1-\lambda_3}$$

Finally, the expression for the ρNN vertex can be written down in the form

$$\left\langle \tfrac{1}{2}\lambda_3 \,\middle|\, \Gamma_\rho \,\middle|1\lambda_{ex}\tfrac{1}{2}\lambda_1\right\rangle = \frac{1}{(2\pi)^{\frac{3}{2}}}\frac{1}{\sqrt{2\omega_q}} g_{\rho NN}\bar{u}_{\lambda_3}(\gamma^\mu - \frac{i\kappa_\rho}{2m}\sigma^{\mu\nu}q_\nu)u_{\lambda_1}\epsilon^{*\lambda_{ex}}_{\mu}(q) \quad (7.23)$$

The polarization vector $\epsilon^{*\lambda_{ex}}_{\mu}(q)$ comes from the numerator of the ρ-meson propagator

$$G_\rho = -g_{\mu\nu} + \frac{q_\mu q_\nu}{m_\rho^2} = \sum_\lambda \epsilon_\nu{}^\lambda(q)\epsilon^{*}_{\mu}{}^{\lambda}(q). \quad (7.24)$$

The other vector, $\epsilon_\nu{}^\lambda(q)$, is contracted with the meson-nucleon amplitude T^{ν}_{MN}. The expression for $\epsilon_\mu{}^\lambda(q)$ is deduced in the appendix 7.6.3.

Now we are going to write down schematically the expressions for the different contributions to (7.23).

$$\begin{aligned}
A_1 &=: \bar{u}_{\lambda_3}\gamma^\mu u_{\lambda_1}\epsilon^{*\lambda_{ex}}_{\mu}(q)\\
&= N_1 N_3 \chi^{\dagger}_{\lambda_3}\left[\epsilon^{*\lambda_{ex}}_0\left(1+\frac{(\vec{\sigma}\vec{p}_3)(\vec{\sigma}\vec{p}_1)}{(\epsilon_1+m)(\epsilon_3+m)}\right) - \frac{(\vec{\sigma}\vec{\epsilon}^{*\lambda_{ex}})(\vec{\sigma}\vec{p}_1)}{\epsilon_1+m} - \frac{(\vec{\sigma}\vec{\epsilon}^{*\lambda_{ex}})(\vec{\sigma}\vec{p}_3)}{\epsilon_3+m}\right]\chi_{\lambda_1}\\
A_2^a &= \bar{u}_{\lambda_3}\sigma^{0i}u_{\lambda_1}\epsilon^{*\lambda_{ex}}_0 q_i = i\epsilon^{*\lambda_{ex}}_0 N_1 N_3 \chi^{\dagger}_{\lambda_3}\left[\frac{(\vec{\sigma}\vec{q})(\vec{\sigma}\vec{p}_1)}{\epsilon_1+m} - \frac{(\vec{\sigma}\vec{q})(\vec{\sigma}\vec{p}_3)}{\epsilon_3+m}\right]\chi_{\lambda_1} \qquad (7.25)\\
A_2^b &= \bar{u}_{\lambda_3}\sigma^{i0}u_{\lambda_1}\epsilon^{*\lambda_{ex}}_i q_0 = -iq_0 N_1 N_3 \chi^{\dagger}_{\lambda_3}\left[\frac{(\vec{\sigma}\vec{\epsilon}^{*\lambda_{ex}})(\vec{\sigma}\vec{p}_1)}{\epsilon_1+m} - \frac{(\vec{\sigma}\vec{\epsilon}^{*\lambda_{ex}})(\vec{\sigma}\vec{p}_3)}{\epsilon_3+m}\right]\chi_{\lambda_1}\\
A_2^c &= \bar{u}_{\lambda_3}\sigma^{ij}u_{\lambda_1}\epsilon^{*\lambda_{ex}}_i q_j = N_1 N_3 \chi^{\dagger}_{\lambda_3}\left[\vec{\sigma}[\vec{\epsilon}^{*\lambda_{ex}}\vec{q}] - \frac{(\vec{\sigma}\vec{p}_1)(\vec{\sigma}[\vec{\epsilon}^{*\lambda_{ex}}\vec{q}])(\vec{\sigma}\vec{p}_3)}{(\epsilon_1+m)(\epsilon_3+m)}\right]\chi_{\lambda_1}
\end{aligned}$$

The numerical calculation of these expressions has been done using simple σ-matrix algebra and equations (7.20). It is worth mentioning that the largest contribution to the ρ meson exchange amplitude is provided by the tensor part, especially by the term $\chi^{\dagger}_{\lambda_3}\vec{\sigma}[\vec{\epsilon}^{*\lambda_{ex}}\vec{q}]\chi_{\lambda_1}$. This is partly due to the large ρNN tensor coupling constant compared to the vector coupling, namely $\kappa_\rho = \frac{f_{\rho NN}}{g_{\rho NN}} = 6.1$ [35]. In addition to this, terms proportional to the final (intermediate) momentum p_3 are rather strongly suppressed in distinction from those proportional to the high initial momentum p_1[1].

[1]This is actually fulfilled even if ISI effects are taken into account, since the relevant intermediate momentum in the ISI loop is close to the on-shell momentum of the initial nucleons.

7.4 Observables

The differential cross section for the reaction $1 + 2 \to 3 + 4 + x$ can be written down in the following form:

$$d\sigma = \frac{4\varepsilon_1\varepsilon_2\, S}{(2S_1+1)(2S_2+1)I} \sum_{\lambda_i,\lambda_f} |M_{fi}|^2 (2\pi)^4 \delta(p_1+p_2-p_3-p_4-p_x) d\vec{p_3} d\vec{p_4} d\vec{p_x} \tag{7.26}$$

In this formula the factor $(2S_1+1)(2S_2+1)$ corresponds to averaging over the spin projections for the initial particles. In the center of mass system (c.m.s.) of the reaction $I = p_i(\varepsilon_1+\varepsilon_2)$ with p_i and $\varepsilon_1, \varepsilon_2$ being the cm-momentum and energies of the incoming nucleons. S is a factor taking into account the statistical properties of the particles in the final state. If final nucleons are identical then we have to integrate only over half of the phase space to avoid a double counting, i.e.

$$S = \begin{cases} \frac{1}{2} & pp\eta \text{ case} \\ 1 & pn\eta \text{ case} \end{cases} \tag{7.27}$$

The reaction amplitude M_{fi} in (7.26) is related to the S-matrix by

$$S_{fi} = \delta_{fi} - i(2\pi)^4 \delta(p_f - p_i) M_{fi}, \tag{7.28}$$

where the indices i and f denote the initial and the final states, respectively.

Introducing Jacobi coordinates (see section 7.1) and performing the integration

$$d\vec{p_3} d\vec{p_4} \delta^4(p_f - p_i) = d\tau_2 = p d\Omega_p m_{34} \tag{7.29}$$

we can rewrite eq. (7.26) in the form

$$d\sigma = \frac{(2\pi)^4\, S}{4v} \sum_{\lambda_i,\lambda_f} |M_{fi}|^2 d\tau_3, \tag{7.30}$$

with

$$v = p_i(\varepsilon_1+\varepsilon_2)/\varepsilon_1\varepsilon_2 \overset{cms}{=} 2p_i/\varepsilon_1 \tag{7.31}$$

$$d\tau_3 = m_{34} p d\Omega_p d^3\vec{q}; \quad m_{34} = \frac{m_3 m_4}{m_3+m_4} = \frac{m}{2}, \tag{7.32}$$

where the final nucleons are treated nonrelativistically.

Since we are interested in the region not far from threshold only the s-wave contributions in the final state play a role (at least for the total cross section). To single out the s-wave terms of the contributions from the higher partial waves we perform a partial wave decomposition of the reaction amplitude:

$$M(\vec{p},\vec{q}) = \sum_{L,M,l,m} Y_{LM}(\vec{p})Y_{lm}(\vec{q})M(p,q,L,M,l,m) \tag{7.33}$$

Finally after the integration over Ω_p and Ω_q the cross section takes the form

$$d\sigma = \frac{(2\pi)^4\,S}{4v}\sum_{L,M,l,m}\sum_{S_z^i,S_z^f}|M_{fi}(\underbrace{L,M,S^f,S_z^f}_{final\;nucleons},\underbrace{l,m}_{meson},p,q;\vec{p}_i)|^2\frac{m}{2}pq^2dq \tag{7.34}$$

We would like to mention that it is convenient to choose the direction of the z-axis along the momentum of the initial nucleons. In this case the projection of the initial angular momentum is zero, i.e. $L_{zi}=0$, what simplifies the calculation. For instance, for the ${}^3P_0 \rightarrow {}^1S_0s$ transition, which is relevant for the reaction $pp \rightarrow pp\eta$, $J_z = L_{zi} + S_{zi} = L_{zf} + S_{zf} = 0$ and due to $L_{zi}=0$ we know that $S_{zi}=0$. Therefore, there is only one relevant transition amplitude:

$$d\sigma = \frac{(2\pi)^4\,S}{4v}|M_{fi}(L\!=\!0,S^f\!=\!0,l\!=\!0,p,q;\vec{p}_i)|^2\frac{m}{2}pq^2dq \tag{7.35}$$

Using the expression (7.3) we can write the momentum p in terms of the total energy Z and the momentum q:

$$p = \sqrt{m\left(Z - 2m - \frac{q^2}{4m} - \sqrt{q^2+m_x^2}\right)} \tag{7.36}$$

For the 2 body reaction $pn \rightarrow d\eta$

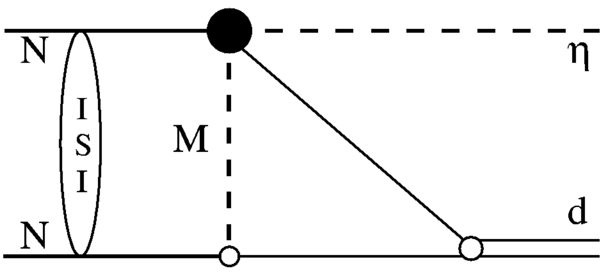

the cross section has the form:

$$
\begin{aligned}
d\sigma &= \frac{1}{4v}\sum_{S_z^i S_z^f} |M_{fi}|^2 (2\pi)^4 \delta(p_f - p_i) d\vec{p_3} d\vec{p_x} \\
&= \frac{(2\pi)^4}{4v}\sum_{S_z^i S_z^f} |M_{fi}|^2 \frac{E_d \omega_\eta}{E_d + \omega_\eta} q d\Omega_q \\
&= \frac{1}{4v}\frac{E_d \omega_\eta}{E_d + \omega_\eta} q \sum_{L,M}\sum_{S_z^i S_z^f} \left|\left\langle\, LM, S^f = 1, S_z^f, q \,\right|\, M_{fi} \,|\vec{p_i}\rangle\right|^2 d\Omega_q
\end{aligned}
\tag{7.37}
$$

where $E_d = \sqrt{m_d^2 + q^2}$; $\omega_\eta = \sqrt{m_\eta^2 + q^2}$.

7.5 Diagrammatic formalism

The calculation of all diagrams described in this appendix is performed in the c.m. system of the final nucleons.The transition to the c.m.s. of the reaction (boost) will be discussed in appendix 7.6.

Born term.

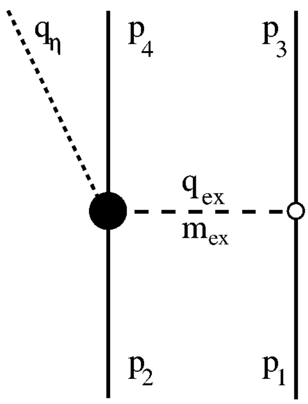

$$= M^{Born} = \Gamma_{NNM} \frac{2\omega_{ex}}{q_{ex}^2 - m_{ex}^2} T_{MN \to \eta N} \tag{7.38}$$

It is interesting to note that in TOPT the sum of the diagrams depicted in Fig. 7.1 correspond to the result deduced with Feynman meson propagator (7.38). However, if we deal with FSI or ISI effects these approaches (TOPT and the so-called Feynman meson propagator) differ from each other since they involve different off-shell extrapolation. Let us consider the calculation of the FSI loop in more detail.

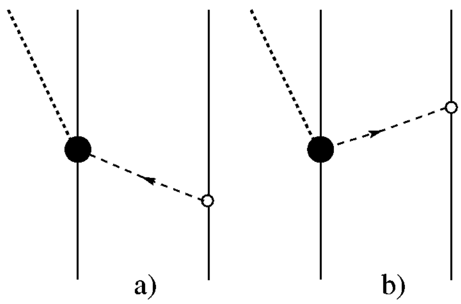

Figure 7.1: Diagrams a) and b) represent the TOPT approach for the intermediate meson.

FSI loop calculus.

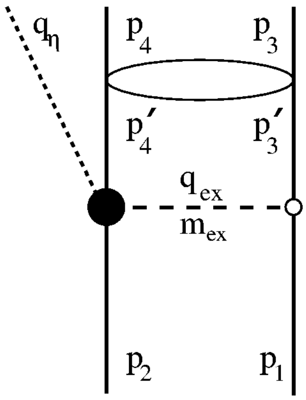

$$p_1 = \begin{pmatrix} E_1 \\ -\vec{p}_i - \vec{q}_\eta/2 \end{pmatrix}, \; p_2 = \begin{pmatrix} E_2 \\ \vec{p}_i - \vec{q}_\eta/2 \end{pmatrix}, \; E_{in} = E_1 + E_2$$

$$E_{1,2} = \sqrt{m^2 + (\vec{p}_i \pm \vec{q}_\eta/2)^2}, \; \omega_\alpha = \sqrt{m_\alpha^2 + p_\alpha^2},$$

$$\vec{p}_3\,' = -\vec{p}_4\,' = \vec{p}\,'$$

Here E_{in} is the energy of the initial particles in the c.m. system of the final nucleons, α is an index which labels different particles in the initial, intermediate or final states (in case of intermediate states a "prime" is added to the energy, i.e. ω'_α). In section 7.6 (cf. eq. (7.58) and (7.59)) it will be shown that the 3-momenta of the initial particles in the c.m.s. of final protons are $\vec{p}_1 \approx -\vec{p}_i - \vec{q}_\eta/2$ ($\vec{p}_2 \approx \vec{p}_i - \vec{q}_\eta/2$). Corrections are of the order of $\sim q_\eta^2/s_{thr}$ which is negligible in the energy region close to η threshold. Here p_i is the momentum of the initial protons in the c.m.s. of the reaction (or equally in the c.m.s. of the initial particles) and $s_{thr} = 2m + m_\eta$.

The expression for the FSI loop in our approach can be written down schematically in the form

$$M_{1loop}^{FSI} = M^{Born} G T_{NN}^{FSI} = \int d\vec{p}\, \frac{M^{Born}(\vec{p}_i; \vec{p}\,', \vec{q}_\eta) T_{NN}^{FSI}(\vec{p}\,', \vec{p})}{E_{in} - \omega_\eta - 2\omega_{p'} + i0}, \qquad (7.39)$$

where M^{Born} is the production amplitude (7.38), G is a Green function and T_{NN}^{FSI} is the NN T-matrix in the final state.

ISI loop.

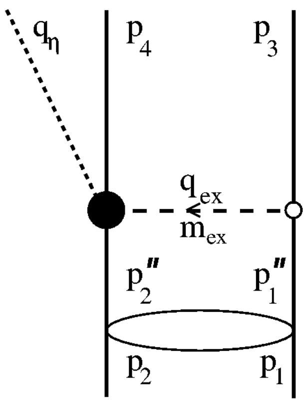

$$\vec{p}_1'' = -\vec{p}\,'' - \vec{q}_\eta/2,$$

$$\vec{p}_2'' = \vec{p}\,'' - \vec{q}_\eta/2.$$

Let us mention again that using formulae (7.58) and (7.59) from appendix 7.6 we find that the intermediate momenta $p''_{1,2}$ (in analogy with initial momenta) are approximately equal to $\vec{p}''_{1,2} \approx \mp\vec{p}'' - \vec{q}_\eta/2$.

The calculation of the one loop integral in the initial state is done similar to the FSI loop.

$$M^{ISI}_{1loop} = \int d\vec{p}'' \, \frac{M^{Born}(\vec{p}''; \vec{q}_\eta, \vec{p}) T^{ISI}_{NN}(\vec{p}_i, \vec{p}'')}{E_{in} - E''_1 - E''_2 + i0}, \tag{7.40}$$

where $E''_1 = \sqrt{m^2 + (\vec{p}'' + \vec{q}_\eta/2)^2}$; $E''_2 = \sqrt{m^2 + (\vec{p}'' - \vec{q}_\eta/2)^2}$ and $\vec{p}$ is the c.m. momentum of the final protons.

To be consistent we should also neglect the terms containing q_η in E''_1 and E''_2. In the following calculations all terms $\sim q^2_\eta/s_{thr}$ will be omitted. Finally the expression for M^{ISI}_{1loop} is

$$M^{ISI}_{1\,loop} = \int d\vec{p}'' \, \frac{M^{Born}(\vec{p}''; \vec{q}_\eta, \vec{p}) T^{ISI}_{NN}(\vec{p}_i, \vec{p}'')}{\sqrt{s} - 2\sqrt{m^2 + p''^2} + i0} \tag{7.41}$$

Two loop integral.

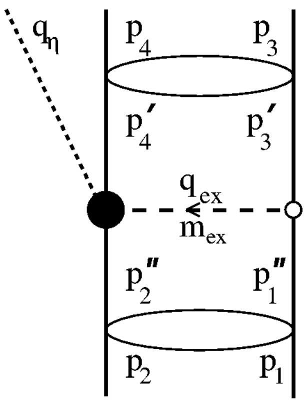

Following the method discussed in previous subsections the amplitude for the two loop diagram can be written down in the form:

$$M_{2\,loop} = \int d\vec{p}' d\vec{p}'' \, \frac{T^{ISI}_{NN}(\vec{p}_i, \vec{p}'') M^{Born}(\vec{p}''; \vec{q}_\eta, \vec{p}') T^{FSI}_{NN}(\vec{p}', \vec{p})}{(\sqrt{s} - 2\sqrt{m^2 + p''^2} + i0)(E_{in} - \omega_\eta - 2\sqrt{m^2 + p'^2} + i0)} \tag{7.42}$$

Direct η production (FSI).

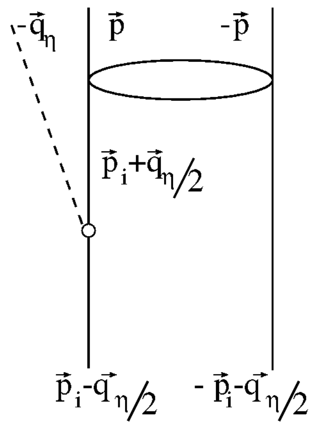

$$M_{dir}^{FSI} = \frac{\Gamma(\vec{p}_i, \vec{q}_\eta) T_{NN}^{FSI}(\vec{p}, \vec{p}_i + \vec{q}_\eta/2)}{E_{in} - \omega_\eta - \sqrt{m^2 + p_i^2}} \tag{7.43}$$

Direct η production (ISI).

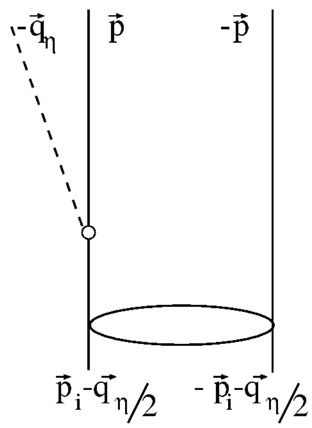

Since $\vec{p}$ is of the same order of magnitude as $\vec{p}_\eta$ the relative momentum of intermediate particles is $\vec{p}'_{cm} = \vec{p} - \vec{q}_\eta/2$

$$M_{dir}^{ISI} = \frac{\Gamma(\vec{p}, \vec{q}_\eta) T_{NN}^{ISI}(\vec{p}_i, \vec{p}'_{cm})}{\sqrt{s} - 2\sqrt{m^2 + {p'}_{cm}^{2}}} \tag{7.44}$$

Direct η production (ISI and FSI).

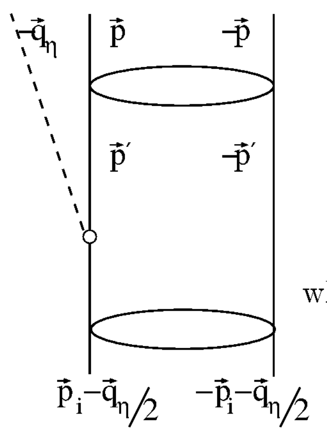

$$M_{dir} = \frac{T_{NN}^{ISI}(\vec{p}_i, \vec{p}'_{cm}) \Gamma(\vec{p}', \vec{q}_\eta) T_{NN}^{FSI}(\vec{p}', \vec{p})}{(E_{in} - \omega_\eta - 2\sqrt{m^2 + p'^2} + i0)(\sqrt{s} - 2\sqrt{m^2 + {p'}_{cm}^{2}} + i0)}, \tag{7.45}$$

where $\vec{p}'_{cm} = \vec{p} - \vec{q}_\eta/2$

7.6 Lorentz transformations

The calculation of the reaction $NN \to NN\eta$ is performed in the c.m.s. of the reaction. However the components of the invariant amplitude $M_{2\to 3}$ consist of the NN and $MN \to \eta N$ 2-body T-matrices which are defined in their center of mass systems. Therefore a Lorentz boost has to be applied to relate the relative momenta of the 2-body systems with those determined in the 3-body case. In this section we use the terminology introduced in Ref. [63].

We introduce some 4 vector $Q^\mu = \begin{pmatrix} Q_0 \\ \vec{Q} \end{pmatrix}$ and transform it to the rest system where $\vec{Q} = 0$, i.e.

$$\Lambda^\mu_\nu Q^\nu = \begin{pmatrix} \sqrt{Q^2} \\ 0 \end{pmatrix} \tag{7.46}$$

The Lorentz matrix Λ^μ_ν satisfying the condition (7.46) is

$$\Lambda^\mu_\nu(Q) = \frac{1}{\mathcal{M}} \begin{pmatrix} Q^0 & -Q^j \\ -Q^i & \mathcal{M}\delta_{ij} - \frac{Q^iQ^j}{Q^2}(\mathcal{M} - Q^0) \end{pmatrix} \tag{7.47}$$

where $\mathcal{M} = \sqrt{Q_0^2 - \vec{Q}^2}$ and the 2-body T-matrix is transformed by

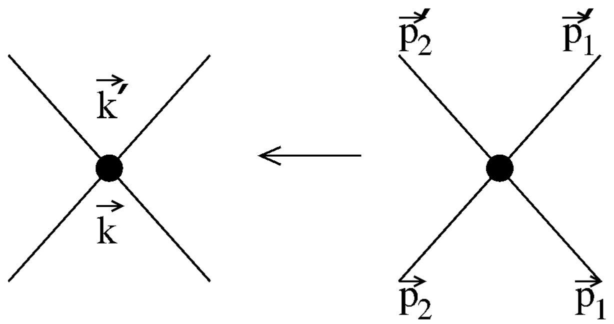

$$T_{2\to 2}(\vec{k}, \vec{k}') = \sqrt{\frac{E_1(k)E_2(k)E_{1'}(k')E_{2'}(k')}{E_1(p_1)E_2(p_2)E_{1'}(p_1')E_{2'}(p_2')}} T_{2\to 2}(\vec{p}_1, \vec{p}_2; \vec{p'}_1, \vec{p'}_2) \tag{7.48}$$

7.6.1 NN boost

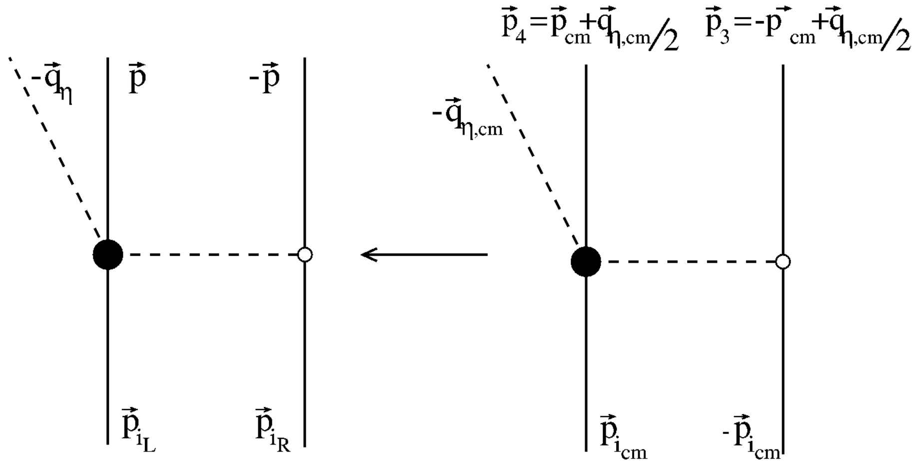

In the c.m.s. of the reaction

$$Q^\mu = \begin{pmatrix} E_3+E_4 \\ \vec{p}_3+\vec{p}_4 \end{pmatrix} = \begin{pmatrix} E_3+E_4 \\ \vec{q}_{\eta,cm} \end{pmatrix}, \tag{7.49}$$

where $E_{3(4)} = \sqrt{m^2+p_{3(4)}^2}, \mathcal{M} = \sqrt{(E_3+E_4)^2 - q_{\eta,cm}^2}$.

Now we are going to find momenta $\vec{p}, \vec{q}_\eta$ (defined in the figure above) in the c.m.s. of the final protons, i.e.

$$\Lambda^\mu_\nu \begin{pmatrix} E_3+E_4 \\ \vec{q}_{\eta,cm} \end{pmatrix} = \begin{pmatrix} 2\sqrt{m^2+p_{cm}^2} \\ 0 \end{pmatrix} \tag{7.50}$$

$$\Downarrow$$

$$\Lambda^\mu_\nu(Q) = \frac{1}{\mathcal{M}} \begin{pmatrix} E_3+E_4 & -q^j_{\eta,cm} \\ -q^i_{\eta,cm} & \mathcal{M}\delta_{ij} - \frac{q^i_{\eta,cm}q^j_{\eta,cm}}{q^2_{\eta,cm}}(\mathcal{M}-E_3-E_4) \end{pmatrix} \tag{7.51}$$

Thus, acting by $\Lambda^\nu_\mu(Q)$ on the 4-momenta $p_4, q_{\eta,cm}$ we obtain

$$\vec{p} = \frac{1}{\mathcal{M}}\left[\mathcal{M}\vec{p}_{cm} + \vec{q}_{\eta,cm}\frac{E_3-E_4}{2} - \frac{\vec{q}_{\eta,cm}\vec{p}_{cm}}{\vec{q}^{\,2}_{\eta,cm}}(\mathcal{M}-E_3-E_4)\right] \tag{7.52}$$

$$-\vec{q}_\eta = -\frac{\sqrt{s}}{\mathcal{M}}\vec{q}_{\eta,cm} \tag{7.53}$$

Taking into account that

$$E_3-E_4 \approx \frac{\vec{q}^{\,2}_{\eta,cm}}{m^2+p^2_{cm}};\ \mathcal{M}-E_3-E_4 \approx \frac{-\vec{q}^{\,2}_{\eta,cm}/2}{(2\sqrt{m^2+p^2})^2};\ \frac{\sqrt{s}}{\mathcal{M}} \approx 1+\frac{E_\eta}{2\sqrt{m^2+p^2_{cm}}} \tag{7.54}$$

we conclude that, neglecting by terms of the order $\sim q_\eta^2/m^2$ which are anyway small near the η threshold, the momenta are

$$\begin{aligned} \vec{p} &\approx \vec{p}_{cm} && (7.55)\\ -\vec{q}_\eta &\approx -\vec{q}_{\eta,cm}\left(1+\frac{E_\eta}{2\sqrt{m^2+p_{cm}^2}}\right) && (7.56)\end{aligned}$$

In a similar way one gets expressions for the initial momenta

$$\begin{aligned} p_{i_L} &= \Lambda^\mu_\nu \begin{pmatrix} \sqrt{s}/2 \\ \vec{p}_{i,cm}\end{pmatrix} \Rightarrow && (7.57)\\ \vec{p}_{i_L} &\approx \vec{p}_{i_{cm}} - \frac{\vec{q}_{\eta,cm}}{2}\frac{\sqrt{s}}{\mathcal{M}} = \vec{p}_{i_{cm}} - \frac{\vec{q}_\eta}{2} && (7.58)\\ \vec{p}_{i_R} &\approx -\vec{p}_{i_{cm}} - \frac{\vec{q}_\eta}{2} && (7.59)\end{aligned}$$

7.6.2 Boost of the meson-nucleon T-matrix

The goal of this section is to find the initial and final c.m. momenta $\vec{k}$ and $\vec{k}'$ as well as the energy of the MN system in terms of the momenta given in the c.m. system of the final nucleons (cf. the Born diagram in the eq. 7.38). We introduce a vector Q^μ as the sum of the final on-shell 4-momenta of the η-meson and the nucleon, i.e.
$Q^\mu = \begin{pmatrix} Q_0 \\ \vec{Q}\end{pmatrix} = \begin{pmatrix} \omega_\eta + \epsilon_4 \\ -\vec{q}_\eta + \vec{p}_4\end{pmatrix}$ with $\omega_\eta = \sqrt{m_\eta^2 + \vec{q}_\eta^{\,2}}$ and $\epsilon_4 = \sqrt{m^2+\vec{p}_4^{\,2}}$. Then the relativistic c.m. momenta $\vec{k}$ and $\vec{k}'$ are determined by the relations

$$\begin{aligned} k'_i = \Lambda^i_\nu \begin{pmatrix} \omega_\eta \\ -\vec{q}_\eta\end{pmatrix} &= -\vec{q}_\eta - \frac{\vec{Q}}{\mathcal{M}}\left(\omega_\eta - \frac{(\vec{Q}\vec{q}_\eta)}{\vec{Q}^2}(\mathcal{M}-Q_0)\right), \\ k_i = \Lambda^i_\nu \begin{pmatrix} \epsilon_2 \\ \vec{p}_2\end{pmatrix} &= \vec{p}_2 - \frac{\vec{Q}}{\mathcal{M}}\left(\epsilon_2 + \frac{(\vec{Q}\vec{p}_2)}{\vec{Q}^2}(\mathcal{M}-Q_0)\right) \qquad (7.60)\end{aligned}$$

If the outgoing $\eta + N$ system is really on-shell (e.g., for the Born term or for the one loop ISI diagram) then the c.m. energy of the ηN system is just $\mathcal{M} = \sqrt{Q_0^2 - \vec{Q}^2}$. In the case of the FSI loop we introduce a 4-vector P^μ in the form $P^\mu = \begin{pmatrix} Z - E_3 \\ \vec{Q}\end{pmatrix}$, i.e. the energy of the ηN-pair is determined as the difference between the total energy of the reaction, Z, and the energy $E_3 = \sqrt{m^2 + \vec{p}_4^{\,2}}$ (where $\vec{p}_4$ is now an off-shell momentum) of the intermediate nucleon in the FSI loop on the right side.

In this case the c.m. energy of the ηN system is

$$E_{cm} = \Lambda^0_\nu P^\nu = \mathcal{M} + \frac{Q_0}{\mathcal{M}}(Z - E_3 - Q_0), \tag{7.61}$$

where $Q_0 = \omega_\eta + \epsilon_4$. Since we are not far from the η-threshold and convergence of the integral in the FSI loop is rather quick (i.e. p_4 is not large) one can assume that $\vec{Q} \ll Q_0$. Therefore $\mathcal{M} \approx Q_0$ and $E_{cm} \approx Z - E_3$, i.e. the boost effect is small (for $\vec{k}$ and $\vec{k}'$ in such a case we get standard non-relativistic expressions.).

7.6.3 Boost of the polarization vector of the ρ-meson

In the rest frame the polarization vector of a particle with spin $S = 1$ can be written down in the form

$$\epsilon_\mu^{\lambda_{ex}=1}(\vec{q}{=}0) = \frac{1}{\sqrt{2}}\begin{pmatrix} 0 \\ -1 \\ -i \\ 0 \end{pmatrix}, \epsilon_\mu^{\lambda_{ex}=-1}(\vec{q}{=}0) = \frac{1}{\sqrt{2}}\begin{pmatrix} 0 \\ 1 \\ -i \\ 0 \end{pmatrix}, \epsilon_\mu^{\lambda_{ex}=0}(\vec{q}{=}0) = \begin{pmatrix} 0 \\ 0 \\ 0 \\ 1 \end{pmatrix} \tag{7.62}$$

In order to obtain this vector in the system where the 4-momentum of the ρ-meson is

$q = \begin{pmatrix} \omega \\ \vec{q} \end{pmatrix}$ with $\omega = \sqrt{m_\rho^2 + \vec{q}^{\,2}}$ we introduce the matrix $(\Lambda^\nu_\mu)^{-1}$ via

$$(\Lambda^\mu_\nu)^{-1}(q) = \frac{1}{m_\rho}\begin{pmatrix} q^0 & q^j \\ q^i & m_\rho\delta_{ij} - \frac{q^i q^j}{q^2}(m_\rho - q^0) \end{pmatrix}. \tag{7.63}$$

It satisfies the relation $(\Lambda^\mu_\nu)^{-1}\begin{pmatrix} m_\rho \\ 0 \end{pmatrix} = \begin{pmatrix} \omega \\ \vec{q} \end{pmatrix}$.

Thus

$$\epsilon_\mu^{\lambda_{ex}}(q) = (\Lambda^\mu_\nu)^{-1}\epsilon_\mu^{\lambda_{ex}}(\vec{q}{=}0) = \begin{pmatrix} \epsilon_0^{\lambda_{ex}}(\vec{q}) \\ \vec{\epsilon}^{\,\lambda_{ex}}(\vec{q}=0) - \vec{q}\,\epsilon_0^{\lambda_{ex}}(\vec{q})\dfrac{(m_\rho - \omega)}{\vec{q}^{\,2}} \end{pmatrix}, \tag{7.64}$$

where $\epsilon_0^{\lambda_{ex}}(\vec{q}) = \dfrac{\vec{q}\vec{\epsilon}^{\,\lambda_{ex}}(\vec{q}=0)}{m_\rho}$

7.7 Partial wave decomposition

According to section 7.4 we need to obtain the reaction amplitude $M_{2\to 3}$ in JLS basis. In this section we will present the formulas for $M^{JLS}_{2\to 3}$ starting from the basis $|\vec{p}, S_i, \lambda_i\rangle$ where the spin and its projection on the z-axis (S_i, λ_i) are fixed for each particles.

First of all we consider the re-scattering process. The transformation of the reaction amplitude to the $LMlm$ basis for the final particles is performed by simple integration over the angular variables,

$$\langle\, LMlm \,|\, M(\vec{p}, \vec{q}_\eta)\, |\vec{p}_i\rangle = \int d\Omega_{\vec{p}} d\Omega_{\vec{q}_\eta} M(\vec{p}, \vec{q}_\eta) Y^*_{LM}(\vec{p}) Y^*_{lm}(\vec{q}_\eta). \qquad (7.65)$$

Let us study now the transformation of initial and final spins.

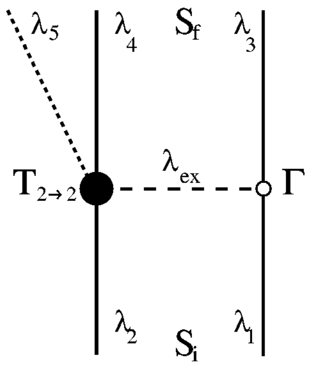

$$\langle\, S_f S_{zf} \,|\, M_{2\to 3} \,|S_i S_{zi}\rangle =$$

$$\sum_{\substack{\lambda_1,\lambda_2,\lambda_{ex}\\ \lambda_3,\lambda_4,\lambda_5}} \left\langle\, S_f S_{zf} \,\middle|\, \tfrac{1}{2}\lambda_3 \tfrac{1}{2}\lambda_4 S_5 \lambda_5 \,\right\rangle \frac{\left\langle\, \tfrac{1}{2}\lambda_3 \tfrac{1}{2}\lambda_4 S_5 \lambda_5 \,\middle|\, T_{2\to 2}\Gamma \,\middle|\, \tfrac{1}{2}\lambda_2 \tfrac{1}{2}\lambda_1 \right\rangle}{q^2_{ex} - m^2_{ex}} \left\langle\, \tfrac{1}{2}\lambda_2 \tfrac{1}{2}\lambda_1 \,\middle|\, S_i S_{zi} \,\right\rangle \qquad (7.66)$$

For the π, η and η' mesons $S_5 = 0$. Therefore the simplified expression is

$$\begin{aligned} \langle\, S_f S_{zf} \,|\, M_{2\to 3} \,|S_i S_{zi}\rangle = & \sum_{\substack{\lambda_1,\lambda_2,\lambda_{ex}\\ \lambda_3,\lambda_4}} C^{S_f S_{zf}}_{\frac{1}{2}\lambda_3 \frac{1}{2}\lambda_4} C^{S_i S_{zi}}_{\frac{1}{2}\lambda_2 \frac{1}{2}\lambda_1} \\ \times \quad & \frac{\left\langle\, \tfrac{1}{2}\lambda_4 00 \,\middle|\, T_{2\to 2} \,\middle|\, \tfrac{1}{2}\lambda_2 S_{ex}\lambda_{ex} \right\rangle \left\langle\, \tfrac{1}{2}\lambda_3 S_{ex}\lambda_{ex} \,\middle|\, \Gamma \,\middle|\, \tfrac{1}{2}\lambda_1 \right\rangle}{q^2_{ex} - m^2_{ex}}, \end{aligned} \qquad (7.67)$$

where $S_{zf} = \lambda_3 + \lambda_4$ and $S_{zi} = \lambda_1 + \lambda_2$.

For the diagram with FSI we derive

$$\langle\, LMS_fS_{zf}, p \,|\, M^{FSI}_{2\to3}\, |\vec{p}_i - \vec{q}_\eta/2, S_iS_{zi}\rangle =$$
$$\sum_{S'S'_z} \int d\vec{p}\,'\langle\, LMS_fS_{zf}, p \,|\, T^{FSI}_{NN}\, |\vec{p}\,', S'S'_z\rangle G(\vec{p}\,')\langle\, S'S'_z, \vec{p}\,' \,|\, M^{Born}_{2\to3}\, |\vec{p}_i - \vec{q}_\eta/2, S_iS_{zi}\rangle \tag{7.68}$$

The NN T-matrix is already given in JLS basis so that we perform the transformation

$$\langle\, LMS_fS_{zf}, p \,|\, T^{FSI}_{NN}\, |\vec{p}\,', S'S'_z\,\rangle =$$
$$\sum_{J,J_z,L'} \langle\, LMS_fS_{zf} \,|\, JJ_zLS_f\,\rangle\langle\, JJ_zLS_f, p \,|\, T^{FSI}_{NN}\, |p\,', JJ_zL'S'\rangle\langle\, JJ_zL'S' \,|\, \vec{p}\,'S'S'_z\,\rangle =$$
$$\sum_{\substack{JJ_z\\ L'M'}} C^{JJ_z}_{LMS_fS_{zf}} C^{JJ_z}_{L'M'S'S'_z} Y_{L'M'}(\vec{p}\,')\langle\, LS_f, p \,|\, T^{J,FSI}_{NN}\, |p\,', L'S_f\rangle. \tag{7.69}$$

To obtain the last equality we used the relation

$$|\vec{p}\,'\rangle = \textstyle\sum_{L'M'} Y^*_{L'M'}(\vec{p}\,')\, |L'M'\rangle. \tag{7.70}$$

We should also mention that the spin is conserved in the NN interaction. Thus, $S_f = S'$ and $L_f = L' \pm 2k, k = 0, 1....$

For the diagram with the ISI the expression is very similar to eq. (7.68):

$$\langle\, LMS_fS_{zf}, p \,|\, M^{ISI}_{2\to3}\, |\vec{p}_i, S_iS_{zi}\rangle =$$
$$\sum_{S''S''_z} \int d\vec{p}\,''\langle\, LMS_fS_{zf}, p \,|\, M^{Born}_{2\to3}\, |\vec{p}\,'', S''S''_z\rangle G(\vec{p}\,'')\langle\, S''S''_z, \vec{p}\,'' \,|\, T^{ISI}_{NN}\, |\vec{p}_i, S_iS_{zi}\rangle, \tag{7.71}$$

where $G(\vec{p})$ is the two nucleon Green function. The NN ISI T-matrix is transformed by

$$\begin{aligned}\langle\, S''S''_z, \vec{p}\,'' \,|\, T^{ISI}_{NN}\, |\vec{p}_i, S_iS_{zi}\rangle = &\sum_{\substack{JJ_z\\ L''M''L_i}} C^{JJ_z}_{L''M''S''S''_z} C^{JJ_z}_{L_iM_iS_iS_{zi}}\\ &\times Y_{L''M''}(\vec{p}\,'')Y^*_{L_iM_i}(\vec{p}_i)\langle\, L''S_i, p'' \,|\, T^{J,ISI}_{NN}\, |p_i, L_iS_i\rangle\end{aligned} \tag{7.72}$$

and the initial momenta are chosen to be parallel to the z-axis, i.e $M_i = 0$ (see comments in section 7.4).

For the double loop the result is simply a combination of the two previous cases:

$$\langle LMS_fS_{zf}, p \,|\, M_{2\to3}^{2\,loop} \,|\vec{p}_i, S_iS_{zi}\rangle = \sum_{\substack{S'S'_z\\ S''S''_z}} \int d\vec{p}'d\vec{p}''\langle LMS_fS_{zf}, p \,|\, T_{NN}^{FSI} \,|\vec{p}', S'S'_z\rangle$$
$$G_1(\vec{p}')\langle S'S'_z, \vec{p}' \,|\, M_{2\to3}^{Born} \,|\vec{p}'', S''S''z\rangle G_2(\vec{p}'')\langle S''S''_z, \vec{p}'' \,|\, T_{NN}^{ISI} \,|\vec{p}_i, S_iS_{zi}\rangle. \quad (7.73)$$

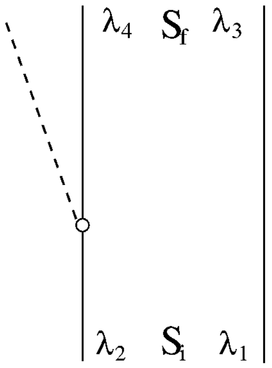

For completeness we also present the result for the Bonn term of the direct η production. The inclusion of FSI and ISI effects is identical to the re-scattering cases.

$$\langle S_fS_{zf} \,|\, M_{dir}^{Born} \,|S_iS_{zi}\rangle = \sum_{\lambda_2,\lambda_3,\lambda_4} C_{\frac{1}{2}\lambda_3\frac{1}{2}\lambda_4}^{S_fS_{zf}} C_{\frac{1}{2}\lambda_2\frac{1}{2}\lambda_3}^{S_iS_{zi}} \langle \tfrac{1}{2}\lambda_4 \,|\, \Gamma \,|\tfrac{1}{2}\lambda_2\rangle \quad (7.74)$$

7.7.1 Partial wave decomposition of the $MN \to \eta N$ amplitudes.

The two body transition amplitude $MN \to \eta N$ is calculated in JLS basis, just like the NN T-matrix. Thus, we are going to convert the matrix element $\left\langle \frac{1}{2}\lambda_4 00, \vec{k}' \,\middle|\, T_{2\to2} \,\middle|\, \vec{k}, \frac{1}{2}\lambda_2 S_{ex}\lambda_{ex}\right\rangle$ appearing in eq.(7.67) into JLS basis. The notation is given in the figure below.

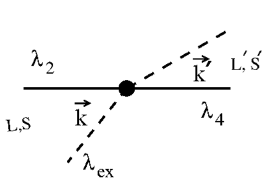

Let us decompose the initial state over the total spin

$$\left|\tfrac{1}{2}\lambda_2 S_{ex}\lambda_{ex}\right\rangle = \sum SS_z C_{\frac{1}{2}\lambda_2 S_{ex}\lambda_{ex}}^{SS_z} \,|SS_z\rangle \quad (7.75)$$

So, finally we get

$$\left\langle \tfrac{1}{2}\lambda_4 00, \vec{k}' \left| T_{MN\to\eta N} \right| \vec{k}, \tfrac{1}{2}\lambda_2 S_{ex}\lambda_{ex} \right\rangle = \sum_{\substack{SLL' \\ JJ_z}} C^{SS_z}_{\frac{1}{2}\lambda_2 S_{ex}\lambda_{ex}} C^{JJ_z}_{LMSS_z} C^{JJ_z}_{L'M'\frac{1}{2}\lambda_4}$$
$$\times Y_{L'M'}(\vec{k}\,')Y^*_{LM}(\vec{k})\langle\, L'\tfrac{1}{2}, k' \,|\, T^J_{MN\to\eta N} \,| k, LS \rangle, \tag{7.76}$$

where $M = J_z - S_z, M' = J_z - \lambda_4, S_z = \lambda_2 + \lambda_{ex}$.

For the π and η exchanges the situation becomes much simpler: $S_{ex} = 0 \to S = 1/2; S_z = \lambda_2$. From the parity conservation we also derive $L = L'$. So we have to sum up only over J, J_z and L and only diagonal transitions ($S \to S, P \to P$ ...) contribute to the result.

For the σ meson we still have $S = 1/2; S_z = \lambda_2$ but the σ is a scalar neson so that only transitions with $L = L' \pm 1$ are allowed. It means that for the s-wave in the final state p-wave will occur in the initial state.

Since ρ is a vector meson we again get $L = L' \pm 2k, k = 0, 1...$ but k can be equal to 1 due to $S_{ex,\rho} = 1$ and hence the total spin $S = 3/2$ is allowed. For the s-wave in the final state we have listed the allowed partial waves for the transition amplitude $\rho N \to \eta N$ in the following table

S	L	S'	L'	J
$\frac{1}{2}$	0	$\frac{1}{2}$	0	$\frac{1}{2}$
$\frac{3}{2}$	2	$\frac{1}{2}$	0	$\frac{1}{2}$

7.8 Isospin coefficients

As it was already discussed in appendix 7.4 it is convenient to perform the calculation using a partial wave decomposition. In this section we will present the transformation procedure for the isospin operators. Since η is isoscalar we only need to consider the transformation of the NN pair into the basis of total isospin. The cross section with respect to the isospin dependent part is

$$\begin{aligned} \sigma_{NN\to NN\eta} &\sim |\langle\, \tfrac{1}{2}I_{1z}\tfrac{1}{2}I_{2z} \,|\, M_{2\to3} \,|\, \tfrac{1}{2}I_{1z}\tfrac{1}{2}I_{2z} \rangle|^2 \\ \langle\, \tfrac{1}{2}I_{1z}\tfrac{1}{2}I_{2z} \,|\, M_{2\to3} \,|\, \tfrac{1}{2}I_{1z}\tfrac{1}{2}I_{2z} \rangle &= \sum_{I,I_z}(C^{II_z}_{\frac{1}{2}I_{1z}\frac{1}{2}I_{2z}})^2\langle\, II_z \,|\, M_{2\to3} \,| II_z \rangle, \end{aligned} \tag{7.77}$$

where $I_{1z}(I_{2z})$ are the isospin projections of the individual nucleons, whereas $I(I_z)$ are the total isospin (its projection) of the reaction.

For the reaction $pp \to pp\eta$ we obtain

$$\begin{aligned} \left\langle \tfrac{1}{2}I_{1z}\tfrac{1}{2}I_{2z} \,\middle|\, M \,\middle|\, \tfrac{1}{2}I_{1z}\tfrac{1}{2}I_{2z} \right\rangle &= \langle 11 \,|\, M \,|11\rangle, \\ \sigma_{pp\to pp\eta} &= \frac{1}{2}\sigma_{1,pp} \end{aligned} \tag{7.78}$$

and for $pn \to pn\eta$

$$\begin{aligned} \left\langle \tfrac{1}{2}I_{1z}\tfrac{1}{2}I_{2z} \,\middle|\, M \,\middle|\, \tfrac{1}{2}I_{1z}\tfrac{1}{2}I_{2z} \right\rangle &= \frac{1}{2}\Big[\langle 10 \,|\, M \,|10\rangle + \langle 00 \,|\, M \,|00\rangle\Big], \\ \sigma_{pn\to pn\eta} &= \frac{1}{4}(\sigma_1 + \sigma_0)_{pn} \end{aligned} \tag{7.79}$$

We should note that σ_1 in the pn case is not the same as for pp reaction. This is related to the fact that pp and pn (with I=1) interactions are different.

For $pn \to d\eta$ we obtain

$$\left\langle \tfrac{1}{2}I_{1z}\tfrac{1}{2}I_{2z} \,\middle|\, M \,\middle|\, \tfrac{1}{2}I_{1z}\tfrac{1}{2}I_{2z} \right\rangle = \tfrac{1}{\sqrt{2}}\langle 00 \,|\, M \,|00\rangle \tag{7.80}$$

Now we are going to calculate the matrix element $\langle II_z \,|\, M^I_{2\to 3} \,|II_z\rangle$ for the exchanges of the π, ρ, η and σ mesons.

For the re-scattering process we apply the expression (7.67) which was already deduced in section 7.7 for the spin variables.

$$\begin{aligned} \langle II_z \,|\, M^I \,|II_z\rangle = \sum_{\substack{\mu_1,\mu_2,\mu_{ex}\\ \mu_3,\mu_4}} & C^{II_z}_{\frac{1}{2}\mu_3\frac{1}{2}\mu_4} C^{II_z}_{\frac{1}{2}\mu_2\frac{1}{2}\mu_1} \\ & \times\left\langle \tfrac{1}{2}\mu_4 \,\middle|\, T_{2\to 2} \,\middle|\, \tfrac{1}{2}\mu_2 I_{ex}\mu_{ex}\right\rangle\left\langle \tfrac{1}{2}\mu_3 I_{ex}\mu_{ex} \,\middle|\, \Gamma_{is} \,\middle|\, \tfrac{1}{2}\mu_1\right\rangle, \end{aligned} \tag{7.81}$$

For isoscalar σ, η mesons $I_{ex} = 0$ and, thus,

$$\left\langle \tfrac{1}{2}\mu_3 I_{ex}\mu_{ex} \,\middle|\, \Gamma_{is} \,\middle|\, \tfrac{1}{2}\mu_1\right\rangle = \delta_{\mu_3\mu_1} \tag{7.82}$$

$$\left\langle \tfrac{1}{2}\mu_4 \,\middle|\, T_{2\to 2} \,\middle|\, \tfrac{1}{2}\mu_2 00\right\rangle = \delta_{\mu_2\mu_4}\left\langle I = \tfrac{1}{2} \,\middle|\, T_{2\to 2} \,\middle|\, I = \tfrac{1}{2}\right\rangle. \tag{7.83}$$

Finally we obtain

$$\langle II_z \,|\, M^I_{\sigma,\eta} \,|II_z\rangle = \left\langle I=\tfrac{1}{2} \,\middle|\, T_{2\to 2} \,\middle|\, I=\tfrac{1}{2}\right\rangle(-1)^{I-1} = \begin{cases} -\left\langle I=\tfrac{1}{2} \,\middle|\, T_{2\to 2} \,\middle|\, I=\tfrac{1}{2}\right\rangle & I=0 \\ \left\langle I=\tfrac{1}{2} \,\middle|\, T_{2\to 2} \,\middle|\, I=\tfrac{1}{2}\right\rangle & I=1 \end{cases} \tag{7.84}$$

For isovector particles the vertex operator Γ contains a term of the form $\vec{\tau}\partial_\mu\vec{\phi}$ for pions ($\vec{\tau}\partial_\mu\vec{\rho}_\nu$ for ρ-meson). The vector field $\vec{\phi}$ has the form:

$$\vec{\phi} = \frac{1}{(2\pi)^3}\int \frac{d\vec{q}}{\sqrt{2\omega_q}} \sum_{\lambda=-1}^{1} (\vec{f}_\lambda a_\lambda(\vec{q})e^{-iqx} + \vec{f}^*_\lambda a^+_\lambda(\vec{q})e^{iqx}), \tag{7.85}$$

where

$$\vec{f}_{+1} = \frac{-1}{\sqrt{2}}\begin{pmatrix}1\\ i\\ 0\end{pmatrix};\ \vec{f}_{-1} = \frac{1}{\sqrt{2}}\begin{pmatrix}1\\ -i\\ 0\end{pmatrix};\ \vec{f}_0 = \begin{pmatrix}0\\ 0\\ 1\end{pmatrix} \tag{7.86}$$

and

$$a_{+1}(q)\,|\pi^+(k)\rangle = |0\rangle\,\delta(\vec{q}-\vec{k}). \tag{7.87}$$

It is convenient to present the matrix element of the vertex operator Γ in the form:

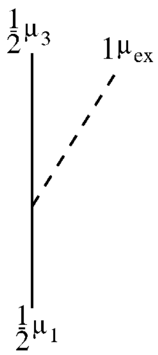

$$= \left\langle \tfrac{1}{2}\mu_3 1\mu_{ex} \,\middle|\, \vec{\tau}\partial_\mu\vec{\phi} \,\middle|\, \tfrac{1}{2}\mu_1 \right\rangle = iq_\mu\sqrt{3}\,C^{\frac{1}{2}\mu_1}_{\frac{1}{2}\mu_3 1\mu_{ex}} \tag{7.88}$$

Converting also the $MN \to \eta N$ T-matrix from particle into isospin basis,

$$\left\langle \tfrac{1}{2}\mu_4 \,\middle|\, T \,\middle|\, \tfrac{1}{2}\mu_2 I_{ex}\mu_{ex} \right\rangle = \left\langle \tfrac{1}{2} \,\middle|\, T \,\middle|\, \tfrac{1}{2} \right\rangle C^{\frac{1}{2}\mu_4}_{\frac{1}{2}\mu_2 I_{ex}\mu_{ex}}, \tag{7.89}$$

we finally arrive at

$$\begin{aligned}\langle II_z \,|\, M^I_{\pi,\rho} \,|II_z\rangle &= \left\langle \tfrac{1}{2} \,\middle|\, T \,\middle|\, \tfrac{1}{2} \right\rangle \sum_{\mu_1\mu_3} C^{II_z}_{\frac{1}{2}\mu_3 \frac{1}{2} I_z-\mu_3} C^{II_z}_{\frac{1}{2} I_z-\mu_1 \frac{1}{2}\mu_1} C^{\frac{1}{2} I_z-\mu_3}_{\frac{1}{2} I_z-\mu_1 1\mu_1-\mu_3} C^{\frac{1}{2}\mu_1}_{\frac{1}{2}\mu_3 1\mu_1-\mu_3} \\ &= \left\langle \tfrac{1}{2} \,\middle|\, T \,\middle|\, \tfrac{1}{2} \right\rangle iq_\mu \begin{cases} \frac{1}{\sqrt{3}} & I=1, I_z=0,1 \\ \sqrt{3} & \text{I=0} \end{cases}\end{aligned} \tag{7.90}$$

For the direct η production we find (compare eq. (7.74) and the corresponding figure)

$$\langle\, II_z \,|\, M^{dir} \,|II_z\rangle = \sum_{\mu_2\mu_4} C^{II_z}_{\frac{1}{2}I_z-\mu_4\frac{1}{2}\mu_4} C^{II_z}_{\frac{1}{2}\mu_2\frac{1}{2}I_z-\mu_2}\delta_{\mu_2\mu_4}$$
$$= (-1)^{I-1} = \begin{cases} 1 & I=1, I_z=0,1 \\ \text{-1} & \text{I=0} \end{cases} \tag{7.91}$$

7.9 Antisymmetrization procedure

Since we work in $JLSI$ basis the nucleons in the initial and final states are considered to be identical for all channels of the reaction $NN \to NN\eta$. Therefore they have to be appropriately symmetrized. Let us describe here this procedure for the re-scattering diagrams. The antisymmetrization in the initial and final states means that we need to add up the following series of diagrams:

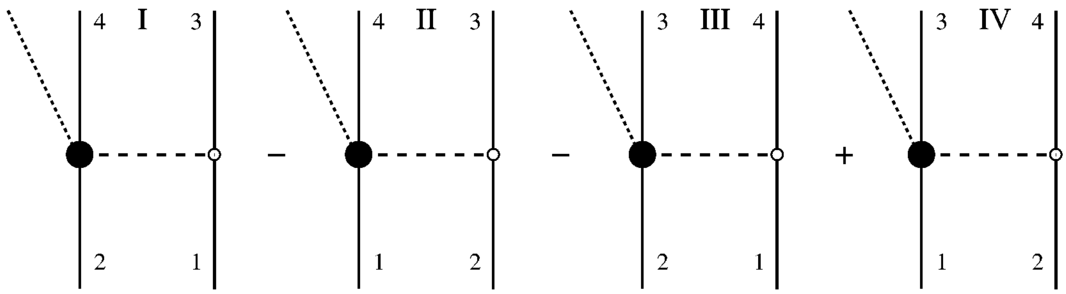

where the index i for each particle contains info about momentum and spin and isospin projections of nucleons $i = (\vec{p}_i, \lambda_i, \mu_i)$.

Let us write down the expression for the diagram II in terms of spin variables.

$$\langle\, S_f S_{zf} \,|\, M^{II}(\vec{p}_2, \vec{p}_1) \,|S_i S_{zi}\rangle = \sum_{\substack{\lambda_1,\lambda_2,\lambda_{ex}\\ \lambda_3,\lambda_4}} C^{S_f S_{zf}}_{\frac{1}{2}\lambda_3\frac{1}{2}\lambda_4} C^{S_i S_{zi}}_{\frac{1}{2}\lambda_2\frac{1}{2}\lambda_1} \langle\, \tfrac{1}{2}\lambda_4 \,|\, T_{2\to 2} \,|\, \tfrac{1}{2}\lambda_1 S_{ex}\lambda_{ex}\rangle$$
$$\times\langle\, \tfrac{1}{2}\lambda_3 S_{ex}\lambda_{ex} \,|\, \Gamma \,|\, \tfrac{1}{2}\lambda_2\rangle \overset{\lambda_1\leftrightarrow\lambda_2}{=} (-1)^{S_i-1}\langle\, S_f S_{zf} \,|\, M^{I}(\vec{p}_2, \vec{p}_1) \,|S_i S_{zi}\rangle \tag{7.92}$$

In the very last equality the property $C^{SS_z}_{S_1S_{1z}S_2S_{2z}} = (-1)^{S-S_1-S_2} C^{SS_z}_{S_2S_{2z}S_1S_{1z}}$ was used. We would arrive at the same factor $(-1)^{I-1}$ by starting from isospin consideration. Then the sum of the four diagrams is

$$I - II - III + IV = \langle\, S_f S_{zf}, I \,|\, M^I(\vec{p}_1, \vec{p}_2, \vec{p}_3, \vec{p}_4) - (-1)^{S_i+I} M^I(\vec{p}_2, \vec{p}_1, \vec{p}_3, \vec{p}_4)$$
$$-(-1)^{S_f+I} M^I(\vec{p}_1, \vec{p}_2, \vec{p}_4, \vec{p}_3) + (-1)^{S_i+S_f} M^I(\vec{p}_2, \vec{p}_1, \vec{p}_4, \vec{p}_3)\, |I, S_i S_{zi}\rangle \tag{7.93}$$

If now we convert our amplitude into LM basis, for example, for the final particles, i.e.

$$M(\vec{p}_3, \vec{p}_4) = M(\vec{p}, -\vec{p});\;\; M(\vec{p}_4, \vec{p}_3) = M(-\vec{p}, \vec{p}) \;\; \text{with}$$
$$\langle\, -\vec{p}\,| \;= \sum_{LM} (-1)^L Y_{LM}(\hat{\vec{p}})\, \langle\, LM\,|\,, \tag{7.94}$$

then for the diagrams responsible for the final antisymmetrization we derive

$$I - III = \langle\, S_f S_{zf}; LM; I \,|\, M^I(\vec{p}_1, \vec{p}_2; \vec{p})\, |I S_i S_{si}\rangle (1 + (-1)^{S_f+L+I}) \tag{7.95}$$

This equality emphasizes that those partial wave amplitudes allowed by the Pauli principle have to be multiplied by a factor 2 due to antisymmetrization, whereas all other terms are equal to 0.

Bibliography

[1] T.-S. H. Lee and D. Riska, Phys. Rev. Lett. **70**, 2237 (1993)

[2] C. J. Horowitz et al, Phys. Rev. **C49**, 1337 (1994)

[3] E. Hernándes, E. Oset, Phys. Lett. **B 350**, 158 (1995)

[4] J. Haidenbauer, C. Hanhart, J. Speth, Acta. Phys. Pol. **27**, 2893 (1996)

[5] C. Hanhart et al., Phys. Lett. **B 444**, 25 (1998)

[6] C. Schütz et al., Phys. Rev. **C57**, 1464 (1998)

[7] A.M. Bergdolt et al., Phys. Rev. **D 48**, 2969 (1993)

[8] E. Chiavassa et al., Phys. Lett. **B 322**, 270 (1994)

[9] H.Calén et al., Phys. Lett. **B 366**, 366 (1996)

[10] F. Hibou et al., Phys. Lett. **B 438**, 41 (1998)

[11] J.Smyrski et al., Phys. Lett. **B474** , 182 (2000)

[12] P. Moskal et al., πN Newsletter **16**, 367 (2002); nucl-ex/0110018

[13] H. Calén et al., Phys. Rev. **C 58**, 2667 (1998)

[14] H.Calén et al., Phys. Rev. Lett. **80**, 2069 (1998)

[15] H.Calén et al., Phys. Rev. Lett. **79**, 2642 (1997)

[16] H. Calén et al., Phys. Lett. **B 458**, 190 (1999)

[17] M. Abdel-Bary et al., nucl-ex/0205016, submitted to the Eur. Phys. J. **A**

[18] P. Winter, diploma thesis, Jül-3943, Forschungszentrum Jülich (2002)

[19] J.M.Laget and F.Wellers, Phys. Lett. **B257**, 254 (1991)

[20] A. Moalem et al., Nucl.Phys. **A 600**, 445 (1996); A. Moalem et al., Nucl. Phys. **A589**, 649 (1995).

[21] E. Gedalin et al., Nucl.Phys. **A 634**, 368 (1998)

[22] V. Bernard, N. Kaiser, and Ulf-G. Meißner, Eur. Phys. J. **A 4**, 259 (1999).

[23] M. Batinić et al., Phys. Scr. **56**, 321 (1997)

[24] J.-F.Germond and C.Wilkin, Nucl. Phys. **A518**, 308 (1990)

[25] G. Fäldt, C. Wilkin, Phys. Scripta **64**, 427 (2001); nucl-th/0104081 (2001)

[26] T.Vetter et al., Phys. Lett. **B 263**, 153 (1991)

[27] M.T. Peña et al., Nucl.Phys. **A683**, 322 (2001)

[28] V. Yu. Grishina et al., Phys. Lett. **B475**, 9 (2000)

[29] K. Nakayama, J. Speth and T.-S. H. Lee, nucl-th/0202012

[30] R. M. Brown. et al., Nucl. Phys. **B 153**, 89 (1979)

[31] B. Krusche et al., Phys. Rev. Lett. **74**, 3736 (1995)

[32] L. A. Kondratyuk, A. V. Lado, Yu. N. Uzikov, Yad. Fiz. **58**, 524 (1995)

[33] S. A. Rakityansky, Phys. Rev. **C53**, 2043 (1996)

[34] P. Moskal et al, Phys. Lett. **B 482**, 356 (2000)

[35] R. Machleidt, K. Holinde und Ch. Elster, Phys. Report **149**, 1 (1987)

[36] O.Krehl et al., Phys. Rev. **C62**, 025207 (2000)

[37] O.Krehl, PhD thesis, Forschungszentrum Jülich, Nr.3692 (1999)

[38] K. M. Watson, Phys. Rev. **88**, 1163 (1952).

[39] A. B. Migdal, Sov. Phys. JETP **1**, 2 (1955).

[40] C. Hanhart and K. Nakayama, Phys. Lett. **B454**, 176 (1999)

[41] J. A. Niskanen, Phys. Lett. **B 456**, 107 (1999)

[42] V. Baru et al., Phys. Atom. Nucl. **64**, 579 (2001); nucl-th/0006075

[43] V. Baru et al., Acta Phys. Polon. **B31**, 2127 (2000)

[44] A. B. Santra, B.K. Jain, Nucl. Phys. **A634**, 309 (1998)

[45] T.-S. H. Lee and A. Matsuyama, Phys. Rev. **C36**, 1459 (1987)

[46] M. L. Goldberger, K. M. Watson, Collision Theory, Wiley, New York 1964, chapter 9.3.

[47] H. Eckstein, Phys. Rev. **101**, 880 (1956)

[48] C. Bennhold, H. Tanabe, Nucl. Phys. **A 530**, 625 (1991)

[49] R. S. Bhalerao and L.C. Liu, Phys. Rev. Lett. **54**, 865 (1985)

[50] A. Sibirtsev et al., Phys. Rev. **C 65**, 044007 (2002); nucl-th/0203039

[51] C. Sauermann, B.L. Friman, W. Norenberg, Phys. Lett. **B341**, 261 (1995)

[52] C. Wilkin, Phys. Rev. **C47**, 938 (1993)

[53] V. V. Abaev and B.M.K. Nefkens, Phys. Rev. **C53**, 385 (1996)

[54] A. M. Green and S. Wycech, Phys. Rev. **C 55**, 2167 (1997)

[55] M. Batinić, et al., Phys. Rev. **C 51**, 2310 (1995); Erratum-ibid. **C57**, 1004 (1998)

[56] M. Arima, K. Shimizu, K. Yazaki, Nucl. Phys. **A 543**, 613 (1992)

[57] E. W. Schmid and H. Ziegelmann, "The quantum mechanical three-body problem", Pergamon press, Braunschweig, Vieweg, 1974

[58] H. Machner and J. Haidenbauer, J. Phys. **G25**, 231 (1999)

[59] R. Machleidt, Advanced Nucl. Phys. **19**, 189 (1989)

[60] J. Haidenbauer, K. Holinde, and M.B. Johnson, Phys. Rev. C **48**, 2190 (1993).

[61] L. Tiator, C. Bennhold and S.S. Kamalov, "The eta coupling and the S_{11} resonance in eta photoproduction on the nucleon", Physics with GeV-Particle Beams, World Scientific, Singapore, p.112 (1995)

[62] M. Kirchbach, L. Tiator, Nucl. Phys. **A 604**, 385 (1996)

[63] C.Hanhart, PhD thesis, Forschungszentrum Jülich, Nr.3476 (1997)

[64] A. M. Gasparyan, PhD thesis, in preparation

[65] G. Höhler, (private communication)

[66] R. Koch, Z. Phys. **C 29**, 597 (1985)

[67] R.A. Arndt et al., Phys. Rev. **C 52**, 2120 (1995)

[68] W. Deinet et al., Nucl. Phys. **B11**, 495 (1969)

[69] F. Bulos et al., Phys. Rev. **187**, 1827 (1969)

[70] W.B. Richards et al., Phys. Rev. **D1**, 10 (1970)

[71] J. Feltesse et al., Nucl. Phys. **B 93**, 242 (1975)

[72] N.C. Debenham et al., Phys. Rev. **D 12**, 2545 (1975)

[73] B. Tippens et al., πN Newsletter **14**, 90 (1998)

[74] T. W. Morrison, PhD thesis, George Washington University, UMI-99-55477-mc (2000)

[75] M. Lacombe et al., Phys. Rev. C **21**, 861 (1980).

[76] M.B. Johnson, Annals of physics **97**, 400 (1976)

[77] W. M. Kloet, J. A. Tjon, Phys. Rev. **C 30**, 1653 (1984)

[78] C. Elster, PhD thesis, Univerität Bonn, June 1986

[79] C. Elster et al., Phys. Rev. **C 38**, 1828 (1988)

[80] SAID library, internet cite: http://gwdac.phys.gwu.edu

[81] R. A. Arndt et al. Phys. Rev. **D 26**, 97 (1983)

[82] R. A. Arndt, Phys. Rev. **C62**, 034005 (2000)

[83] V. Baru et al., η-meson production in the reaction $pp \to pp\eta$, IKP/COSY Annual report 2000, jül-3852, p.114

[84] V.Baru et al., On the η-meson production in nucleon-nucleon collisions, Preprint ITEP (in russian), **36** (2001)

[85] N. Kaiser, Phys. Rev. **C60**, 057001 (1999).

[86] Yu. N. Uzikov, C. Wilkin, Phys. Lett. **B 511**, 191 (2001)

[87] B. L. Druzhinin, A. E. Kudryavtsev, and V. E. Tarasov, Z. Phys.**A359**, 205 (1997).

[88] G. Fäldt and C. Wilkin, Phys. Lett. **B 382**, 209 (1996).

[89] R. Shyam and U. Mosel, Phys. Lett. **B 426**, 1 (1998).

[90] A. Sibirtsev and W. Cassing, nucl-th/9904046; Eur. Phys. J. **A 2**, 333 (1998).

[91] A. I. Titov, B. Kämpfer, and B. L. Reznik, Eur. Phys. J. **A 7**, 543 (2000).

[92] A. E. Kudryavtsev, B. L. Druzhinin, V. E. Tarasov, JETP Lett. **63**, 235 (1996)

[93] V.Baru et al., Eur. Phys. J. A **6**, 445 (1999)

[94] P. Moskal, ..., V. Baru, ..., et al., Phys. Lett. **B474**, 416 (2000)

[95] H.v.Haeringen, Nucl. Phys. A **253**, 355 (1975)

[96] H.v.Haeringen, Charged-Particle-Interactions, Theory and Formulas, Leyden: Coulomb Press 1985

[97] C. Hanhart, J. Haidenbauer, A. Reuber, C. Schütz, and J. Speth, Phys. Lett. **B 358**, 21 (1995).

[98] Cf. the Appendix of C. Hanhart and K. Nakayama, `nucl-th/9809059`.

[99] N.A.Törnqvist, Phys. Rev. Lett. **49**, 624 (1982).

[100] V.V.Anisovich, E-print hep-ph/9712504.

[101] A.Veinstein et al., EPAN (Elementarnie Chastizi Atomnoe Yadro) **13**, 542 (1982).

[102] E.v.Beveron, Phys. Lett. **B 495**, 300 (2000)

[103] N.N.Achasov and G.N.Shestakov, Sov. Phys. Uspechi **161**, N.6, 53 (1991); **142**, 361 (1984); Z.Phys. **C 41**, 309 (1988); N.N.Achasov hep-ph/9803292

[104] V.N.Gribov, LU-TP-91-7;ORSAY Lectures on Confinement1, LPT HE-ORSAY-92-60; V.N.Gribov, Eur. Phys.J. **C10**, 91 (1999); F.Close et al., Phys. Lett. **B319**, 291 (1993).

[105] J.Weinstein, N.Isgur., Phys. Rev. **D41**, 2236 (1990); N.Isgur, K.Maltman, J.Weinstein and T. Barnes, Phys.Rev.Lett. **64**, 161 (1990).

[106] G.Janssen, B.C. Pearce, K. Holinde and J.Speth, Phys. Rev. **D52**, 2690 (1995).

[107] O. Krehl, R. Rapp, J. Speth, Phys. Lett. **B 390**, 23 (1997)

[108] L. A. Kondratyuk et al., Preprint ITEP-19-97, Moscow (1997); V.Tchernishev et al., COSY proposal N.55: "Study of a_0^+-mesons at ANKE" (1997).

[109] J. B. Gay et al., Phys. Lett. **63**, 220 (1976).

[110] S. M. Flatté, Phys. Lett. **63**, 224 (1976).

[111] N. N. Achasov, S.A. Devyanin, G.N.Shestakov., Yad. Fiz. **32**, 1098 (1980).

[112] S .Teige et al., Phys. Rev. **D59**, 012001 (1999)

[113] D.Bugg et al., Phys. Rev. **D50**, 4412 (1994)

[114] V. Baru et al., The perspectives to study lightest scalar $a_0^-(980)$ in the reaction $pd \to ppa_0^- p(s)$ close to threshold, preprint ITEP-30-00, Moscow (2000)

[115] E. L. Bratkovskaya et al., nucl-th/0107071

[116] D.M.Binnie et al., Phys. Rev. **D8**, 9, 2789 (1973).

[117] B.Abramov et al., Z. Phys. **C69**, 409 (1996).

[118] F.Duncan et al., Phys. Rev. Lett. **80**, 4390-4393, (1998)

Acknowledgments

First of all I would like to express my gratitude to Prof. J. Speth for hospitality, support of this work and useful discussions.

Dr. J. Haidenbauer, Dr. C. Hanhart and Prof. A. E. Kudryavtsev I thank for cooperation, constant interest in this work, careful reading of this manuscript and helpful critical remarks and suggestions.

I would like to thank my friend and coauthor Ashot Gasparyan for valuable discussions and assistance with the programming of my code which was used in performing the calculations.

Dr. Pawel Moskal I acknowledge for fruitful cooperation and for quick providing me by the new experimental data from COSY 11 collaboration.

I would like to acknowledge Prof. L. A. Kondratyuk, Prof. V. M. Kolybasov and Dr. Yu. N. Uzikov for agreement to be the official referees of this thesis in Russia.

I thank Dr. K. Nakayama and Dr. A. Sibirtsev for numerous discussions.

I am grateful to Mrs. R. Bley for the readiness to help with any administrative matter.

Thanks a lot to all my russian and german colleagues and friends. It is pleasant for me to work in such a collective.

Forschungszentrum Jülich
in der Helmholtz-Gemeinschaft

Jül-4004
Oktober 2002
ISSN 0944-2952